



HAL
open science

Structural vibration damping with synchronized energy transfer between piezoelectric patches

Kaixiang Li

► **To cite this version:**

Kaixiang Li. Structural vibration damping with synchronized energy transfer between piezoelectric patches. Other. INSA de Lyon, 2011. English. NNT : 2011ISAL0088 . tel-00735788

HAL Id: tel-00735788

<https://theses.hal.science/tel-00735788>

Submitted on 26 Sep 2012

HAL is a multi-disciplinary open access archive for the deposit and dissemination of scientific research documents, whether they are published or not. The documents may come from teaching and research institutions in France or abroad, or from public or private research centers.

L'archive ouverte pluridisciplinaire **HAL**, est destinée au dépôt et à la diffusion de documents scientifiques de niveau recherche, publiés ou non, émanant des établissements d'enseignement et de recherche français ou étrangers, des laboratoires publics ou privés.

THÈSE

présentée devant

L'INSTITUT NATIONAL DES SCIENCES APPLIQUÉES DE LYON

par

Kaixiang LI

pour obtenir le grade de DOCTEUR

École doctorale : Électronique, Électrotechnique et Automatique de Lyon

Spécialité : Énergie et Systèmes

Soutenue le xx Sept 2011 devant la commission d'examen

Amortissement vibratoire avec échange d'énergie synchronisé entre des éléments piézoélectriques

-

Structural vibration damping with synchronized energy transfer between piezoelectric patches

Membres du jury :

Pr.	Emmanuel	FOLTETE	Professeur à l'ENSMM de Besançon	Examineur
Dr.	Jean-Yves	GAUTHIER	Maître de Conférences à l'INSA de Lyon	Co-directeur
Pr.	Daniel	GUYOMAR	Professeur à l'INSA de Lyon	Directeur
Pr.	Mohamed	ICHCHOU	Professeur à l'Ecole Centrale de Lyon	Rapporteur
Dr.	Dejan	VASIC	Maître de conférence H.D.R. à Université de Cergy-Pontoise	Rapporteur
Pr.	Zhichun	YANG	Professeur à Northwestern Polytechnical University (Chine)	Examineur

Laboratoire de Génie Electrique et Ferroélectricité (LGEF) de l'INSA de Lyon

INSA Direction de la Recherche - Ecoles Doctorales - Quinquennal 2011-2015

SIGLE	ECOLE DOCTORALE	NOM ET COORDONNEES DU RESPONSABLE
CHIMIE	CHIMIE DE LYON http://www.edchimie-lyon.fr Insa : R. GOURDON	M. Jean Marc LANCELIN Université de Lyon – Collège Doctoral Bât ESCPE 43 bd du 11 novembre 1918 69622 VILLEURBANNE Cedex Tél : 04.72.43 13 95 directeur@edchimie-lyon.fr
E.E.A.	ELECTRONIQUE, ELECTROTECHNIQUE, AUTOMATIQUE http://edeea.ec-lyon.fr Secrétariat : M.C. HAVGOUDOUKIAN eea@ec-lyon.fr	M. Gérard SCORLETTI Ecole Centrale de Lyon 36 avenue Guy de Collongue 69134 ECULLY Tél : 04.72.18 60 97 Fax : 04 78 43 37 17 Gerard.scorletti@ec-lyon.fr
E2M2	EVOLUTION, ECOSYSTEME, MICROBIOLOGIE, MODELISATION http://e2m2.universite-lyon.fr Insa : H. CHARLES	Mme Gudrun BORNETTE CNRS UMR 5023 LEHNA Université Claude Bernard Lyon 1 Bât Forel 43 bd du 11 novembre 1918 69622 VILLEURBANNE Cédex Tél : 04.72.43.12.94 e2m2@biomserv.univ-lyon1.fr
EDISS	INTERDISCIPLINAIRE SCIENCES- SANTÉ http://ww2.ibcp.fr/ediss Sec : Safia AIT CHALAL Insa : M. LAGARDE	M. Didier REVEL Hôpital Louis Pradel Bâtiment Central 28 Avenue Doyen Lépine 69677 BRON Tél : 04.72.68 49 09 Fax : 04 72 35 49 16 Didier.revel@creatis.uni-lyon1.fr
INFOMATHS	INFORMATIQUE ET MATHEMATIQUES http://infomaths.univ-lyon1.fr	M. Johannes KELLENDONK Université Claude Bernard Lyon 1 LIRIS - INFOMATHS Bâtiment Nautibus 43 bd du 11 novembre 1918 69622 VILLEURBANNE Cedex Tél : 04.72. 43.19.05 Fax 04 72 43 13 10 infomaths@bat710.univ-lyon1.fr
Matériaux	MATERIAUX DE LYON	M. Jean-Yves BUFFIERE Secrétaire : Mériem LABOUNE INSA de Lyon École Doctorale Matériaux Mérim LABOUNE Bâtiment Antoine de Saint-Exupéry 25bis Avenue Jean Capelle 69621 VILLEURBANNE Tel : 04 72 43 71 70 Fax : 04 72 43 72 37 ed.materiaux@insa-lyon.fr
MEGA	MECANIQUE, ENERGETIQUE, GENIE CIVIL, ACOUSTIQUE (ED n°162)	M. Philippe BOISSE Secrétaire : Mériem LABOUNE Adresse : INSA de Lyon École Doctorale MEGA Mérim LABOUNE Bâtiment Antoine de Saint-Exupéry 25bis Avenue Jean Capelle 69621 VILLEURBANNE Tel : 04 72 43 71 70 Fax : 04 72 43 72 37 mega@insa-lyon.fr Site web : http://www.ed-mega.com
ScSo	ScSo* M. OBADIA Lionel Sec : Viviane POLSINELLI Insa : J.Y. TOUSSAINT	M. OBADIA Lionel Université Lyon 2 86 rue Pasteur 69365 LYON Cedex 07 Tél : 04.78.69.72.76 Fax : 04.37.28.04.48 Lionel.Obadia@univ-lyon2.fr

*ScSo : Histoire, Géographie, Aménagement, Urbanisme, Archéologie, Science politique, Sociologie, Anthropologie

Every experiment proves something. If it does not prove what you wanted it to prove, it proves something else.

Anonymous

Abstract

Advanced materials such as carbon fiber, composite materials *et.al.* are more and more used in modern industry. They make the structures lighter and stiffer. However, they bring vibration problems. Researchers studied numerous methods to eliminate the undesirable vibrations. These treatments are expected to be a compact, light, intellectual and modular system. Recently, a nonlinear technique which are known as Synchronized Switch Damping (SSD) technique was proposed. These techniques synchronously switched when structure got to its displacement extremes that leading to a nonlinear voltage on the piezoelectric elements. This resulting voltage showed a time lag with the piezoelectric strain thus causing energy dissipation. Based on the developed SSD techniques, a new synchronized switch damping *e.g.* Synchronized Switch Damping with Energy Transfer (SSDET) was proposed in this document. This method damped the vibration by using the energy from other vibrating form. The objectives of the work reported in this document were threefold. The first one consisted of introduction of SSDET principle and developing its control law. This part aimed at establishing the mathematical model and verifying the proposed method by mathematical tools. Then, the experiment validations were carried out. Three experiments with different configurations demonstrated that SSDET can be implement not only between structures but also vibrating modes in one structure. A SSDET scheme with multi-patches was also investigated for improving the damping. Finally, a bidirectional SSDET concept was introduced based on the original SSDET technique. This technique be regarded as a multimode control SSDET. Since it privileged the target vibration while keeps a decent control effect on the source vibration.

Keywords: piezoelectric materials, synchronized switch damping technique, non-linear vibration control, semi-passive, semi-active, energy transfer.

Résumé

Les matériaux évolués tels que les matériaux composites ou les fibres de carbone sont de plus en plus utilisés dans l'industrie. Ils rendent les structures plus légères et plus résistantes mais en contrepartie, ils apportent de nouveaux problèmes de vibration. De nombreuses recherches sont ainsi en cours pour apporter des solutions afin d'éliminer les vibrations indésirables tout en restant compactes, légères, intelligentes et modulaires. Récemment, des techniques de contrôle non-linéaires, dénommées en anglais S.S.D. (Synchronized Switch Damping) ont été proposées et validées. Ces méthodes font commuter un élément piézoélectrique collé à la structure mécanique à amortir sur un circuit électrique de manière synchronisée avec la déformation de celle-ci. Un effet amortissant peut ainsi être obtenu en utilisant l'énergie de vibration de la structure mécanique elle-même. Basée sur ces concepts, une nouvelle technique appelée S.S.D.E.T. (Synchronized Switch Damping with Energy Transfer) est proposée dans ce manuscrit. Cette méthode permet d'amortir une vibration en utilisant de l'énergie extraite à partir d'autres vibrations. Les résultats de ce travail de thèse sont présentés de la manière suivante. Premièrement, le principe et les lois de commande de la technique S.S.D.E.T. sont introduits. Ainsi, un modèle mathématique est établi et permet de vérifier les concepts proposés par simulation. Ensuite, des validations expérimentales menées sur différentes configurations sont décrites et démontrent l'augmentation de l'amortissement sur un système composé de deux structures mécaniquement indépendantes, sur un système composé d'une seule structure qui vibre selon plusieurs modes et sur une combinaison des deux précédents. Enfin, une extension de la technique S.S.D.E.T. est introduite dans un cadre d'échange d'énergie bidirectionnel. Celle-ci permet d'obtenir un amortissement privilégié sur un mode tout en conservant un contrôle correct des autres modes.

Mots-clés : matériaux piézoélectriques, technique d'amortissement par commutation synchronisée, contrôle de vibration non-linéaire, semi-passif, semi-actif, transfert d'énergie

Acknowledgment

The acknowledgment of this thesis, without a doubt, is the most difficult section to write. It is really impossible to list all of the people who help me to finish this thesis. However, some contributors are definitely deserve to be recognized for all of their time and effort.

First and foremost, I am deeply indebted to my supervisor, Professor Daniel Guyomar. I would like to thank him for bringing me to LGEF and making it possible to complete this work. His vision in directing my work and his encouragement have helped me tremendously.

I would like to express my gratitude to my co-supervisor, Dr. Jean-Yves Gauthier. His guidance and support from the initial to the final level enabled me to develop an understanding of the subject. Without his guidance and patience, I would not have the drive to finish this work.

I would like to acknowledge all the members of my Ph.D. Jury for evaluating the present work. In particular, I am grateful to Prof. Mohamed Ichchou and Dr. Dejan Vasic for reviewing this manuscript and for their constructive criticism. I would like to thank Prof. Emmanuel Foltete and Prof. Zhichun Yang for examining the present work. My special thanks go to Prof. Zhichun Yang who was my supervisor in my master stage. For attending my Ph.D. defense, he comes to France by taking a long-range flight from China.

I would like to thank Dr. Michaël Lallart and Dr. Thomas Monnier for their help in the work of structural health monitoring.

I appreciate the help from our secretary Mrs. Evelyne Dorieux and technicien Mr. Frédéric Defromerie. As a poor French speaker, it is really hard to make kinds of affairs alright in my life. Without their help (introduction the life in France, translation of so many documents, even negotiation with my landlord ...), I can not devote myself to this work without annoyances.

I would like to thank all members and colleagues in LGEF laboratory for their administrative and scientific supports though I can't list all of their names. Without their companionship and their wonderful sense of humor, it is impossible to finish this thesis.

For financial support, I would like to thank China Scholarship Council (CSC).

Last but not the least, my deepest and most sincere appreciation goes to my parents. They have been a constant source of support-emotional, moral and of

course financial - during those years, and this thesis would certainly not have existed without them.

Contents

Abstract	iii
Résumé	v
Acknowledgements	vii
Table of contents	1
Notations and abbreviations	13
Introduction	17
1 General introduction	19
1.1 Vibration control	19
1.2 Smart materials	22
1.2.1 Common smart materials	22
1.2.2 Piezoelectricity	23
1.3 Shunt damping techniques	26
1.3.1 Resistive shunt technique	28
1.3.2 Inductive shunt technique	28
1.3.3 Capacitive shunt technique	30
1.3.4 Switched shunt technique	31
1.4 Objectives of research topic	32
2 Review of synchronized switch damping techniques	33
2.1 SSD techniques principles	34
2.1.1 Mathematical model of piezo-element coupled structure	34
2.1.2 SSDS principles	36
2.1.3 SSDI principles	38
2.1.4 SSDV and adaptive SSDV principles	39

2.2	Energy analysis and transfer functions	42
2.2.1	General energy analysis	42
2.2.2	Transfer functions of SSD approaches	44
2.3	Broadband and multimode control of SSD techniques	47
2.3.1	Mathematical model of multimode SSD techniques	47
2.3.2	Original SSD broadband control	49
2.3.3	Mode distinguishing based multimode control	50
2.3.4	Time window based SSD multimode control	52
2.4	A brief introduction for self-powered SSD techniques and blind switch damping techniques	54
2.4.1	Self-powered SSD technique	54
2.4.2	Blind switch damping techniques	56
2.5	Conclusion	58
3	General SSDET principles	61
3.1	Principles of the SSDET	61
3.1.1	Idea of energy transfer in SSD technique	62
3.1.2	SSDET circuit and control law	62
3.1.3	Voltages cycle in SSDET	66
3.2	Mathematical modeling in time domain	67
3.2.1	Modeling by state space approach	69
3.2.2	Introduction of simulink model and configurations	71
3.2.3	System parameter identification	71
3.2.4	Simulations and results discussions	74
3.3	Mathematical modeling in frequency domain	79
3.3.1	Mathematical modeling	80
3.3.2	Simulations and discussions	84
3.4	An enhanced SSDET control law based on a threshold setting	85
3.4.1	Threshold setting principles	85
3.4.2	Simulation validation	87
3.5	Conclusion	89
4	SSDET experiments and discussions	93
4.1	Introduction of the control system	93
4.2	Energy transfer between different structures	94
4.2.1	Experimental setup	94
4.2.2	Results and discussion	99

4.2.3	Stability analysis	100
4.3	Energy transfer in one structure between different modes: Harmonic response	103
4.3.1	Experimental setup	104
4.3.2	Results and discussion	105
4.3.3	Comparison between the experiment results and mathematical predictions in frequency domain	107
4.4	Energy transfer in one structure between different modes: Impulse response	111
4.4.1	Experimental setup	111
4.4.2	Impulsing torsion motion while the structure vibrates under its bending mode	112
4.4.3	Impulsing bending mode while the structure vibrates under its torsion mode	113
4.4.4	Impulsing both the bending and torsion mode at the same time	119
4.5	Energy transfer between multi piezoelectric patches	120
4.5.1	Experimental setup	121
4.5.2	Results and discussion	123
4.6	Conclusion	125
5	Bidirectional SSDET: A preliminary research	127
5.1	A bending-torsion coupling vibration case	127
5.2	Damping behavior comparisons between four connections with SSDI control	129
5.2.1	Case-A: Each patch is connected into a standalone SSDI circuit	130
5.2.2	Case-B: Two patches connected in parallel	130
5.2.3	Case-C: Two patches connected in series	132
5.2.4	Case-D: Two patches with two switches sharing an inductor	132
5.3	Principle of bidirectional SSDET	136
5.3.1	Idea of bidirectional SSDET	137
5.3.2	Control law of the bidirectional SSDET	137
5.4	Experimental validation	142
5.4.1	Experimental setup	142
5.4.2	Results and Discussions	143
5.5	Conclusion	146

Conclusion and perspective	149
Bibliography	160
Publications	161
French part	163
Folio	178

List of Figures

1.1	Quartz watch. ¹	20
1.2	Sonicare-toothbrush designed by Philips corporation.	20
1.3	Earthquake in Wenchuan,China.	20
1.4	Tacoma narrows bridge collapse under 64 km/h winds. ²	20
1.5	Structural brackets added to the FA-18 vertical tail. ³	21
1.6	Tuned mass damped erected on Taipei101 skyscraper.	21
1.7	Conventional active vibration control.	22
1.8	polarization of polycrystal materials.	25
1.9	Piezoelectric effect. ⁴	25
1.10	piezoelectric patch bonded on a vibrating mechanical structure.	26
1.11	Classification of piezoelectric shunt circuits[1].	27
1.12	Wu's multimode R-L shunt damping circuit[2].	29
1.13	Representative optimization of the resistance on R-L shunt damping[3].	29
1.14	Davis' ladder capacitive shunt circuit[4].	30
2.1	Type II mechanical spring[5].	35
2.2	An electromechanical model.	35
2.3	A classic circuit for SSD techniques.	36
2.4	SSDS circuit.	37
2.5	SSDS waveforms.	37
2.6	SSDI circuit.	39
2.7	SSDI waveforms.	39
2.8	Ten-bay truss structure with piezoelectric transducers[6].	40
2.9	SSDV circuit.	41
2.10	SSDV waveforms.	41
2.11	SSDV damping absolute value versus proportional coefficient[7].	42
2.12	Extracted energy cycle.	44
2.13	Extracted energy cycle for SSD techniques.	45

2.14	Schematic diagram of cantilever beam. $u(x, t)$ is the beam deflection along the transverse direction(y) and $F(t)$ is the excitation force at the tip of the beam($x = L$)[8].	48
2.15	An acoustic box with SSD control[9].	50
2.16	A brass pulse tube with a separator wall consisting of a piezoelectric buzzer driven by SSD control board[10].	50
2.17	Multimode control schema with numerical filter[11].	51
2.18	Waveforms under enhanced switching law[12].	52
2.19	Estimation of the piezoelectric voltage after an inversion process[10].	53
2.20	Vibration control effect with different algorithm[13].	53
2.21	Sketch of the autonomous shunt circuit that does not require power for operation[14].	55
2.22	Self-powered SSDI control block diagram[15].	55
2.23	Self-powered adaptive SSDI control block diagram[15].	55
2.24	Low power circuit for self-powered SSDV[16].	56
2.25	BSDS technique[17].	57
2.26	BSDV techniques[17].	57
3.1	Energy flow in SSD techniques. (a) SSDS or SSDI. (b)SSD technique with energy transfer.	63
3.2	SSDET circuit.	64
3.3	Comparisons between SSDI and SSDET techniques:(a) SSDI waveforms and (b) SSDET waveforms.	65
3.4	The voltage waveforms in SSDET.	66
3.5	Voltages versus current in coil.	68
3.6	Sideviews of Fig.3.5.	68
3.7	A diagram of the simulink model.	72
3.8	Simulink model.	73
3.9	Time simulation results.	75
3.10	Details of the simulation waveform(Without control).	76
3.11	Details of the simulation waveform(SSDI).	77
3.12	Details of the simulation waveform(SSDET).	78
3.13	Extracted energy from source and target.	79
3.14	Representative current waveforms in SSDET.	80
3.15	Voltage waveforms under SSDET technique.	81
3.16	Target displacement versus several parameters.	86
3.17	Flow chart.	88

3.18	Normalized values under different normalized threshold.	89
3.19	The extract energy power versus threshold with each frequency ratio.	90
4.1	A schematic diagram of the experimental system.	94
4.2	Control system designed in Simulink.	95
4.3	Control user interface designed in Controldesk.	95
4.4	A schematic diagram of the experiment (SSDET between different structures).	97
4.5	Energy source structure: A cantilever beam.	97
4.6	Energy target structure: A four edge clamped plate.	97
4.7	The switching control scheme.	98
4.8	The damping of the plate by SSDI and SSDET.	99
4.10	The theoretical and experimental damping effect of SSDET beyond SSDI versus the displacement of the energy-source structure.	103
4.11	A spectrum comparison between experimental SSDI and SSDET.	104
4.12	A cantilever plate with the bonded PZTs.	105
4.13	A schematic diagram of the experiment. (a) The experimental setup. (b) The switching control scheme.	106
4.14	Mode shapes of the plate. (a) the first bending mode shape($f_s=23.5\text{Hz}$) and the electrical charge distribution (b) the first torsion mode($f_t=81.7\text{Hz}$) and the electrical charge distribution.	107
4.15	Control effect in time domain.	108
4.16	Transfer function of the plate with different control strategies.	108
4.17	Details during different control stage. (a) Without control (b) SSDI control (c) SSDET control.	109
4.18	The comparison between the experiment and prediction (Increasing bending case). (a) Transfer times per second vs. bending displacement (b) Extracted power vs. bending displacement (c) Torsion displacement vs. extracted power.	110
4.19	The comparison between experiment and prediction (Increasing threshold case). (a) Transfer times per second vs. threshold (b) Extracted power vs. threshold (c) Torsion displacement vs. extracted power.	110
4.20	An experimental scheme of transient case (top view).	112
4.21	Torsion displacement as the function of time for the impulse experiment.(Impact on torsion while bending is under harmonic excitation).	113
4.22	Torsion voltage as the function of time for the impulse experiment.(Impact on torsion while bending is under harmonic excitation).	114

4.23	Bending displacement as the function of time for the impulse experiment.(Impact on torsion while bending is under harmonic excitation).	114
4.24	Bending voltage as the function of time for the impulse experiment.(Impact on torsion while bending is under harmonic excitation).	115
4.25	Torsion displacement as the function of time for the impulse experiment.(Impact on bending while torsion is under harmonic excitation).	115
4.26	Torsion voltage as the function of time for the impulse experiment. (Impact on bending while torsion is under harmonic excitation).	116
4.27	Bending displacement as the function of time for the impulse experiment. (Impact on bending while torsion is under harmonic excitation).	116
4.28	Bending voltage as the function of time for the impulse experiment.(Impact on bending while torsion is under harmonic excitation).	117
4.29	Torsion displacement as the function of time for the impulse experiment.(Both of bending and torsion mode are impacted by a force hammer).	117
4.30	Torsion voltage as the function of time for the impulse experiment.(Both of bending and torsion mode are impacted by a force hammer).	118
4.31	Bending displacement as the function of time for the impulse experiment.(Both of bending and torsion mode are impacted by a force hammer).	118
4.32	Bending voltage as the function of time for the impulse experiment.(Both of bending and torsion mode are impacted by a force hammer).	119
4.33	The envelope of the torsion displacement with different control strategies.	119
4.34	SSDET circuit for multi piezoelectric patches.	120
4.35	Experimental setup for multi-patches.	122
4.36	Experimental results in time domain.	123
4.37	Damping during different control stages.	124
5.1	A bending torsion coupled vibrating plate.	128
5.2	Displacement and voltage waveforms when structure vibrates under bending and torsion modes.	129
5.3	Electrical scheme for two electrically separated SSDI control (Case-A).	130

5.4	Normalized voltages, piezoelectric forces and displacements for two separate SSDI control (Case-A: simulation results).	131
5.5	Electrical scheme for the SSDI control with two patches in parallel (Case-B).	131
5.6	Normalized voltages, piezoelectric forces and displacements with SSDI control of two patches in parallel (Case-B: simulation results).	132
5.7	Electrical scheme for the SSDI control with two patches in series (Case-C).	133
5.8	Normalized voltages, piezoelectric forces and displacements with SSDI control of two patches in series (Case-C: simulation results).	133
5.9	Electrical scheme for the SSDI control with two patches sharing an inductor (Case-D).	134
5.10	Normalized voltages, piezoelectric forces and displacements with SSDI control of two patches sharing one inductor with two switches (Case-D: simulation results).	134
5.11	Voltage waveforms during the transferring and the equivalent circuit scheme.	135
5.12	Bidirectional SSDET circuit.	138
5.13	Waveforms of displacements and voltages under case $\dot{u}_s > 0$ and u_t at its maximum.	140
5.14	Normalized voltages, piezoelectric forces and displacements with SSDI control of two patches sharing one inductor with two switches (simulation results).	142
5.15	Experimental setup.	143
5.16	Experimental waveforms (Without control).	144
5.17	Experimental waveforms (CASE-B).	144
5.18	Experimental waveforms (CASE-D).	145
5.19	Experimental waveforms (CASE-E).	145

List of Tables

1.1	The relationship between the stimuli and response of some types of smart material.	24
2.1	Energy terms.	44
2.2	Extracted energy with different SSD techniques.	45
2.3	h definitions in SSD techniques.	47
2.4	SSD techniques damping effect[18].	47
3.1	System parameters in SSD techniques.	72
3.2	System properties in simulation.	74
4.1	Geometric characteristics.	98
4.2	System characteristics in simulation.	100
4.3	System parameters of the clamped plate.	109
4.4	System properties in multi-patches SSDET experiment.	122
5.1	A comparison of the damping between different electrical schemes.	137
5.2	Direction of the energy transfer in bidirectional SSDET technique.	138
5.3	Bidirectional SSDET control law.	141
5.4	Damping comparison between different control strategies.	146

Notations and abbreviations

Notations

Symbol	signification
<i>Alphabetic character</i>	
A	state matrix
B	Input matrix
<i>C</i>	capacitance
C_0	natural capacitance of piezoelectric material
<i>c</i>	structural damping coefficient,
<i>D</i>	electric displacement,
$[d]$	direct piezoelectric effect
$[d^t]$	converse piezoelectric effect
d_{31}	piezoelectric elements with 3-1 effect
<i>E</i>	electrical field
$E_{dissipated}$	total energy dissipation in SSDET
E_s	extracted energy from source
$E\bar{I}$	flexural rigidity
s^E	compliance of piezoelectric material
<i>F</i>	exerted-force
<i>f</i>	frequency
f(t)	force matrix
<i>i</i>	current
i_0	initial current
<i>j</i>	imaginary unit
<i>k</i>	stiffness
<i>L</i>	inductance
<i>m</i>	mass
P_s	extracted power from source

Q_i	electrical quality factor
Q_M	mechanical quality factor
q_i	modal displacement of i^{th} mode
R	resistance
S	material strain
T	material stress
<i>threshold</i>	source voltage threshold
T_{LCR}	oscillation period of LCR oscillator
t	time
t_a or t'_a	switch closing time for step 1
t_b or t'_b	switch closing time for step 2
u	displacement
u_M	displacement amplitude
U_0	initial voltage
V	voltage
\tilde{V}_0	piecewise function of voltage
V_M	voltage before inverted
V_m	voltage after inverted
\tilde{V}_{sM}	RMS value of source voltage at the inversion instant (before inverted)
\tilde{V}_{tM}	RMS value of target voltage at the inversion instant (before inverted)
\tilde{V}_{tm}	RMS value of target voltage at the inversion instant (after inverted)
\tilde{V}_t	equivalent target voltage
V_{cc}	voltage of the voltage source
\mathbf{x}	state vector
Z	electrical impedance

Greek character

Symbol	signification
α	Force factor
β	User defined coefficient in adaptive SSDV
γ	Inversion factor
ρ	Density
ω	Circular frequency
ω_0	Natural circular frequency
ζ	Structural damping ration
φ_i	Model coordinate of i^{th} mode

η	Efficiency factor
λ	Ratio between voltage and displacement
δ	RMS value of displacement
<i>Superscripts</i>	
Symbol	signification
s	source
t	target
<i>Subscripts</i>	
Symbol	signification
E	open circuit
D	short circuit

Abbreviations

Symbol	signification
ABSV	ABSolute Value
AC	Alternating Current
AVS	Active Variable Stiffness
BSDS	Blind Switch Damping on Short circuit
BSDV	Blind Switch Damping on Voltage source
BSDVp	Blind Switch Damping on Piecewise constant Voltage source
BSDVa	Blind Switch Damping on Adaptive constant Voltage source
DVF	Direct Velocity Feedback
ER	Electro-Rheological
FEM	Finite Element Method
FFT	Fast Fourier transfer
I/O	Input/Output
LCR	Inductance-Capacitance-Resistance
MOSFET	Metal-Oxide-Semiconductor-Field-Effect-Transistor
MR	Magneto-Rheological
Neg	Negative
Pos	Positive
PZT	Lead-Zieconate Titanate
PMVA	Passive Mechanical Vibration Absorber

RMS	Root Mean Square
SSD	Synchronized Switch Damping
SSDS	Synchronized Switch Damping on Short circuit
SSDI	Synchronized Switch Damping on Inductor
SSDV	Synchronized Switch Damping on Voltage source
SSDET	Synchronized Switch Damping with Energy Transfer
SSH	Synchronized Switch Harvesting
SW	SWitch
TMD	Tuned Mass Damper

Introduction

Undesired mechanical vibration harms the running mechanical equipments. It could lead to material fatigue, deterioration of system performance, also increase the noise level. Particularly, structure could be damaged due to the high amplitude vibration when the excitation just locates around structure eigenvalue frequencies. Several catastrophes such as bridge collapse, airplane crash have been ascribed to vibration caused problems. Thus, vibration control becomes to an urgent issue to the mechanical engineers.

The main vibration control methods can be cataloged as passive, active and semi-passive or semi-active methods. Passive control methods are usually considered to be stable. Since there is no external feedback exerted on the target structure directly. However, it is usually bulky and sensitive to the environmental changes. On the contrary, active control can achieve broadband control but it consumes great amount of energy. Besides, it is also confined by the caused instability problems such as spillover. Semi-passive or semi-active methods inherit the advantages of both passive and active control and become a hot topic in vibration control domain.

This document proposes a semi-passive vibration technique called synchronized switch damping with energy transfer. The basis of this technique is the popular synchronized switch damping techniques (reviewed in chapter 2). This technique aims at reducing the structural vibration (target) level by using the energy pumped from another vibrating structure or vibrating mode (source) via bonded piezoelectric materials.

In this thesis, two types of SSDET technique are discussed. The first one is an ordinary SSDET technique in which the energy transfer path is constantly from one piezoelectric patches group to another. The investigation of this type SSDET concerns with control law development, mathematical modeling and simulations in both time and frequency domain (in chapter 3) and the experimental validations on different testbenches (in chapter 4). The other one is bidirectional SSDET technique in which the energy transfer between piezoelectric patches is in both direction (in chapter 5). In this part, We also discuss the damping effect by using several different connections between two patches for damping a bending-torsion coupling vibration structure. Comparisons are carried out both in simulation and experiment to reveal the advantage of the bidirectional SSDET.

Chapter 1

General introduction

Effective vibration control can improve the precision of the machining, reduce the fatigue load and prolong the operational life of industrial structures. Plenty of vibration control methods have been developed and already applied into the commercial arena. Smart materials especially piezoelectric material based vibration control techniques grows rapidly during the past two decades. In this chapter, we give a general idea of vibration control. Piezoelectricity and their usage in vibration control are simply introduced. Among kinds of piezoelectric materials based damping treatments, we emphasize in reviewing four basic shunt damping techniques due to their advantages.

1.1 Vibration control

Vibration is a basic physical phenomenon in universe. People utilize desirable vibrations to make a better life. For instance, orchestral music are played by vibration based instruments such as drums, violin, clarinet and so on. These instruments are tuned to vibrate with certain frequencies that equals to integer multiples of a fundamental frequency in order to generate pleasant sound. Crystal oscillators are used to make quartz watch which runs much preciser than a automatic one as shown in Fig.1.1. Electric and sonic toothbrushes vibrate as high as 13 thousand Hz, show a superiority to traditional toothbrushes in removing plaque and surface stains on teeth as shown in Fig.1.2.

However, undesirable vibrations can bring lots of problems. Working in a high level noise environment can severely damage human's health. Structural vibrations can cause material fatigue, structural failure and excessive equipment wear which



Figure 1.1: Quartz watch.¹



Figure 1.2: Sonicare-toothbrush designed by Philips corporation.



Figure 1.3: Earthquake in Wenchuan,China.



Figure 1.4: Tacoma narrows bridge collapse under 64 km/h winds.²

would shorten the structure operational life and increase the maintenance costs. Moreover, Disasters could occur if there is a inherent shortage of the structural design. People would lost their lives in a strong earthquake if their residences without anti-seismic design as shown in Fig.1.3. Long span bridge such as suspension bridge or cable-stayed bridge is vulnerable to the wind which could induce the self-excited vibration of the bridge as shown in Fig.1.4.

Consequently, people call for vibration control methods to avoid the problems induced by the undesirable vibrations. In the past decades, such techniques grow rapidly in kinds of industry domain. These approaches can be generally classified as three catalogs which are passive control, active control and semi-active or semi-passive control.

¹<http://www.hautehorlogerie.org/fr/horlogere-culture/watches/modeles-de-legende/1981-1990/swatch/> due to 2011

²[http://en.wikipedia.org/wiki/Tacoma_Narrows_Bridge_\(1940\)](http://en.wikipedia.org/wiki/Tacoma_Narrows_Bridge_(1940)) due to 2011

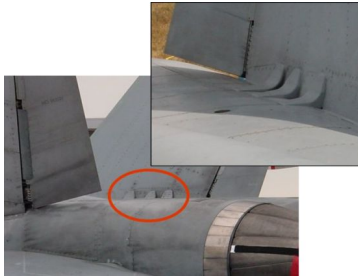


Figure 1.5: Structural brackets added to the FA-18 vertical tail.³



Figure 1.6: Tuned mass damped erected on Taipei101 skyscraper.

Passive control is the earliest developed vibration control methods. These methods are easy to implement, sensor and power needless and unconditional stable. The simplest passive vibration control method is isolation. On the one hand, we can isolate the vibrating structure from its support to prevent the vibration transmit to other equipments. This application has been applied to the some mechanical structures such as central air condition and air compressor. On the other hand, we can also isolate the structure from the vibrating base like adding a spring under the seats in the vehicles. However, the vibration source is not be damped in these applications. Another simple way is to add mass or stiffness to the structure in order to change the dynamic behaviors. Thus the structure can keep away from their resonant frequencies during working time. Besides the above treatments, several passive control ways are also developed. Tuned mass damper (TMD) is a popular passive control approach[19]. This device is normally mounted in a host structure to absorb the structural mechanical energy when the structure vibrates at its resonant frequency. The main disadvantage of the passive control is that the control bandwidth is too narrow. Once the structure dynamic properties changes, the control system would need to be retuned. In addition, the passive control need to add non negligible mass to the structure which could be unacceptable in aerospace field.

Active control is developed based on the development of the computer science[20, 21]. The control system need sensors to monitor the displacement or velocity of the structure. The sensed signals then send to a controller (microchip or computer embedded I/O board) in order to obtain a control signal by employing specific algorithms. The control signal would be amplified by power amplifier or directly exert on actuators to generate feedback force on the structure which usually has the opposite phase with the external excitation. Depending on the modern control

³<http://www.aerospaceweb.org/question/planes/q0176.shtml> due to 2011

theories, people can design specific control laws to solve kinds of vibration problems. However, the power consumption would be large and the spill-over could be induced for high frequency control leading to instability.

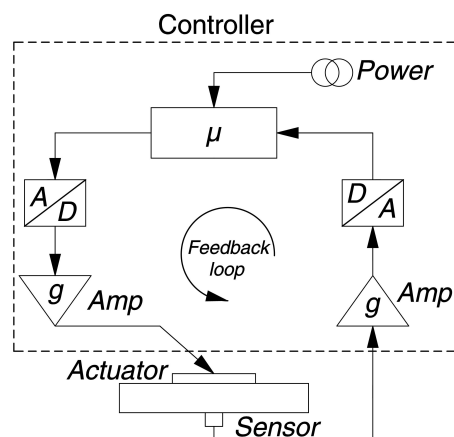


Figure 1.7: Conventional active vibration control.

Semi-active control or semi-passive control possesses partial advantages of both passive and active control. Usually, these control strategies are hysteretic or non-linear in nature. By using small amount of energy, these methods can change the structural dynamic properties by changing the control state thus achieving the damping. The semi-passive and semi-active methods can be distinguished by how we use the *small amount external energy*. The criterion is that if this energy is only used for power-up the control system but not used for inducing the control force, such method can be ranged with semi-passive method. Otherwise, it is a semi-active control. However, the energy used for inducing the control force is very small comparing with conventional active control. Several control systems have been proposed and investigated in the literatures, include active variable stiffness (AVS) in which the stiffness can be switched between high and low values[22], electro-rheological (ER) dampers and magneto-rheological (MR) dampers which damp the structural vibrations by tuning the intensity of electric field or magnetic field with the structural motion[23, 24].

1.2 Smart materials

1.2.1 Common smart materials

The definition of smart material could be depicted as *smart material can sense and respond to the external stimuli in a predictable and useful manner*. These stimuli

could be stress, temperature, electric or magnetic fields, moisture, pH value. For example, shape memory alloy can remember their original shape and cold-forged shape and return to it when heated. Magnetorheological fluid can increase its apparent viscosity when subjected to a magnetic field. The relationship between the stimuli and response of some types smart material are described in Tab. 1.1.

Compared with other smart materials, piezoelectric materials were extensively used in vibration control field due to four reasons. (1) Piezoelectric material is one of crystalline materials which are usually used to produce high performance devices. (2) Piezoelectric material is solid state making it easier to be fixed on the structure. (3) Piezoelectric can transfer the mechanical energy into electrical energy and *vice versa*, it could be used as actuators for either passive or active control. (4) The electrical field is also easy to be generated and controlled compared with other stimuli. We will give a more detailed introduction of piezoelectricity in next section.

1.2.2 Piezoelectricity

Piezoelectricity was firstly discovered in 1880 by Pierre Curie and Jacques Curie, two French physicists who were also brothers. They demonstrated that crystals of tourmaline, quartz, cane sugar and Rochelle salt generate electrical polarization from mechanical stress. They found twenty natural crystal classes exhibit piezoelectricity. One year after the discovery of the piezoelectricity, Gabriel Lippmann predicted the existence of the converse piezoelectricity from the deducing of the fundamental thermodynamic which was soon confirmed by the Curies. Despite these exciting discoveries, they were not used for applications rather than the interests of the physicists until the early twentieth century.

The piezoelectric materials are usually made by polycrystal which has random polar axis inside. In order to generate the piezoelectric effect, the polycrystal is heated firstly in order to give more freedom to the domain of the materials. Meanwhile, a strong electrical field is applied to the polycrystal to align the dipoles in nearly piezoelectric effect after the electrical field is canceled. The procedure can be shown in Fig.1.8

When mechanical stress is acting on the piezoelectric body, which manifests the dipole moments in the materials, an electric field can be observed between the insulated electrodes. This effect is known as direct piezoelectric effect. A ordinary lighter in our daily life comes from this effect. More than 10k volts voltage can be generated when pushing the button. Then the resulting electro spark can

<i>Response</i> \ <i>Stimuli</i>	Electrical	Magnetic	Optical	Thermal	Mechanical
Electrical			Electrochromic Electroluminescent Electro-optic	Thermoelectric	Piezoelectric Electrostrictive ER Fluids
Magnetic			Magneto-optic		MR Fluids
Optical	Photoconductor		Photochromic		
Thermal			Thermochromic Thermoluminescent		Shape memory
Mechanical	Piezoelectric	magnetostrictive	Mechanochromic		Negative poisson ratio

Table 1.1: The relationship between the stimuli and response of some types of smart material.

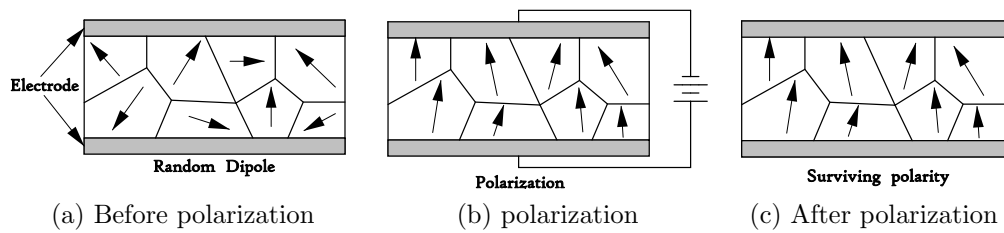
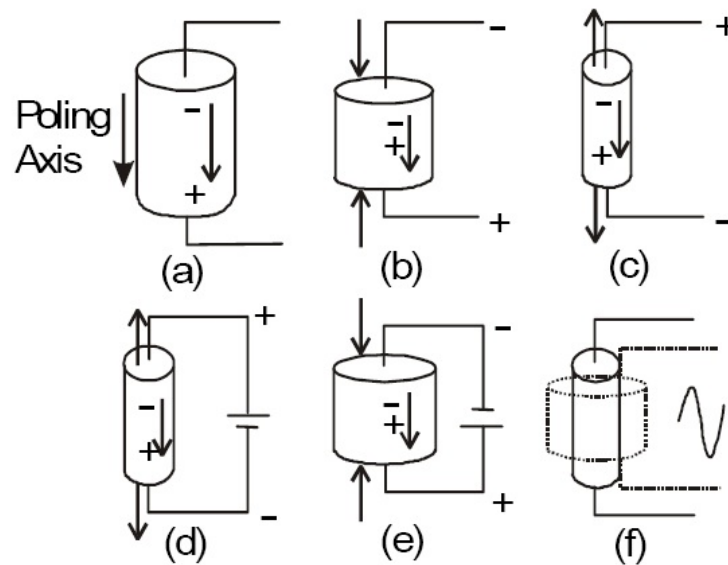


Figure 1.8: polarization of polycrystal materials.

Figure 1.9: Piezoelectric effect.⁴

ignite the gas. In industry field, direct piezoelectric effect is more applied to produce the sensors. Due to its high sensitivity and broad bandwidth sensing, It is applied to many domains such as underwater wave detection, earthquake prediction, loudspeaker production and so on.

On the contrary, the converse piezoelectric effect is that when a voltage is applied on the two piezoelectric electrodes, the material will deform. The ceramic will be expanded if the applied voltage has the same direction with the poling direction and be compressed if this voltage direction is different from it. If the exerting voltage is a AC voltage, the piezoelectric materials will vibrate with the frequency of the AC signal. This effect is utilized for making actuators which relates to vibration control, supersonic engineering, precise motion driving and so on. The piezoelectric effect is shown in Fig.1.9.

⁴<http://www.aurelienr.com/electronique/piezo/piezo.pdf> due to 2011

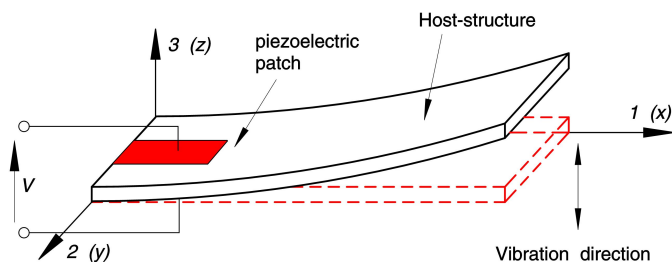


Figure 1.10: piezoelectric patch bonded on a vibrating mechanical structure.

Piezoelectricity results a coupling effect between electricity and mechanics thus the constitutive equation of tensors as shown in Eq. 1.1.

$$\begin{bmatrix} S \\ D \end{bmatrix} = \begin{bmatrix} s^E & d^t \\ d & \varepsilon^T \end{bmatrix} \begin{bmatrix} T \\ E \end{bmatrix} \quad (1.1)$$

where D is the electrical displacement (surface charge density), S is the material engineering strain. E and T are the electrical field in the material (volts/meter) and the material stress(force/area). The matrix $[d]$ and $[d^t]$ represent the direct piezoelectric effect and the converse piezoelectric effect. The parameters ε^T and s^E correspond to the permittivity and the compliance of the piezoelectric material. The superscript E indicates a zero, or constant, electric field. The superscript T indicates a zero, or constant, stress field and the superscript t is transposition of a matrix.

In vibration control, the piezoelectric patch with 3-1 effect ($d = d_{31}$) is usually utilized as the transducers. When structure is vibrating in the direction as shown in Fig.1.10, the piezoelectric patch will strain along the x-axis and the resulting strain S_x will generate a AC voltage between the two electrodes of the patch. In this thesis, the piezoelectric patches are composed of PZT (lead-zirconate titanate) which are fabricated by LGEF laboratory. We also use some PZT patches which are produced by commercial companies like Midé corporation.

1.3 Shunt damping techniques

Piezoelectric shunt damping techniques were an important branch in structure vibration control by smart materials[25]. By connecting an optimized electrical impedance between piezoelectric elements, which are bonded to or embedded in the structure, an obvious damping effect has been observed when the structure vibrates around its natural frequency. These techniques require no feedback sensor

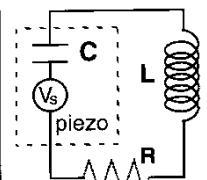
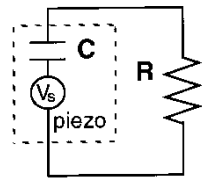
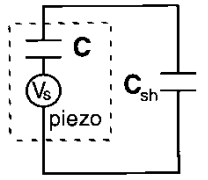
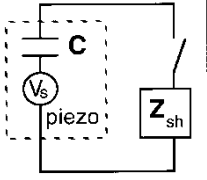
INDUCTIVE	RESISTIVE	CAPACITIVE	SWITCHED
 <p>Resonant (damped) absorber</p>	 <p>Frequency dependent damping</p>	 <p>Frequency dependent stiffness</p>	 <p>Controlled energy transfer</p>
<p>Tuning strategies</p> <ul style="list-style-type: none"> Passive vs synthetic inductors Single vs multimode Active (slow) tuning Circuit topology Effects of: <ul style="list-style-type: none"> structural damping nonlinearities RL-shunted CLD Hybrid active-passive Power efficiency 	<p>Peak damping</p> <p>Frequency dependence tuning distribution</p> <p>Modal strain energy</p> <p>Effects of: <ul style="list-style-type: none"> electrode size local stiffening </p> <p>Damped composites <ul style="list-style-type: none"> particulate fiber-reinforced </p>	<p>Adjust stiffness of part of mechanical vibration absorber</p> <p>Active (slow) tuning</p>	<p>Active (fast) shunting <ul style="list-style-type: none"> rectifier resistance inductance rate </p>

Figure 1.11: Classification of piezoelectric shunt circuits[1].

and only need a few simple electronic components. Some of them are pure passive control methods which get rid of the power source and the stability problems. The preliminary shunt damping technique is proposed by Forward in 1979[26]. In this research, they tried both inductive shunting and active feedback control to damp the structure dynamic response. Their work lay a foundation for the future researches on shunt damping techniques. In 1988, Uchino and Ishii experimentally demonstrated the feasibility of the resistive damping[27].

Starting from the electromechanical coupling effect between structure and bonded piezoelectric elements, Hagood *et.al* systematically analyzed the resistive and inductive shunt damping circuit behaviors[28]. Their works focused on the principles of the shunt circuits and the optimization of the circuit parameters. This remarkable work is significant to the subsequent shunt damping researches.

In a review article, Lesieutre reported on four basic shunt circuits, i.e., inductive, resistive, capacitive and switched circuits as shown in Fig.1.11, and each shunt circuit could give rise to a different mechanical behavior[1]. In the following sections, we will briefly review the developed treatments of these shunt circuits.

1.3.1 Resistive shunt technique

Since a AC voltage appears on the piezoelectric elements, a resistor connected between the terminals of the piezo-elements can dissipate the electrical energy through Joule heat. Hagood and Flotow proved that the damping increased at first, and then decreased if the resistor increased monotonously[28]. The maximum damping value was determined by the electromechanical coupling effect. Lesieutre *et.al* used multi piezoelectric elements and distribute resistors to build piezoelectric shunt damping circuit. They obtained a broadband control ability[29, 30]. Tanimoto *et.al* applied the resistive shunt circuit to damping a composite plate and they gave the optimized resistance value for each controlled mode[31].

1.3.2 Inductive shunt technique

Due to its simplicity and low power cost, the R-L (resistor-inductor) shunt circuit is one of the most researched and it shunts the terminals of piezoelectric elements with serial or parallel resistors and inductors. The oscillation frequency of this circuit (LCR oscillator) is well tuned to the structural eigenvalue frequency in order to get a maximum damping effect. Such method was interpreted in terms of an analogy with tune mass damper (TMD) or passive mechanical vibration absorber (PMVA)[28]. Wu *et.al.* proposed a parallel resistor and inductor circuit to damp a cantilever beam. They pointed out that the structure parameters change or unoptimized inductor choosing would decrease the damping around the natural frequencies[32, 33]. Wu demonstrated that the R-L shunt circuit have the multi-mode control ability. He developed a multimode R-L shunt damping circuit. As shown in Fig.1.12, the circuit contains n branches aiming at controlling n vibrating modes, and each branch have $(n - 1)$ anti-resonant oscillators which play a role as bandwidth filter to prevent the current passing except one target mode component[34]. Then, this technique was successfully applied to damp the vibration also the acoustical response of cut-out panel from an F-15 fighter aircraft, CD-ROM, hard disc drive beam and other structures[2, 35–40].

The optimization for R-L shunt damping technique had also got much attention. Many researches focused on tuning the resistance for the sake of obtaining a flat system transfer function[3, 41, 42]. Fig.1.13 shows a representative system transfer function with different optimized resistances. The bonding placement and profile of the piezoelectric elements were also considered in some researches[39, 43].

The main drawback of the R-L shunt damping technique is huge inductance requirement even up to thousands of henries for low frequency control. In prac-

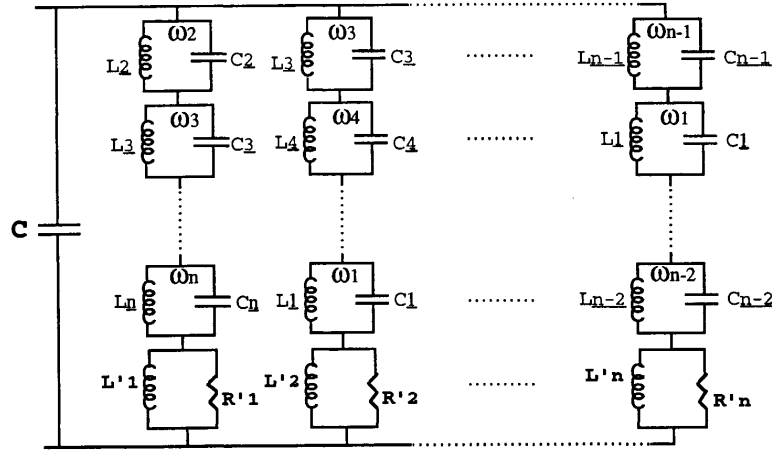


Figure 1.12: Wu's multimode R-L shunt damping circuit[2].

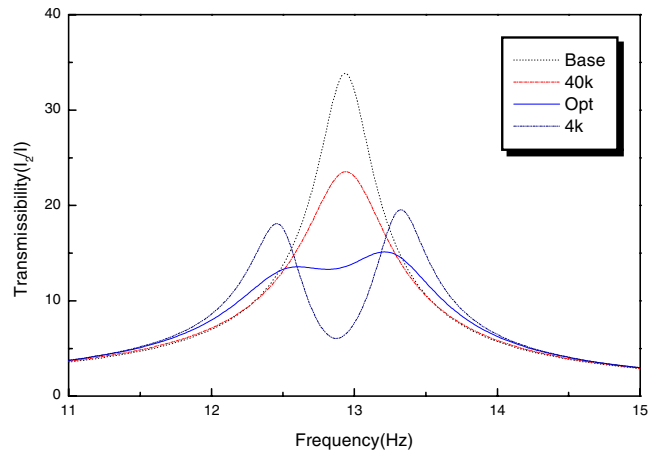


Figure 1.13: Representative optimization of the resistance on R-L shunt damping[3].

tice, discrete inductors are limited in size to around 1 H. Fleming *et.al* advised to place an additional capacitance across the terminals of the PZT in order to decrease the inductance need. However, it could decrease the force generated by the piezoelectric elements[44]. In their another research, a synthetic impedance was developed by a DSP system avoiding to use the inductor component in the circuit[45]. More popular method is called Negative capacitance which run with a similar electrical behavior of an inductor[46]. Moreover, it could be designed as an adaptive one which can trace the structure vibration frequency changes[47, 48]. But these designs need an external power supply, that makes the R-L shunting no longer a passive method.

1.3.3 Capacitive shunt technique

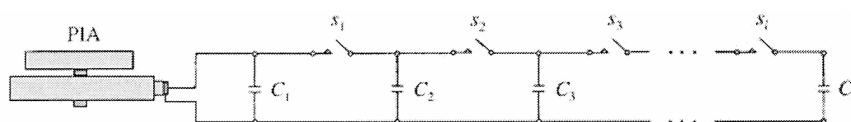


Figure 8. Conceptual "ladder" capacitive shunt circuit.

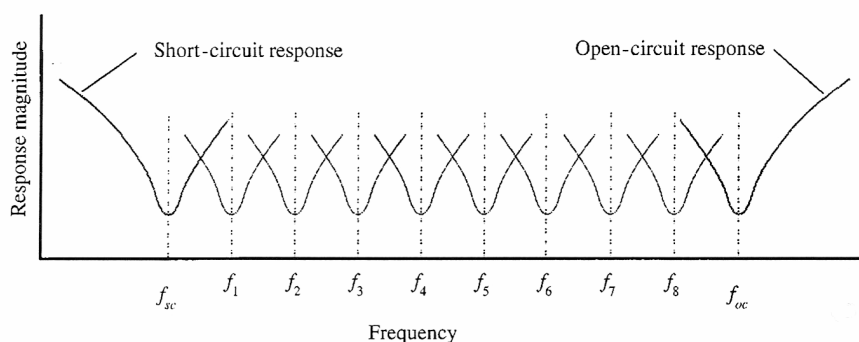


Figure 1.14: Davis' ladder capacitive shunt circuit[4].

Capacitive shunt technique tuned the stiffness of the global system by changing the stiffness of the bonded piezoelectric elements, meanwhile keeping the system damping a constant value. So far, there are several literatures concern this topic[49, 50]. Davis *et.al* tuned the system frequency-response curve by connecting or disconnecting capacitors using switches as shown in Fig.1.14[4]. Thus, the structure response would be low if the excitation frequency was between open-circuit and short-circuit frequency. Kurdila *et.al* used averaging analysis for qualitative and quantitative study of this method. They suggested two control strategies. One is to increase the capacitance by step; another is to alternatively set the capaci-

tance as the optimized values for only open-circuit or short-circuit frequency[51]. Tylikowski applied capacitive shunt technique to suppress the vibration of a ring structure. He pointed out that the precise impedance tuning is critical to the control effect[52].

1.3.4 Switched shunt technique

By intermittently on-off the switches in the circuit, a non-linear voltage will be generated over the piezoelectric elements[53]. In 1994, Larson proposed the state switch conception from the stiffness change of a sound actuator which is made of piezoelectric material[54]. Cunefare *et.al* developed a State Switch Absorber (SSA) which aiming at minimizing the mechanical energy of the system. He also introduced the control law based on the velocity response of the host structure[55]. The most popular switched shunt techniques are called state switch shunt technique and synchronized switch damping techniques.

- *State switch damping technique.* Clark *et.al* proposed the state switch damping technique[56, 57]. In this technique, the switch is close in one-half of the structure vibration period and open in rest of the time. The damping effect can be be ascribed to the stiffness change between the two switch states. He also studied the damping effected by the switch closing duration[58]. As key parameters in a switched shunt circuit, the timing and duration of the switching have also been investigated. It is pointed out that the optimal timing should be at the peak of the vibration cycle for closing and the peak of the next electrical cycle for reopening that makes the state switch technique close to the synchronized switch damping technique. Corr *et.al* explained the enegy dissipation from the angle of the stiffness change. He figured out that the synchronized switching damping can perform better than state switch damping technique[59, 60].
- *Synchronized switch damping techniques.* Synchronized switch damping (SSD) techniques get great attention in the recent years due to its simplicity and decent control ability. We will give a particular review in chapter 2. Moreover, the techniques have been successfully transplanted into the energy harvesting field for power up small electrical devices[8, 61–64].

1.4 Objectives of research topic

The researches introduced in this thesis are developed based on the well-known Synchronized switch damping techniques. SSD techniques have been studied in many literatures. These works cover many aspects like principles, control laws, broadband control also their applications. However, most of these researches only use one patch (group) in the control system. In this thesis, multi patches are bonded on the host structure and they are not connected in series or in parallel as before. With such configuration, we propose a new SSD conception while named as synchronized switch damping with energy transfer (SSDET) technique. In this method, we transfer the energy which comes from the different vibrating modes, between different patches in order to enhance the damping on one particular structure or mode.

The entire thesis is organized as follows. Chapter 2 reviews the published SSD techniques in detail. Chapter 3 presents the principles as well as the control law of the SSDET technique. The mathematical model in time and in frequency domain are established. Simulations are carried out in matlab/simulink environment to verify its feasibility. An enhanced control law based on a voltage threshold is also developed in this chapter. Chapter 4 experimentally demonstrates the SSDET. Three different type experiments are implemented to show that the SSDET can be applied between different structures or modes in one structure. Experimental results also show that it can be adopted for reducing both harmonic and transient response. Chapter 5 introduces a preliminary research on bidirectional SSDET technique. Different connections between two patches are illustrated and dynamic behaviors are researched based on the simulations. Then, the bidirectional SSDET technique and its control law are introduced. Experimental results are compared between several connections. Finally, Chapter 6 concludes the thesis.

Chapter 2

Review of synchronized switch damping techniques

Among kinds of semi-active and semi-passive vibration control methods, Synchronized Switch Damping (SSD) techniques are proved to be an effective treatment. Compared with the passive methods, the system has the immunity against the structure dynamic properties shift due to the environmental change. They are also compact, lightweight which is convenient to apply to specific structure with weight or size restriction. Compared with the active control, SSD control system is very simple to implement and can easily be self-powered from the vibration itself. In these techniques, the switch in the circuit is intermittently switched leading to a non-linear voltage processing. The piezo-force induced by such voltage always shows an opposite sign with the structure velocity which leading the vibration suppression on the structure. Such behavior is similar with the well-known direct velocity feedback control[65, 66].

This chapter reviews the developed SSD techniques in four main aspects. At first, SSD principles are introduced. After that, the energy analysis in SSD techniques are listed. The broadband frequency control attempts of SSD techniques are exhibited which are classified as mode distinguished based approaches and time window based approaches. Finally, the self-powered SSD techniques and Blind Switch Damping (BSD) techniques are briefly introduced.

2.1 SSD techniques principles

SSD technique could be studied analogously to variable-stiffness control which is devised by Onoda in[67]. In his proposed methods, the type II is the most interesting one as shown in Fig.2.1. A secondary stiffness Δk can be added or canceled by a switch. The switching timing can be determined by several control laws such as maximum strain law, maximum amplitude law[67] or maximum energy benefit[5]. In SSD technique, the stiffness of the piezo-elements is different under different electrical boundary. By switching these piezo-elements between different electrical boundary, the mechanical energy is converted as electrical energy and stored on the piezoelectric element itself. The collected energy could be dissipated due to the electric loss or harvested in a battery. However, strictly speaking, SSD technique is not variable stiffness technique. In variable stiffness control, we do not add additional damping into system but only shift the transfer function of the controlled system to avoid resonant. That is we do not extract or dissipate system energy. In SSD technique, the piezoelectric force is always opposite to velocity which shows similar behavior like dry friction. The mechanical energy of the host structure is extracted by SSD technique.

2.1.1 Mathematical model of piezo-element coupled structure

This section presents a general mathematical model of a piezo-structure. The basic equations are introduced to exhibit the electromechanical relations.

The structure coupled with piezoelectric elements is often described by a model with a single degree of freedom as shown in Fig.2.2. Here, m is the structure mass, c is the damping coefficient and k^E is the short-circuit stiffness. Furthermore, F is an external force exerting on the structure, C_0 is the natural capacitance of the piezoelectric elements on the structure, u is the displacement of the structure and V is the voltage between two electrodes of the piezoelectric element. This electromechanical coupling system can generally be formulated according to Eq.(2.1). Here, i is the outgoing current from the piezoelectric elements and α is the force factor related to the piezoelectric material.

$$\begin{cases} m\ddot{u} + c\dot{u} + k^E u = F - \alpha V \\ i = \alpha\dot{u} - C_0\dot{V} \end{cases} \quad (2.1)$$

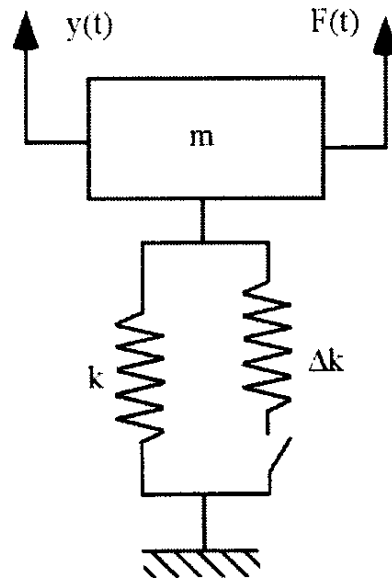


Figure 2.1: Type II mechanical spring[5].

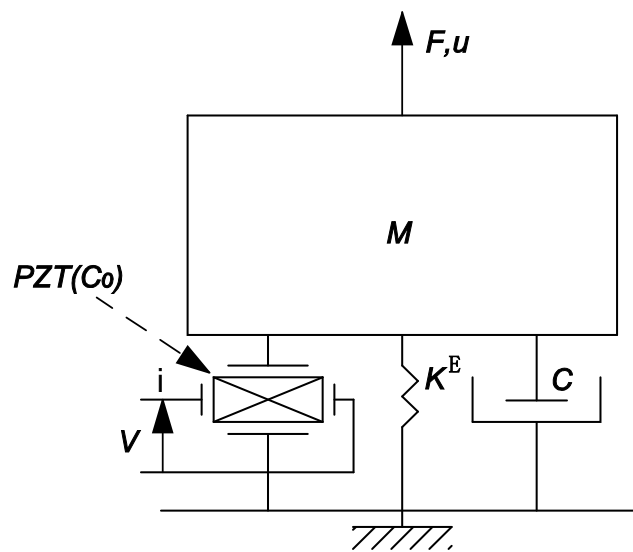


Figure 2.2: An electromechanical model.

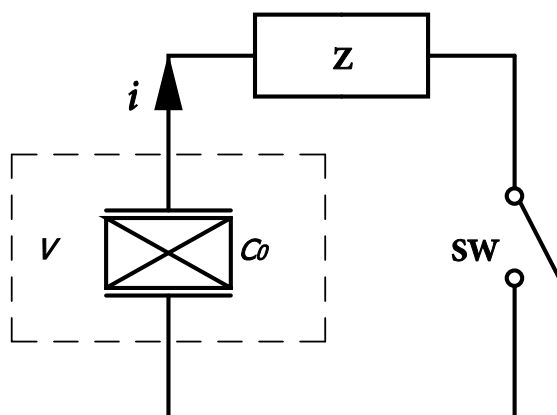


Figure 2.3: A classic circuit for SSD techniques.

The general circuit schema for SSD techniques can be shown in Fig.2.3. The piezoelectric elements with capacitance C_0 are usually bonded on the surface of the structure. The switch is usually achieved by combining MOSFET transistors and diodes. The driving signal consists in pulses with short duration synchronizing with the structure motion. The impedance Z could be a small resistor (SSDS), an inductor(SSDI) or a battery source (SSDV) as discussed in the following sections.

2.1.2 SSDS principles

Synchronized Switch Damping on Short circuit (SSDS) was proposed by Richard *et.al.* in 1999[68]. The circuit of SSDS is very simple which only consists of a wire, a switch and a small resistor as shown in Fig.2.4. Once the structure gets to its extrema (maximum or minimum) of displacement, the switch will be closed for a very short time and then re-opened. That is the circuit is in short circuit. Thus, the electrical charge with different polarities store on the piezoelectric patches surface will be canceled during the closing time and the piezoelectric voltage will return to zero in the closing duration. Fig.2.5 shows the waveforms of the structural displacement and voltage. From this figure, we know that the piezoelectric voltage increases in most of the time which indicates the mechanical energy is extracted from the structure and stored in the piezoelectric elements as electrical energy. Such voltage only drops when the switch is closed. That means the electrical energy is dissipated in the circuit as joule heat. So, the mechanical energy of the vibration finally dissipated in the circuit. It could also be noticed that the voltage always has the same sign with the velocity. Therefore, the induced piezoelectric force which equals to $-\alpha V$ always has the opposite sign with the velocity. That

behavior is like the dry friction effect. This behavior shows a similar manner to the Direct Velocity Feedback[66].

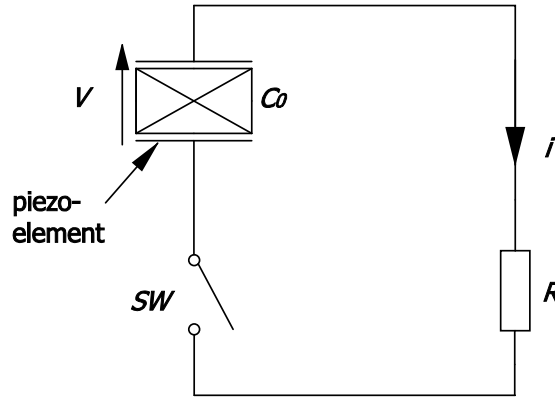


Figure 2.4: SSDS circuit.

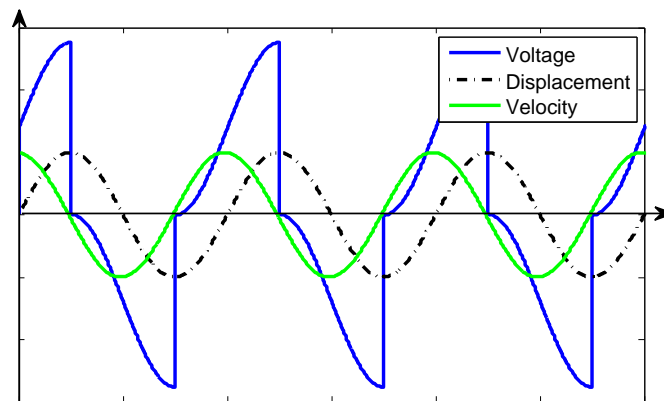


Figure 2.5: SSDS waveforms.

Due to its simplicity, SSDS gets much researchers' attention. Corr and Clark analyzed the energy dissipation of SSDS technique and compared with state switch control technique[59, 69]. They pointed out that SSDS always outperform the state switch technique. Then, they experimentally compared the state switch control, SSDS and the RL resonant shunt by using a aluminum beam. Experiment show that state switch can only obtain 2 dB reduction while that is 12 dB for SSDS and RL shunt. However, the RL shunt circuit needs 2870 times greater inductor than SSDS does[60]. In[70], it is demonstrated that SSDS technique can be achieved by self-sensing method.

2.1.3 SSDI principles

It can be shown that the converted energy is directly related to the voltage jump during the switching. In order to maximizing the damping, Synchronized Switch Damping on Inductor (SSDI) is proposed by Richard *et.al.* in[71]. The electrical circuit of SSDI is shown in Fig.2.6. Compared with SSDS circuit, an additional inductor is added into the circuit. The capacitance C_0 of the piezoelectric elements, the inductance L and the resistance R of the circuit constitute an LCR oscillator. The switch is open at most of the time and just briefly closed at the selected instants. The closing duration t_i is one-half of the electrical oscillation period T . Hence, the voltage V can be inverted during the closing time. Considering that the resistance in the circuit is very small, the closing time t_i could be approximately shown in Eq.(2.2). It can be known smaller inductance L will lead to a smaller t_i . The closing time issue is also discussed in[58] in which it concludes that the switch should be closed on the peak of a vibration cycle and reopen it on the first peak of the electrical cycle for optimal performance. Compared with the passive $R - L$ shunt circuit, the inductance is much smaller. Usually, it is chosen to get an inversion time roughly between 10 and 50 times lower than the shortest mechanical vibration period. The voltage and displacement typical waveforms are shown in Fig.2.7 in the case of sinusoidal excitation. From Fig.2.7, we know that the inversion occurs at the displacement extrema. The amplitude of voltage after inversion is always less than that before inversion which indicates the energy loss during the inversion process. Such loss can be contributed to the resistance of the circuit (switch+inductor+wire) and can be reflected by an electrical quality factor Q_i which is defined in Eq.(2.3). The before-after voltage relation can be presented by using this quality factor which is given by Eq.(2.4). An inversion factor γ which is given by Eq.(2.5), can be defined as the ratio of the before-after voltage inversion.

Under such definition, the inversion factor of SSDS γ_{SSDS} will be zero. In SSD techniques, it has been demonstrated that the damping is particularly up to the inversion factor[72]. Larger inversion factor usually leads to better damping effect. Hence, SSDI can perform a better control performance than that of SSDS. SSDI got researched in many literatures[6, 73–79]. In[75], SSDI control is compared with one kind of active control. Though the active control show a better damping than SSDI, the authors suggest that the SSDI is better choice for single mode control considering the tradeoff between control performance and system complexity. In[6, 75, 77], SSDI is adopted to control the vibration of a ten-bay truss structure as

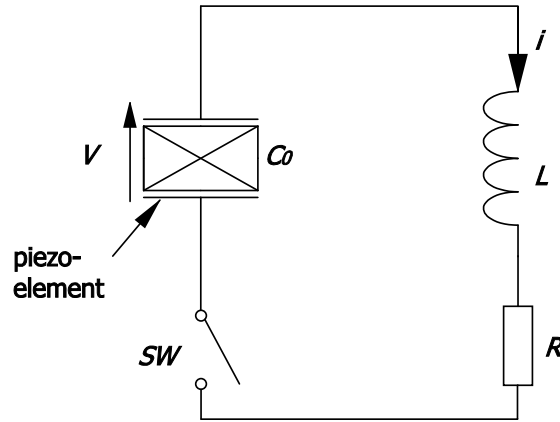


Figure 2.6: SSDI circuit.

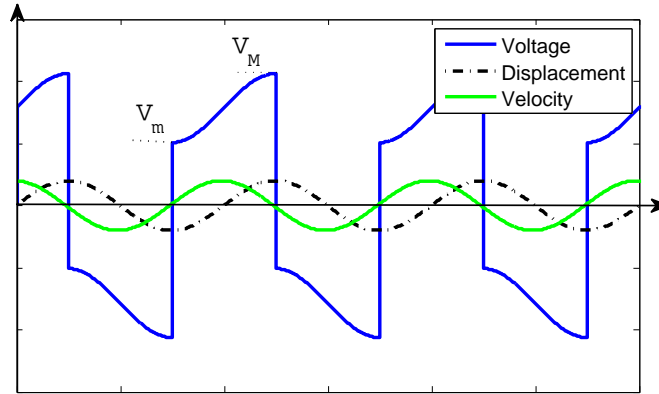


Figure 2.7: SSDI waveforms.

shown in Fig.2.8. Results proved that SSDI is an effective, robust and low-energy-consumed vibration control method, and it could be also self-sensing.

$$t_i = \frac{T_{LCR}}{2} \approx \pi \sqrt{LC_0} \quad (2.2)$$

$$Q_i = \frac{1}{R} \sqrt{\frac{L}{C_0}} \quad (2.3)$$

$$V_m = V_M e^{-\frac{\pi}{2Q_i}} \quad (2.4)$$

$$\gamma = \frac{V_m}{V_M} = e^{-\frac{\pi}{2Q_i}} \quad (2.5)$$

2.1.4 SSDV and adaptive SSDV principles

As we know, the voltage amplitude in SSD techniques is significant. Synchronized Switch Damping on Voltage source (SSDV) technique is proposed to artificially

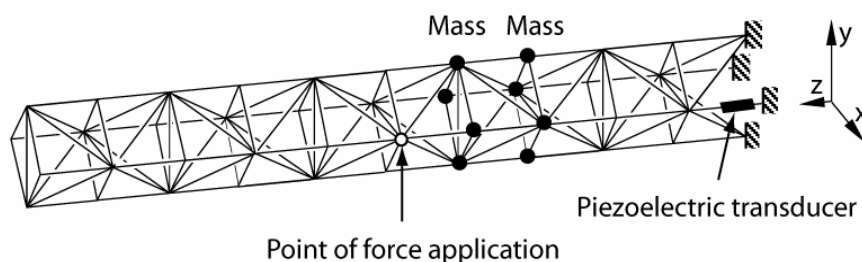


Figure 2.8: Ten-bay truss structure with piezoelectric transducers[6].

enhance such voltage especially for systems with low electromechanical coupling. This section introduces the original SSDV which uses a constant voltage source in the circuit. SSDV with an adaptive voltage source techniques which possess better stability than original one, are reviewed as well.

- Original SSDV

SSDV circuit is similar with the that of SSDI but adding an addition voltage source in series as shown in Fig.2.9. The role of these additional constant voltage sources, having respectively a $+V_{cc}$ and a $-V_{cc}$ value, is to increase the voltage amplitude of V , thus increasing the damping effect[80, 81]. The control strategy of the switches is to alternatively close the SW_1 or SW_2 when the maximum or minimum displacement u occurs. The switch closing duration is totally same with that in SSDI technique which is given in Eq.(2.2). The typical SSDV waveforms are plotted in Fig.2.10. These waveforms also show a similarity with SSDI but with a higher inversion factor due to the additional energy source. Here, the inversion factor has the same definition with Eq.(2.5). The relationship between voltages before-and-after inversion V_m and V_M can be expressed as Eq.(2.6).

$$(V_m - V_{cc}) = \gamma(V_M + V_{cc}) \quad (2.6)$$

- SSDV on adaptive voltage source

In the original SSDV, the sign of the continuous voltage source changes with the structural speed direction that increases the piezo-voltage during the inversion process. However, it would lead stability problems. Since the absolute value of the voltage source is constant, which images the force induced by this voltage is also constant. It could excite the structure when the structural vibration level is low instead of suppressing the vibration. Badel *et.al* developed an enhanced SSDV so called SSDV on adaptive voltage source[7]. The

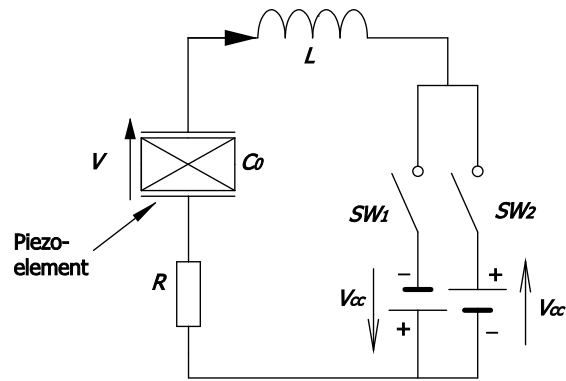


Figure 2.9: SSDV circuit.

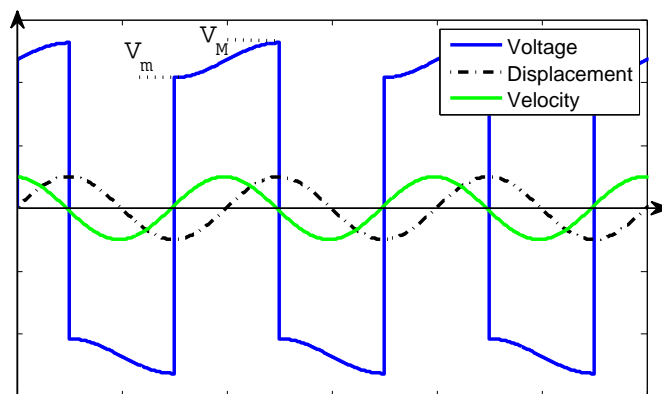


Figure 2.10: SSDV waveforms.

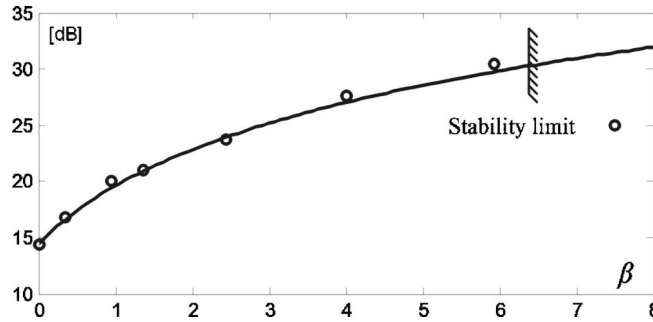


Figure 2.11: SSDV damping absolute value versus proportional coefficient[7].

applied voltage is automatically adjusted by the controller proportionally with the structure deflection. The proportional coefficient β is empirically set by users. This coefficient can not set too large, otherwise instability would occur as shown in Fig.2.11. Ji *et.al.* employed LMS algorithm to find the same coefficient as mention above. However, the system would become definitely complex[82]. Lallart *et.al.* systematically analyzed the stability of SSDV and SSDV on adaptive voltage source[72]. They pointed out that the unstable phenomenon happened in experimental would be induced by the delay of the switching. For SSDV on adaptive voltage source, the system can always be stable as long as the margin modulus is less than a certain value which shows good agreement with the research[7].

2.2 Energy analysis and transfer functions

2.2.1 General energy analysis

The mechanical property of the piezo-elements coupled 1-D structure can be written in Eq.(2.7). If multiplying both terms by the velocity \dot{u} and integrating over the time variable leads to the following energy Eq.(2.8):

$$m\ddot{u} + c\dot{u} + k^E u = F - \alpha V \quad (2.7)$$

$$\int m\ddot{u}\dot{u}dt + \int c\dot{u}^2dt + \int k^E u\dot{u}dt + \int \alpha V\dot{u}dt = \int F\dot{u}dt \quad (2.8)$$

Considering only the steady state, integration over a finite number of periods gives:

$$\left[\frac{1}{2} m \dot{u}^2 \right]_0^T + \left[\frac{1}{2} k^E u^2 \right]_0^T + \int_0^T c \dot{u}^2 dt + \int_0^T \alpha V \dot{u} dt = \int_0^T F \dot{u} dt \quad (2.9)$$

If we consider the initial conditions of the displacement u and velocity \dot{u} are zero, then the Eq. (2.9) becomes:

$$\frac{1}{2} m \dot{u}^2 + \frac{1}{2} k^E u^2 + \int_0^T c \dot{u}^2 dt + \int_0^T \alpha V \dot{u} dt = \int_0^T F \dot{u} dt \quad (2.10)$$

Eq.(2.10) shows that the provided energy is distributed into the kinetic energy and potential elastic energy of the structure, the structural damping loss and the extracted energy. These terms are listed in Tab.2.1. The vibration control of SSD techniques is reflected as the *extracted energy* part which is firstly extracted from the structural mechanical energy and transferred as electrical energy stored on the capacitor, and finally dissipated in the circuit by joule heat. Thus, greater extracted energy certainly brings better control ability. This energy can be expressed as the following integral function of voltage V and displacement u shown in Eq.(2.11). Due to

$$\int \alpha V \dot{u} dt = \int \alpha V du \quad (2.11)$$

Considering the harmonic motion of the structure, the extracted energy can be plotted as the cycle shown in Fig.2.12. It is clear that the voltage inversions occurs at the displacement extrema moment. Since the inversion time is very short comparing with mechanical period, the structure can hold at its position (the displacement variation is zero) in this duration. In the open circuit, the voltage variations are proportional to the displacement with a factor α/C_0 . The circumscribed surface by this cycle is the extracted energy with a factor $1/\alpha$ in one mechanical period. The surface can also be expressed as Eq.(2.12). Enlarging the surface means that more energy is extracted from the structure which can be achieved by increasing the voltage.

The extracted energy in one period of SSDS, SSDI and SSDV are listed in Tab.2.2 and plotted in Fig.2.13. It shows that SSDV possesses the largest area which images the best damping effect. Due to the larger inversion factor, SSDI can perform better control ability than SSDS (the inversion factor of SSDS is zero). If the switch is open all the time, the area surrounded by hysteresis loop of the voltage is null, which indicates the extracted energy from SSD is zero. However,

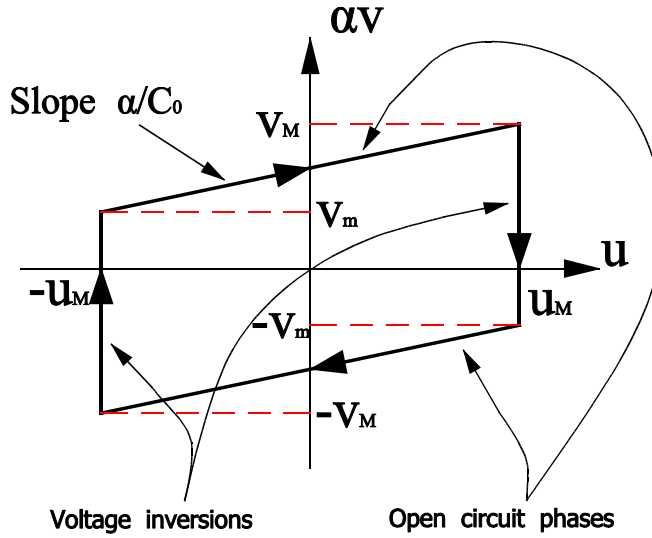


Figure 2.12: Extracted energy cycle.

it should be also pointed that though SSDV shows the best control performance, it consumes more energy than SSDI or SSDV in which the external energy is only used to control the switches state. Moreover, the force induced by the energy source is directly exerted on the structure which potentially brings the instability. As the matter of fact, SSDV could loses its stability if the voltage source has a high voltage output.

$$\int_{period} \alpha V du = 2\alpha u_M (V_M + V_m) \quad (2.12)$$

Table 2.1: Energy terms.

$\int_0^T F \dot{u} dt$	Provided energy
$\frac{1}{2} m \dot{u}^2$	Kinetic energy
$\frac{1}{2} k^E u^2$	Potential elastic energy
$\int_0^T c \dot{u}^2 dt$	Structural damping loss
$\int_0^T \alpha V \dot{u} dt$	Extracted energy

2.2.2 Transfer functions of SSD approaches

open circuit

Without control, the electrical circuit is in open circuit condition ($i = 0$), thus

Table 2.2: Extracted energy with different SSD techniques.

E_{ssds}	$4 \frac{\alpha^2}{C_0} u_M^2$
E_{ssdi}	$4 \frac{\alpha^2}{C_0} \cdot \frac{1+e^{-\pi/2Q_i}}{1-e^{-\pi/2Q_i}} u_M^2$
E_{ssdv}	$(4 \frac{\alpha^2}{C_0} u_M^2 + 4\alpha u_M V_{cc}) \cdot \frac{1+e^{-\pi/2Q_i}}{1-e^{-\pi/2Q_i}}$

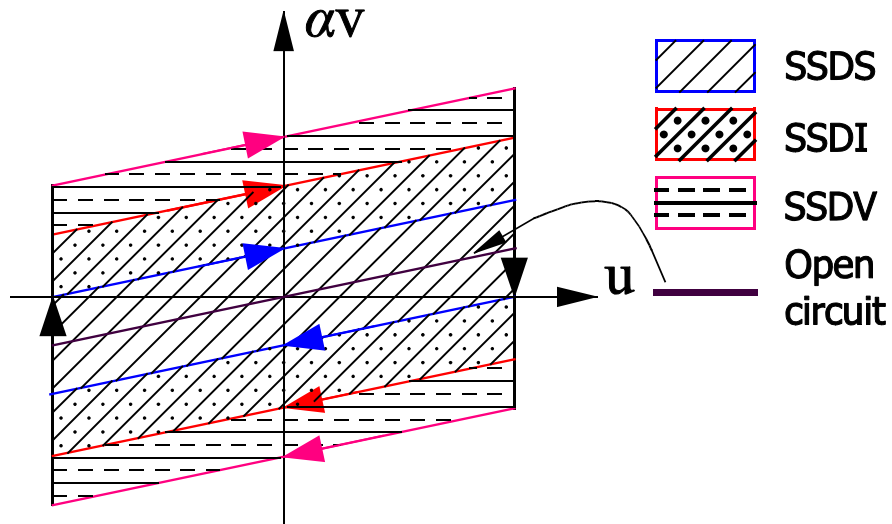


Figure 2.13: Extracted energy cycle for SSD techniques.

yield Eq.(2.13)

$$V = \frac{\alpha}{C_0}u \quad (2.13)$$

Inserting Eq.(2.13) into Eq.(2.1) leads to:

$$m\ddot{u} + c\dot{u} + k^E u = F - \frac{\alpha^2}{C_0}u \quad (2.14)$$

Eq.(2.1) can be written by using the open circuit stiffness k^D which is described in Eq.(2.16) :

$$m\ddot{u} + c\dot{u} + k^D u = F \quad (2.15)$$

$$k^D = k^E + \frac{\alpha^2}{C_0} \quad (2.16)$$

Thus, the transfer function of the uncontrolled system can be expressed in Eq.(2.17) by Fourier transformation. If the structure vibrates under its open-circuit resonant frequency $\omega_0^D = \sqrt{k^D/m}$, then the transfer function becomes Eq.(2.18)

$$\left(\frac{\tilde{u}}{\tilde{F}}\right)_{without} = \frac{1}{-m\omega^2 + jc\omega + k^D} \quad (2.17)$$

$$\left(\frac{\tilde{u}}{\tilde{F}}\right)_{without} = \frac{1}{jc\omega_0} \quad (2.18)$$

With SSD techniques

The dynamic behavior of the piezo-coupled structure can be written as Eq.(2.19). The V is the voltage between piezoelectric elements electrical poles and it can be expressed as the sum of a sinusoidal signal and a piecewise function as Eq.(2.20). The amplitude of the piecewise function in different SSD techniques can be shown in Tab.2.3. By inserting V into Eq.(2.19) and transferring it to the Laplace domain, the transfer function of SSD techniques can be obtained. Assuming the external force is constant, SSD damping thus can be derived by comparing with the Eq.(2.18) as shown in Tab.2.4. Readers can refer to[7] for more information about the derivation.

$$m\ddot{u} + c\dot{u} + k^E u = F - \alpha V \quad (2.19)$$

$$V = \frac{\alpha}{C_0}(u + h) \quad (2.20)$$

Technique	h value
SSDS	$u_M \text{sign}(\dot{u})$
SSDI	$u_M \frac{1+\gamma}{1-\gamma} \text{sign}(\dot{u})$
SSDV	$(u_M + \frac{C_0}{\alpha} V_{cc}) \frac{1+\gamma}{1-\gamma} \text{sign}(\dot{u})$
Adaptive SSDV	$u_M(1 + \beta) \frac{1+\gamma}{1-\gamma} \text{sign}(\dot{u})$

Table 2.3: h definitions in SSD techniques.

Technique	Inversion factor γ	Source voltage V_{cc}	Damping coefficient
SSDS	0	0	$\frac{c\omega_0}{c\omega_0 + \frac{4\alpha^2}{\pi C_0}}$
SSDI	γ	0	$\frac{c\omega_0}{c\omega_0 + \frac{4\alpha^2}{\pi C_0} \frac{1+\gamma}{1-\gamma}}$
SSDV	γ	V_{cc}	$\frac{c\omega_0}{c\omega_0 + \frac{4\alpha^2}{\pi C_0} \frac{1+\gamma}{1-\gamma}} \times \left(1 - \frac{4}{\pi} \frac{1+\gamma}{1-\gamma} \frac{\alpha V_{cc}}{F_M}\right)$
Adaptive SSDV	$\frac{(1+\beta)(1+\gamma)-1}{(1+\beta)(1-\gamma)+1-\gamma}$	βV_{cc}	$\frac{c\omega_0}{c\omega_0 + \frac{4\alpha^2}{\pi C_0} \frac{(1+\beta)(1+\gamma)}{(1-\gamma)}}$

Table 2.4: SSD techniques damping effect[18].

2.3 Broadband and multimode control of SSD techniques

During the early research stage, SSD techniques usually deal with the monomodal vibration case. However, researchers' put more and more attention to the multimode vibration control in the recent years.

2.3.1 Mathematical model of multimode SSD techniques

In the model of the multimode vibration control, the structure properties are usually represented by model coordinate. Guyomar *et.al.* built a multimode model for a Euler-Bernoulli beam[8]. The schema of the beam is shown in Fig.2.14 and

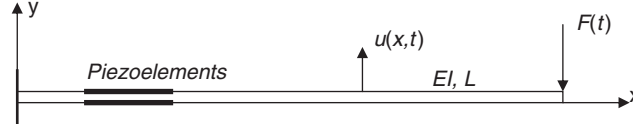


Figure 2.14: Schematic diagram of cantilever beam. $u(x, t)$ is the beam deflection along the transverse direction (y) and $F(t)$ is the excitation force at the tip of the beam ($x = L$) [8].

the corresponding governing equation is given in Eq.(2.21). $E\bar{I}$ is the flexural rigidity of the beam. ρ , c and $F(t)$ are the mass, damping coefficient and external force per unit length. Then, this model can be discretized by the modal function $\varphi(x)$ into the interested modes as Eq.(2.21). Here, the Q_i is the generalized forces and q_i is the displacement of the i th mode. Since the Q_i can be expressed by the sum of the excitation force and the piezoelectric force, Eq.(2.21) can be written as Eq.(2.23). The global current I can be also presented by the modal displacement as Eq.(2.24).

$$\rho \frac{\partial^2 u(x, t)}{\partial t^2} + c \frac{\partial u(x, t)}{\partial t} + \frac{\partial^2}{\partial x^2} \left[E\bar{I} \frac{\partial^2 u(x, t)}{\partial x^2} \right] = f(x, t) \quad (2.21)$$

$$\ddot{q}_i + 2\zeta_i \omega_i \dot{q}_i + \omega_i^2 q_i = \frac{\bar{Q}_i}{M_i} \quad (2.22)$$

$$\ddot{q}_i + 2\zeta_i \omega_i \dot{q}_i + \omega_i^2 q_i = \frac{1}{M_i} f_i(t) - \frac{\alpha_i}{M_i} v_i(t) \quad (2.23)$$

$$I = \sum_{i=1}^N \alpha_i \dot{q}_i \varphi_i - C_0 \dot{v} \quad (2.24)$$

Ciminello *et.al.* developed a multimode SSD model by using Finite Element Method (FEM) [83]. In this research, they extracted the mass, damping and stiffness matrix from a commercial software. The PZT mass, damping and stiffness matrix are obtained by its constitutive relation. By adding or dropping the PZT matrix from the global matrix synchronizing with the structural motion, the simulation for SSDI technique can be achieved. Badel *et. al.* investigated both FEM

and simple lumped model for SSD techniques. They compared the simulation results between these two methods. It reveals that the simple lumped model shows good agreement with the FEM model while possessing 100 times faster speed calculation than FEM[84].

2.3.2 Original SSD broadband control

At first, SSD techniques designed for single mode control was directly used to suppress the motion under broadband excitation. In research[80], SSDI is used to control the vibration of a steel cantilever beam. The switching occurred at each extrema which leads to 9dB and 12dB to the the first two bending modes. Then, the identical control method is applied to a four edge clamped plate. The results show that six modes which distributed between 190Hz to 280Hz, are suppressed at least 20%. The results are also compared with the tradition $L - R$ resonant shunt circuit which only works in four modes. Ciminello *et.al.* established a FEM model to verify the broadband control ability of SSD techniques, and the experiment also successfully damped the first eight modes by using 6 PZT inserts[85]. Guyomar *et.al.* introduced these techniques to reduce the acoustic transmission. One of their attempt is to adopt SSDI and SSDV to suppress the sound transmission in an acoustic box shown in Fig.2.15[9]. It shows that sound pressure is weaken at selected five resonant modes. In addition, the electromechanical coupling coefficient variation with different piezoelement's size (thickness, width and length) are considered. Their another try is to attenuate both the sound transmission and reflection in a brass pulse tube with a separator wall shown in Fig.2.16[10]. Experiments show an apparent control effect for both two modes. Meanwhile, simulations show a good agreement with the experimental results. A similar work is implemented by Faiz *et.al.* also demonstrates SSD effectiveness for wave transmission reduction[86].

As we know, SSD techniques need to detect the extrema of the sensed displacement or piezovoltage to determine the closing instant. It had been demonstrated that the switching at each extrema of structural displacement is the most effective for single mode control, but it is no longer the optimal algorithm for the multimode vibration control. Multimode vibration generates plenty of extrema in the displacement signal. If switching occurs at every extrema, highest mode will be privileged (since the detected extrema are mainly caused by the highest mode), while degenerating the control effect on the lower mode which usually has larger vibration amplitude. Several methods listed below are developed to refine SSD

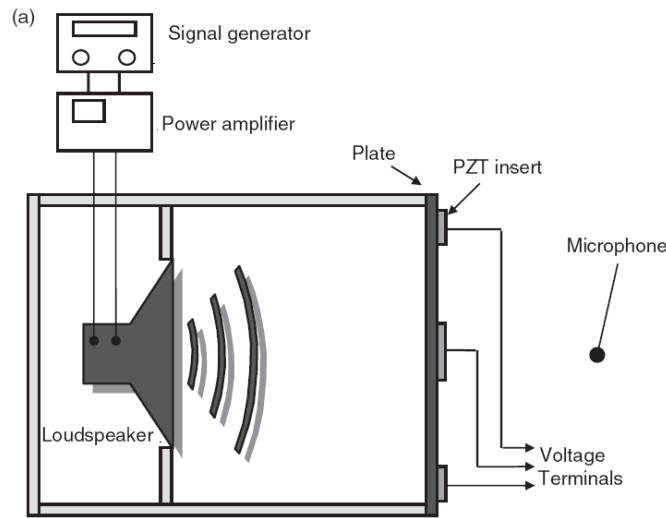


Figure 2.15: An acoustic box with SSD control[9].

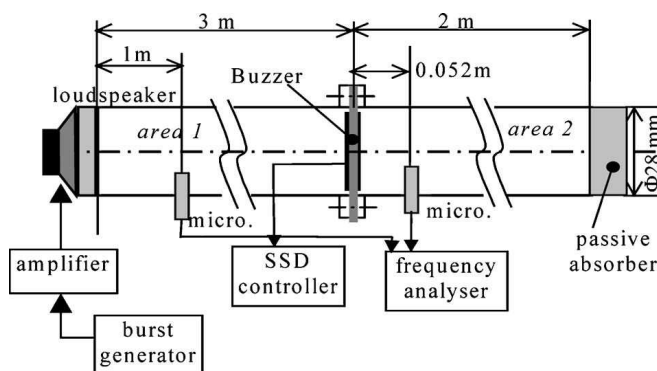


Figure 2.16: A brass pulse tube with a separator wall consisting of a piezoelectric buzzer driven by SSD control board[10].

application for lower mode control in the multimode vibration. They could be classified as two catalogues: mode distinguish based approaches and time window based approaches.

2.3.3 Mode distinguishing based multimode control

For multimode vibration, the sampled signals usually consists of the information from different modes. Mode distinguish based approaches are used to separate this signal into several components in which contains only single mode information. Corr and Clark firstly proposed to use a numerical filter to distinguish the each mode in the sensed hybrid frequency signal. The control schema is shown in Fig.2.17. The switching can be assigned at the selected control mode. However,

numerical filter inevitably generates a time lag between the input and output signals. The time lag depends on the order of the filter as well as the filtering algorithm. Consequently, the switching will occur later than the exact extrema instant decreasing the control effect. Meanwhile, the energy consumption of the filter is also a drawback to such a semi-passive control.

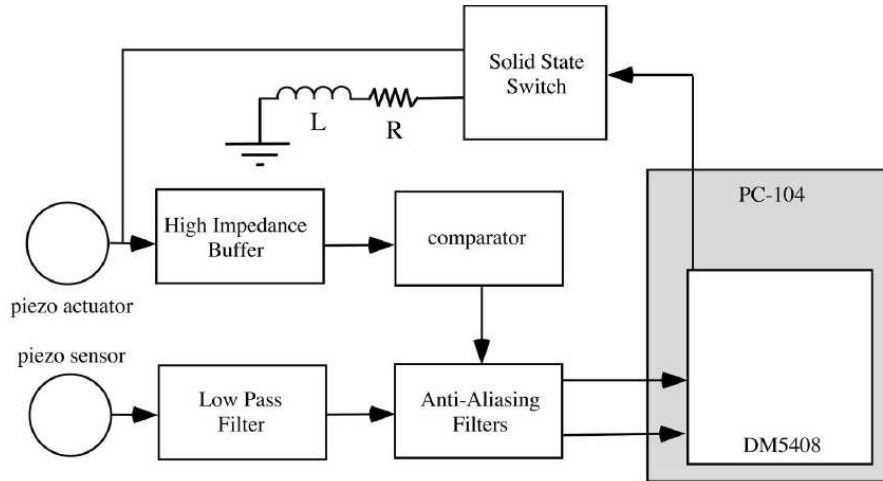


Figure 2.17: Multimode control schema with numerical filter[11].

Harari *et.al.* proposed to use modal observer to select the desired modes[87]. The propose of modal observer is similar with numerical filter, that is to distinguish each mode from the global motion. In their research, the modal observer is built by the mechanical parameters from FE model. Then, the modal displacements can be calculated by the observer to detect its extrema. Since only one mode can be selected as the target, the damping for the rest modes are not optimal. The further researches found that even the switching occurs at the extrema of the distinguish mode, it may still not be the optimal control for the target mode[88]. A $SSDI_{max}$ is then developed with an enhanced switching law for a bimodal vibration control[12, 87, 89, 90] aiming at dissipated more energy of the structure. In this approach, the modal observer remains for obtaining the modal displacement firstly, then the switching does not occur at the exact extrema but with little time shift which ranges $[-\frac{T_2}{2}, \frac{T_2}{2}]$ around the extrema, where T_2 is the period of the higher mode. The waveforms under this control is illustrated in Fig.2.18. Switching will occur in the gray period at the extrema of the higher mode which has the same sign with the lower mode exterma (both maximum or minimum instant). By doing so, the voltage will be enhanced by using the vibration energy of the higher mode. Experiments also show more structural energy can be dissipated by utilizing the proposed control law. But it should be pointed out that the switching is not

synchronized with neither lower mode motion nor higher mode motion, which leads to a tradeoff between the voltage and the control effect. The energy and frequency ratio of the neighboring mode could also play an important role in this method. Moreover, the modal observer should have a fast running performance to give the modal displacement. Otherwise, it will have the same problems with numerical filter such as time delay of the switching.

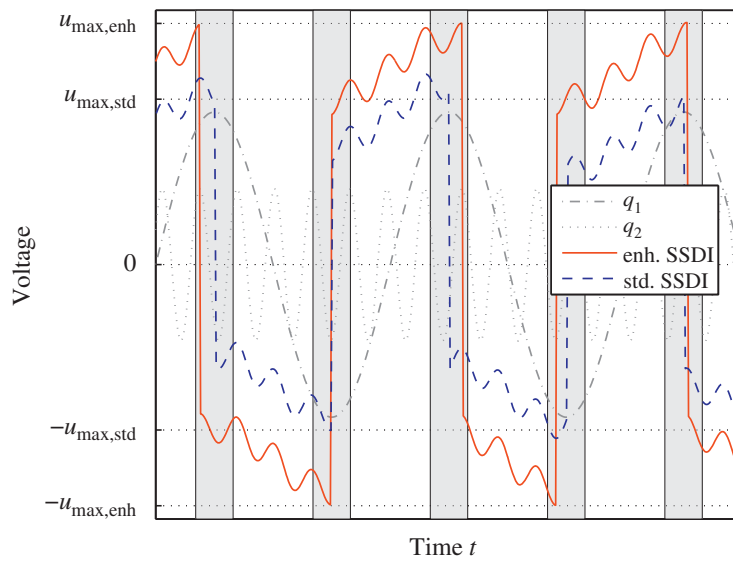


Figure 2.18: Waveforms under enhanced switching law[12].

2.3.4 Time window based SSD multimode control

Time window based SSD approaches aim at optimizing the dissipated energy in the circuit without taking into account any information related to the different modes to the structures. A fixed length time window is generally needed to evaluate the voltage threshold for the forthcoming switching. Guyomar and Badel proposed an efficient probabilistic approach to get the voltage threshold[10]. In their research, the dissipated energy in a fixed time regime can be expressed as Eq.(2.25). Where, the subscript k is the switching times and V_k is the voltage before the k^{th} switching. The employed approach is to maximize the Eq.(2.25) so as to reach an optimal global control effect. The structural displacement of piezovoltage in the past time (in the window) are used to estimate the future piezovoltage by a cumulative distribution function as shown in Fig.2.19. If the voltage exceeds the statistically probable value, the switching will be triggered once $\frac{\partial u}{\partial t} = 0$. Simulations are carried out to verify the approach. In a following research, they employed several statistic

algorithms for example average value and standard deviation or root mean square value to calculate the threshold[13]. The authors also discussed about the effect of the window length. When the length is too short, the control would not be sensitive to the lower mode because the their extrema may not include into the window. Conversely, if it is too long, this would induce delays in the control which would decrease its frequency band. The comparison between different algorithms are illustrated in Fig.2.20

$$\int_0^t V I dt = \frac{1}{2} C_0 \sum_k V_k^2 (1 - \gamma^2) \tag{2.25}$$

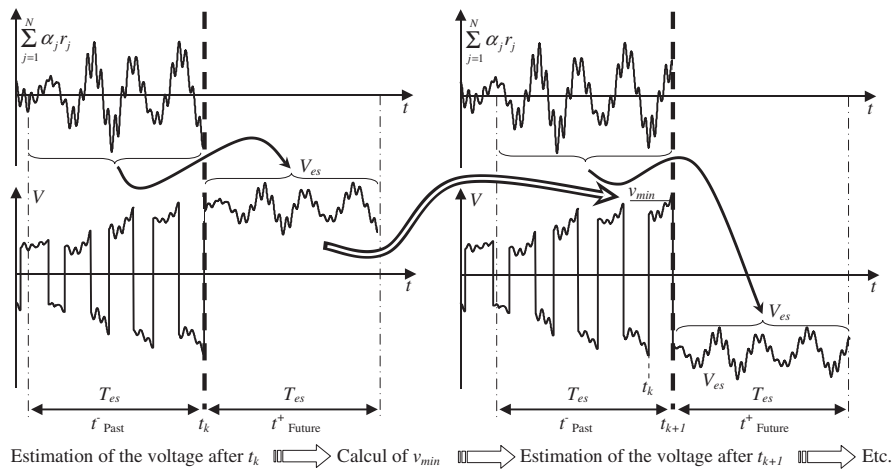


Figure 2.19: Estimation of the piezoelectric voltage after an inversion process[10].

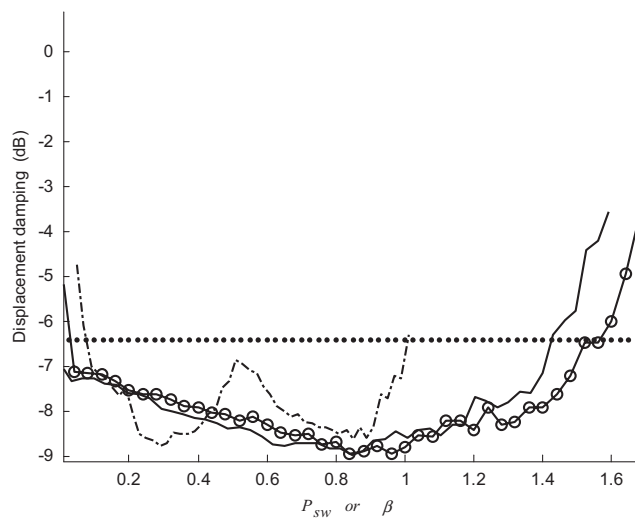


Figure 2.20: Vibration control effect with different algorithm[13].

Ji *et. al.* did a similar work as that mentioned above[91]. They recorded the absolute value of the displacement at the latest 10 switching instants. The mean value multiplied by an adjustment coefficient is then set as the threshold. Switch is triggered only when the structural displacement exceeds this threshold while a local extreme is respected. His another attempt is to maximize converted energy which is shown in Eq.(2.26)[92]. Thus, the problem can be summarized as to find out the largest distance difference of the neighboring switching. These approaches perform well in the experiments. However, the algorithms mainly privilege the lower mode since the largest displacement difference usually occurs around the displacement extreme of the lowest mode motion.

$$\int_0^T \alpha V_{SW} du = \frac{1 + \gamma}{1 - \gamma} \frac{\alpha^2}{2C_0} 2n |\Delta u_j|^2 \quad (2.26)$$

2.4 A brief introduction for self-powered SSD techniques and blind switch damping techniques

2.4.1 Self-powered SSD technique

In this section, self-powered techniques in SSD techniques are briefly introduced. The ultimate goal of SSD techniques should be a low cost and self-powered system. Most of the current researches still use external rigs such as DSP or microcontroller to implement peak detection and switching. In order to achieve real self-powered goal, some preliminary researches have been done by smart circuit design. Niederberger *et.al.* designed an autonomous shunt circuit which performs SSDI without any power supply[14]. This circuit schema is shown in Fig.2.21. The switching is achieved as follows. The sensor charges a capacitor whose capacitance is smaller than the sensor. If the voltage absolute value of the damping insert is larger than that of the small capacitor, the switching is trigger due to the MOSFET physical property. Since two piezoelectric elements are collocated, their voltage amplitude will show almost the same value which ensure the switching occurs at the instant close to the exact extrema. Richard *et.al.* proposed another self-powered SSD schema in which the sensor is needless[15]. The control block diagram is shown in Fig.2.22. An envelope detector is embedded in the circuit which can be powered up by the damping patch. The switching is trigger once the input voltage is less than the envelope value. This technique switches at all local extrema decreasing

its multimode control performance. Lallart *et.al.* improved this method by using two voltage envelope detectors with different time constants as shown in Fig.2.23. The detector with larger time constant works like a threshold mentioned in[91] and it is used to active the detector with smaller time constant. Such a circuit only picks the global extrema so as to get a global control propose.

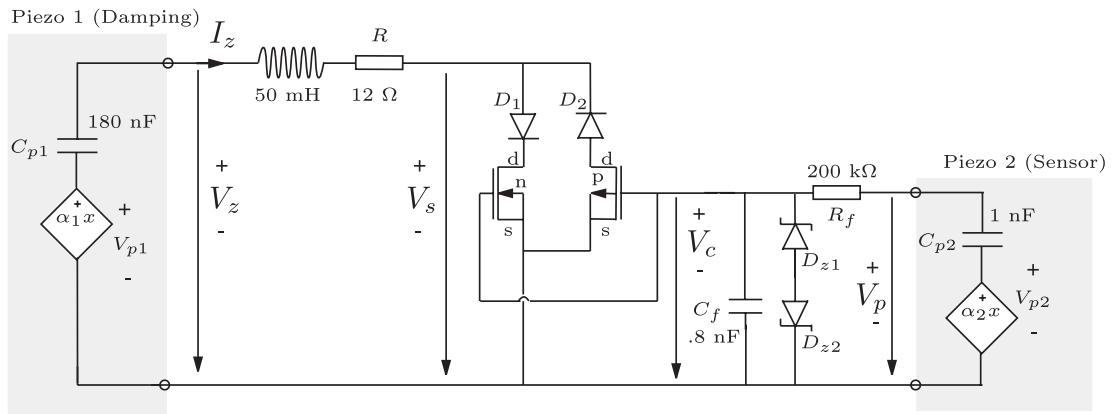


Figure 2.21: Sketch of the autonomous shunt circuit that does not require power for operation[14].

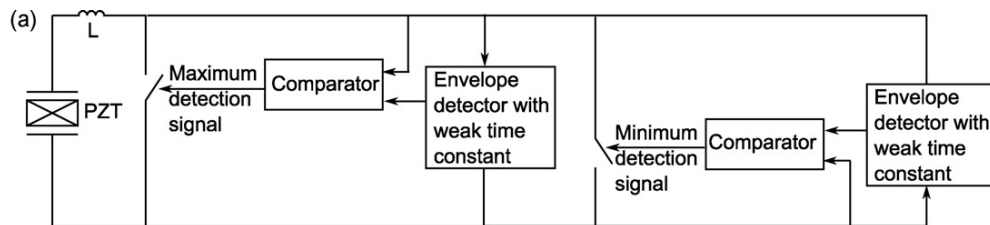


Figure 2.22: Self-powered SSDI control block diagram[15].

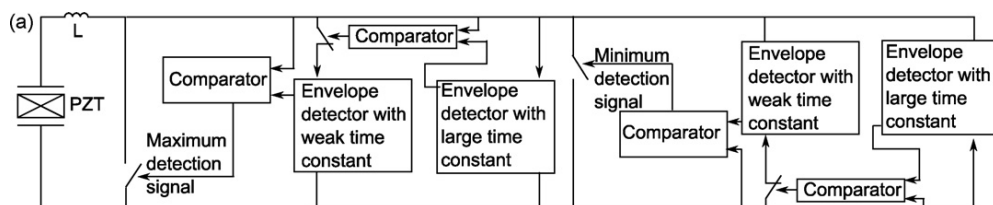


Figure 2.23: Self-powered adaptive SSDI control block diagram[15].

Shen *et. al.* proposed a low-power circuit for SSDV version in[16, 63]. In this research, two structures are used to verify this technique. One is used to harvest energy and another is the structure need to be damped. A low power circuit shown

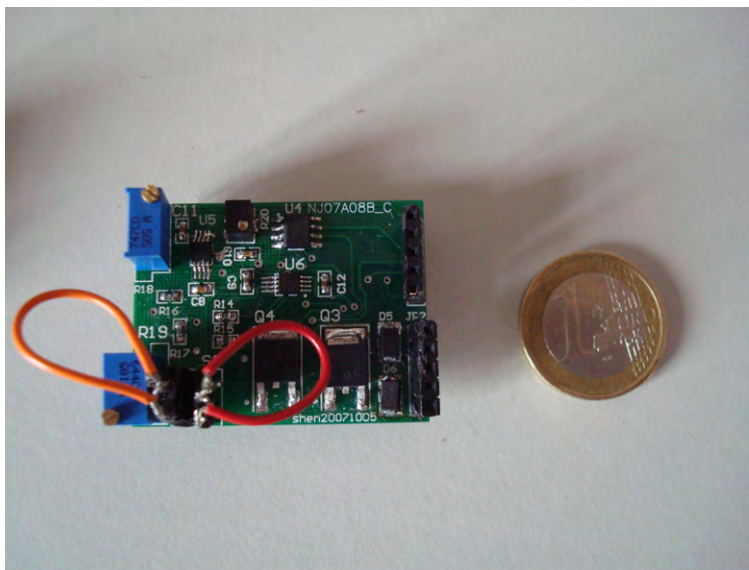


Figure 2.24: Low power circuit for self-powered SSDV[16].

in Fig.2.24 is designed to manage the harvest energy for switching and providing the voltage V_{cc} and V_{EE} used in SSDV. However, this technique is supplied by external device but not the structure itself, so it is not truly self-powered system. In addition, the energy consumed in the circuit is critical for this technique.

2.4.2 Blind switch damping techniques

Blind Switch Damping (BSD) techniques are investigated by Lallart *et al.* in[17]. They proposed three BSD methods namely *Blind Switch Damping on Short circuit* (BSDS) and *Blind Switch Damping on Voltage source* (BSDV) including *Blind Switch Damping on Adaptive Voltage sources* (BSDVa) and *Blind Switch Damping on Piecewise constant Voltage source* (BSDVp). Strictly speaking, the BSD techniques are not synchronized switch damping techniques since the switching is not synchronizing with the structure motion. However, the BSD techniques do not need to detect the displacement peak thus making it easier to implement. They also allow a control of the re-injected harmonics¹.

Fig.2.25 shows the BSDS circuit and waveforms. In BSDS, the switches usually switch with a random frequency (usually, this frequency is higher than the structure frequency. Since the mechanical energy is always transferred as electrical energy

¹SSD techniques can induce the harmonics motion. In order to suppress these harmonics, a larger inductance should be used to smooth the inversion. This issue is discussed in[80]. BSD techniques can control these harmonics thus the required inductance could be much smaller than that in SSD techniques. It allows the BSD easier for integration on an electrical board.

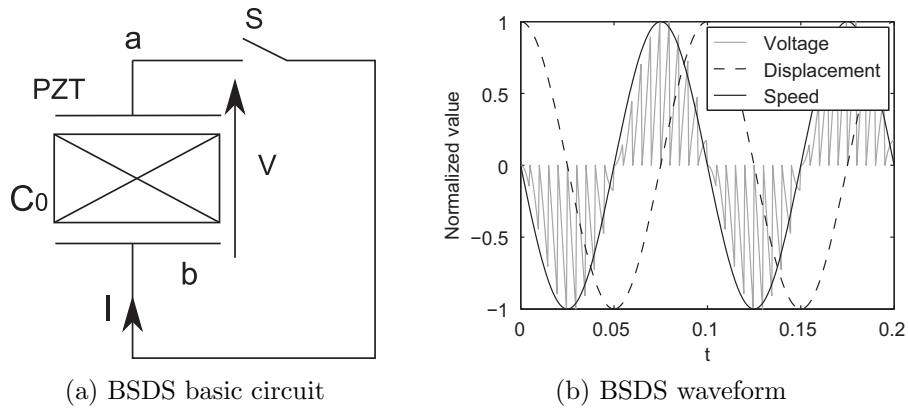


Figure 2.25: BSDS technique[17].

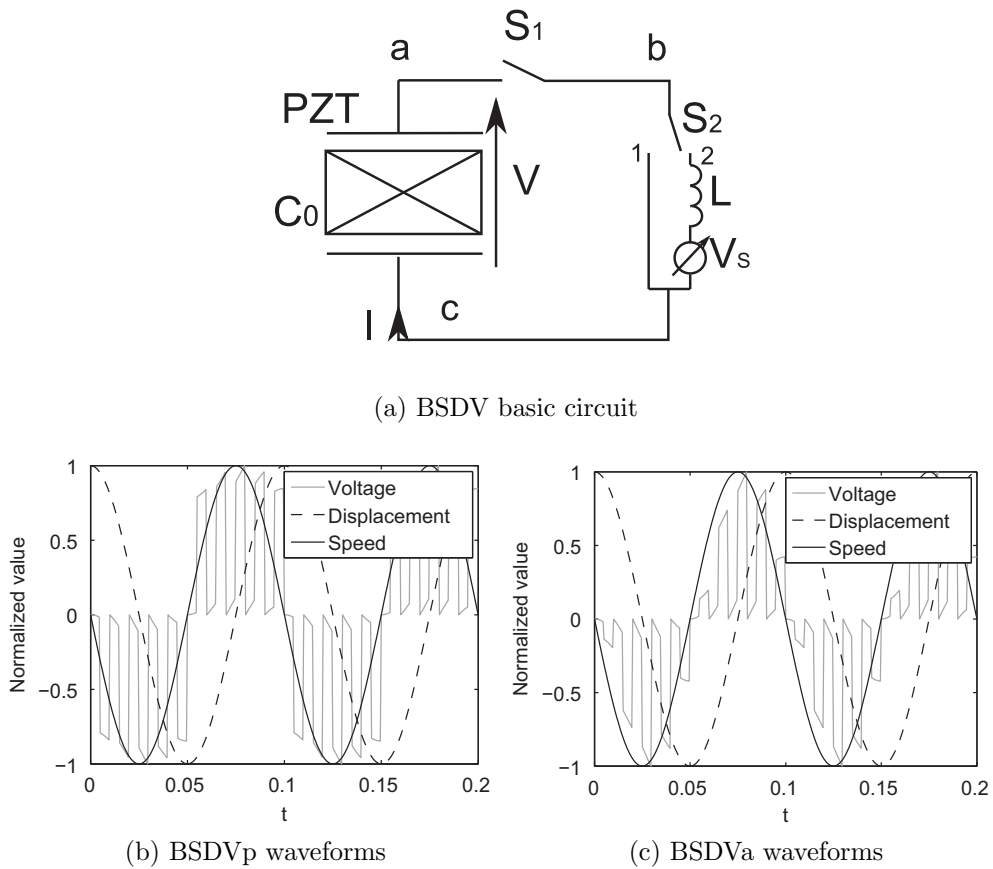


Figure 2.26: BSDV techniques[17].

and can be dissipated in the circuit during the switching, the BSDS should be a robust control. However, the switching is not synchronized with the structural displacement, the damping effect should be worse than that of SSDS.

Fig.2.26 shows the BSDV circuit and waveforms. It shows that the voltage always has same sign with the speed. That means the piezo-induced force always has the different sign with the speed. Since there is external voltage source in the circuit, the BSDV techniques exhibit a better control performance than that of BSDS.

In BSD techniques, the switching frequency is directly related to the damping effect. Experimental results show that too much switching in one period will decrease the damping. It could be imaged that the best switching instant should be just at the extrema of the structural displacement that reducing the BSD techniques to SSD techniques.

2.5 Conclusion

In this chapter, we review the state-of-the-art of synchronized switch damping techniques. The conclusion can be summarized as follows:

- First, the classical mathematical model for piezo-coupled structure is given. Then, three representative SSD techniques are introduced namely SSDS, SSDI and SSDV both in their working principles and the corresponding waveforms. Their similarities can be summarized as three parts: (a), the switching always occurs at the displacement extrema; (b), the piezo-voltage increases most of the time but only drops to zero or inverts to an opposite value during the switching. That indicates the mechanical energy can be only transferred into electrical energy and finally dissipated as heat in the circuit. The electrical energy can not be transferred back as the mechanical energy; (c), the signs of the induced voltage are always same with that of the velocity. That is to say the induced piezo-force has the different signs with the velocity. As energy-recycling techniques, SSDS and SSDI are always robust since we can consider that the energy used for control is extracted from the controlled structure. While SSDV could be instable because the energy for control is partly from external voltage source. However, SSDV on adaptive source can solve such problem.
- Second, we introduce the energy analysis for general SSD techniques. It shows that the damping ability of SSD technique particularly depend on

the voltage on the piezoelectric elements. The energy cycle reveals that the damping ability ranking is $SSDS < SSDI < SSDV$. However, the energy consumption ranking is $SSDS \approx SSDI < SSDV$. The transfer function of kinds of SSD techniques are also listed in the section.

- Third, we conclude the broadband control and multimode control of SSD methods which were developed in past five years. The mathematical model of multi-mode SSD methods are usually built under model coordinate. Researchers also establish the model by means of FEM methods. The main difference between single mode control and multimode control is the switching instant selection. we summarized these techniques as three catalogs. (a), The method with original control law. In these methods, the control law is identical with that in single mode control. They show the control ability for broadband excitation in the experiments. However, they are not the best control law for multimode control; (b), The mode distinguish based methods. These methods identify the interested modes from sensing signals so as to determine the switching instant; (c), The time window based methods. The switching instant is determined by statistical prediction which is obtained from a fixed time window.
- Fourth, two distinctive SSD techniques are reviewed which are self-powered SSD techniques and blind switch damping techniques (BSD). In the research, the switches On/Off states are controlled by DSP devices. Therefore, the energy consumption of these devices is would be large. elf-powered SSD technique can open and close the switch without any outer energy supply but by smart circuit design. In the reviewed literature, this technique can even possess multimode control ability. BSD techniques do not need to detect the displacement peak thus making them easier to implement. But BSD techniques can not be considered as SSD techniques. Because the switching is not synchronized with displacement extreme. However, it has the same circuit schema with SSD technique. In addition, the BSDS technique is partially similar with Synchronized switch damping with energy transfer technique which will be presented in the next chapter.

Chapter 3

General SSDET principles

Due to it differing from most of the published vibration control techniques, this chapter proposed a new SSD scheme so called Synchronized Switch Damping with Energy Transfer (SSDET) technique. In this technique, vibration energy can be transferred between structures or different vibrating modes in order to achieve damping effect. The remainder of this chapter continues as follows. At first, the SSDET principles are introduced including the circuit design and the control law. Then, the mathematical modeling in time domain is established by the state-space approach. The simulation work is carried out by using the matlab/simulink software to verify its feasibility. The system parameter identification technique for SSD techniques are explained as well. After that, the mathematical model in frequency domain is derived. The effect of several parameters are discussed by employing this model. Finally, an enhanced control law by using threshold setting is developed. A simple simulation demonstrates this control strategy can significantly increase the control effect.

3.1 Principles of the SSDET

In this section, we proposed a new SSD schema named synchronized switch damping with energy transfer. The electrical circuit and the operation steps (control law) are introduced to explain how the energy between different objects can be transferred for the sake of vibration control.

3.1.1 Idea of energy transfer in SSD technique

Compared with the passive vibration control, active control gets better damping effect in most cases. However, it usually needs a strong external energy source to power the control system especially to drive actuators. That brings hazard risks in industrial applications. For instance, the control system will lose its effectiveness once the external power is cutoff by accident. SSDI technique do not need external energy while performs a decent vibration control. However, its control ability is limited by the electromechanical coupling coefficient which can not be easily altered after the piezoelectric elements are bonded on the structure.

In SSD techniques, it has been demonstrated that the voltage amplitude plays an important role. Higher amplitude always leads to better damping. Moreover, this voltage can be enhanced by artificially adding a small battery (SSDV). However, it still need change the battery termly.

That drives us to develop an *autonomous energy-feeding* or *self-powered* system to enhance such voltage. Energy harvesting techniques[93–97] for mechanical system could be suitable for combining with SSD technique to achieve this goal. The hypothetical system could be composed of two parts. One of them should be energy harvesting part which collect the energy and store them on an energy storage device. The rest part should be SSD part which use the collected energy to enhance the voltage amplitude. The energy flow in traditional SSD techniques and the proposed energy transfer based SSD technique are depicted in Fig.3.1a. As shown in this Fig.3.1a, the mechanical energy is partially extracted by the piezo-elements and then simply dissipated into heat in the circuit in SSDS or SSDI technique. While in energy transfer based SSD technique, the mechanical energy (from a source structure or mode) is delivered to an energy storage device by the coupled piezoelectric elements and then transferred to the other piezo-element which coupled with a mechanical target. A greater voltage amplitude will appear on the piezoelements which receives the transfer energy thus causing better damping for the target. The energy flow routing is illustrated in Fig.3.1b.

3.1.2 SSDET circuit and control law

The ideal SSDET control scheme is described in Fig.3.2. It consists of two *LCR* circuits sharing an inductor L which is used as temporary energy storage and a resistor R . C_0 and V are the capacitance of and the voltage on the piezoelectric elements, respectively. The subscripts s and t indicate the variables related to the energy source and the target respectively. The two switches are in the opened

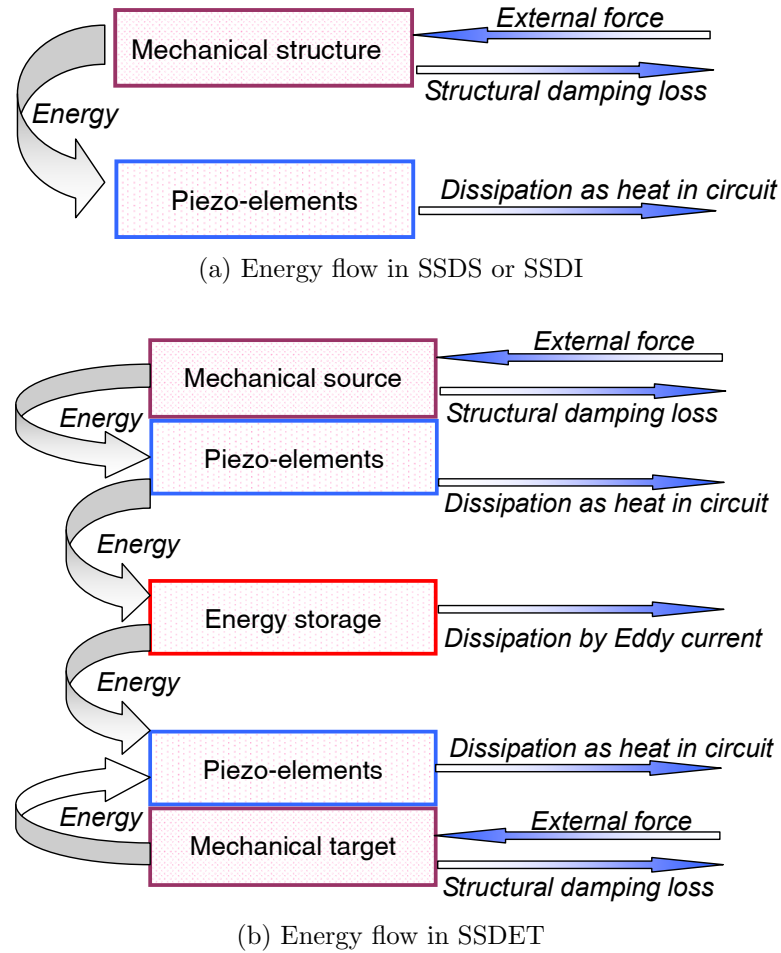


Figure 3.1: Energy flow in SSD techniques. (a) SSDS or SSDI. (b) SSD technique with energy transfer.

state most of the time and only need to be switched on when the target voltage, which images the displacement, reaches either a maximum or a minimum value. The capacitor C_{0s} is used to extract the mechanical energy of the source while the C_{0t} is used to receive the transfer energy for a better damping on the target. The corresponding operations could be carried out in the two following steps:

- **step 1:**

When the target vibration reaches its extreme displacement, SW_s is switched on till V_s drops to zero. In other words, the current i increases to its first extreme, and then SW_s is switched off. During this period, the electrical energy which has been converted from energy-source mechanical energy is stored in the inductor. This process is shown in the right part of Fig.3.2 which could be called an energy storing process.

- **step 2:**

Considering that the LCR resonant frequency is much higher than the structure vibration frequency, step 1 could be implemented in a very short time while the displacement of the target u_t would be maintained around its extreme during this period. When SW_s is re-opened, SW_t is immediately switched on till V_t is inverted. Subsequently, SW_t is opened again. This process is shown in the left part of Fig.3.2, and can be referred to as an energy transferring process.

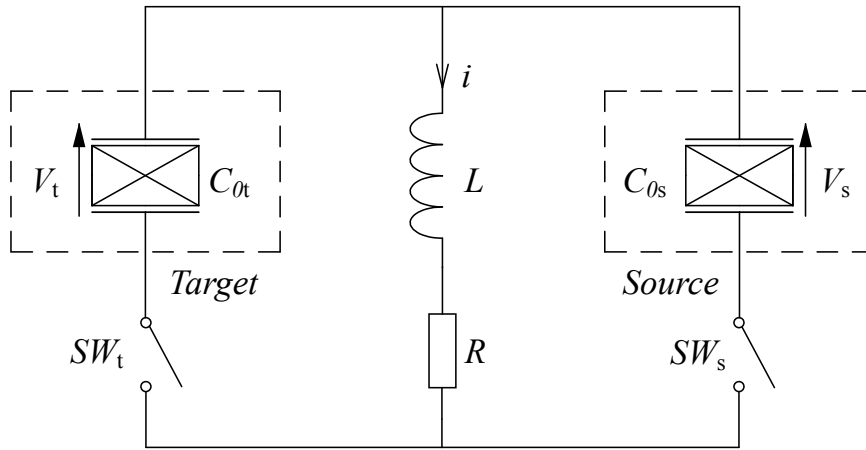


Figure 3.2: SSDET circuit.

To some extent, the operation in step one is similar with Synchronized Switch Harvesting on Inductor technique(SSHI)[8, 61, 64, 72, 98, 99]. In these SSHI techniques, the energy is stored in a capacitor. However, in our proposed SSDET circuit, the energy storage media is a inductor but not capacitor. That is because using capacitor would decrease the transfer efficiency. Since large capacitor would be preferred in order to store more energy from source, but it needs longer charging time which would be unaccepted in the synchronizing system. Moreover, the energy stored in C_{0s} can not be totally transferred to C_{0t} in step 1 no matter what capacitance we choose due to the parallel connection of the capacitors. On the contrary, the inductor can perfectly transfer the energy and transfer speed would be very fast if using a small inductor. Moreover, the voltage cross the inductor can be inverted by tuning the switching duration in order to correspond to the voltage on the target. However, it needs two capacitors to accomplish this goal (one's voltage is positive and another's voltage is negative) making the system more complex. These advantages make inductor be a better component than a capacitor does.

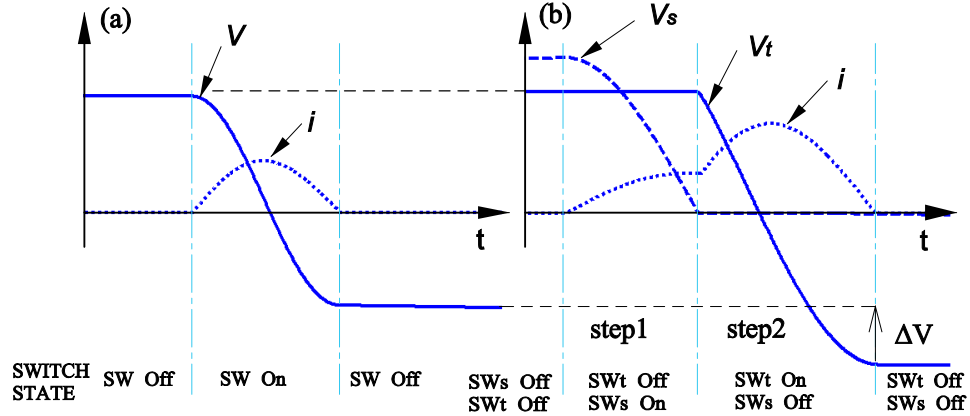


Figure 3.3: Comparisons between SSDI and SSDET techniques:(a) SSDI waveforms and (b) SSDET waveforms.

Fig.3.3 exposes the waveforms of SSDI and SSDET techniques during the closing of the switches. For classical SSDI method, the piezoelectric voltage is simply inverted during one-half of the circuit period. The current i increases when the voltage V decreases. It reaches a maximum when V drops to zero and then decreases till V is inverted to its opposite extreme. As compared to SSDI technique, the proposed SSDET method contains two steps. In the first inversion, V_s is not totally inverted but cut off at zero. The operation in step 2 is the same with SSDI but begins with an initial inductor current, thus giving rise to a greater inversion. Due to the initial current, the inversed voltage could be even larger than one¹.

As shown in Fig.3.4, the signs of V_s and V_t could be either the same (at point e) or opposite (at point b) at the beginning of the step 1 as shown in Fig.3.4(a), which determines different switch closing durations. If the signs of V_s and V_t are the same(fig:voltage-time-schema(c)), SW_s should be closed for a quarter of an oscillation period, which roughly equals $2\pi\sqrt{LC_{0s}}$ in the energy storing process (assuming that the resistance is small). Otherwise(Fig.3.4(b)), the SW_s should be closed for a longer time to make sure that the sign of the voltage on the inductor was the same as for V_s at the end of step 1. By doing so, the energy stored in the inductor consistently enhanced the voltage inversion in step 2. The switching duration t_b in step2 was not constant but depended on the initial conditions. Based on the second-order circuit relations, the switch-closing duration in each step, i.e., the control law, can be summarized in Eq.(3.1).

¹Only in some inversions, but it can not be always larger than one in all inversion

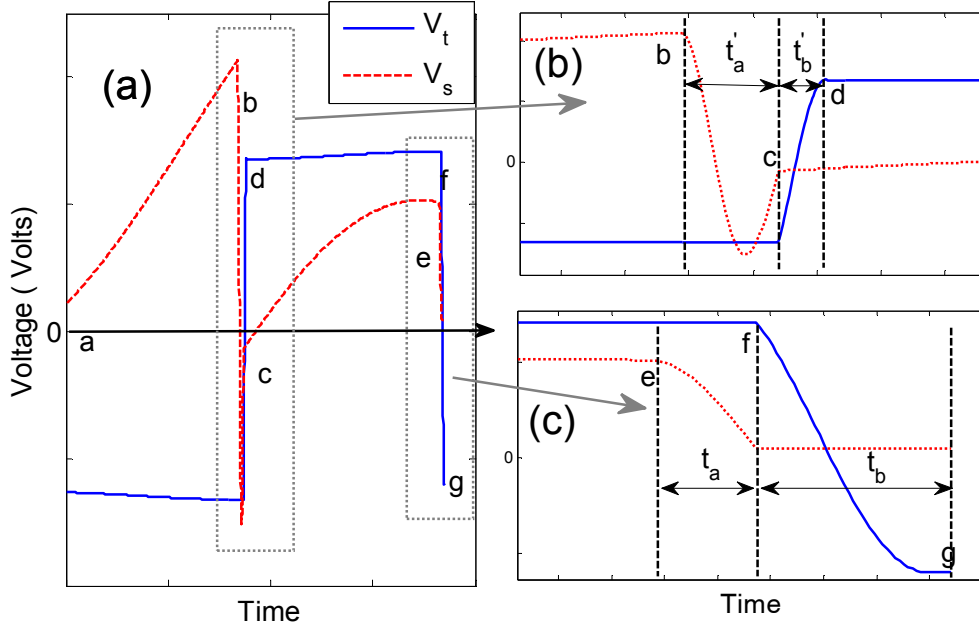


Figure 3.4: The voltage waveforms in SSDET.

$$\begin{aligned}
 \text{When } \dot{i}_t = 0 \text{ and } \text{sign}(V_s \cdot V_t) \geq 0 & \begin{cases} t_a = \frac{1}{\omega_s} \arctan\left(\frac{\omega_s}{\beta}\right) \\ t_b = \frac{1}{\omega_t} \left[\arctan\left(\frac{-i_0 \omega_t L}{U_0 - i_0 \beta L}\right) + \pi \right] \end{cases} \\
 \text{When } \dot{i}_t = 0 \text{ and } \text{sign}(V_s \cdot V_t) < 0 & \begin{cases} t'_a = \frac{1}{\omega_s} \left[\arctan\left(\frac{\omega_s}{\beta}\right) + \pi \right] \\ t'_b = \frac{1}{\omega_t} \left[\arctan\left(\frac{-i_0 \omega_t L}{U_0 - i_0 \beta L}\right) + \pi \right] \end{cases}
 \end{aligned} \quad (3.1)$$

Here, $\beta = \frac{R}{2L}$. U_0 and i_0 are the initial voltage of the V_s and the initial current in the inductor at the beginning of step 2, ω_s and ω_t are the resonant circular frequency of the energy storing circuit and the energy transferring circuit. These parameters can be obtained from Eq.(3.2). It should be pointed out that t_a and t'_a are always constant since they are only determined by the L , C_0 and R properties. Nevertheless, the t_b and t'_b are variable due to the different initial conditions (V_0 and i_0) under each transfer time.

$$\omega = \sqrt{\frac{1}{LC} - \left(\frac{R}{2L}\right)^2} \quad (3.2)$$

3.1.3 Voltages cycle in SSDET

Fig.3.5 shows the voltages cycle versus the current in coil. The time flows from point a to point g which brings into correspondence with Fig.3.4. The side view

Figures are also plotted in Fig.3.6. SSDET can damp not only the target but also the source. It clarifies that the voltage inversion on target begins with a initial current leading to a larger area indicating the dissipated power compared with that of SSDI. This cycle can be described as follows.

- $a \rightarrow b$: Both V_s and V_t increase, the energy are extracted from their corresponding structure or mode.
- $b \rightarrow c$: SW_s is closed. The electrical energy on source mode are transferred to the coil. Note that V_s and V_t have the different signs. Hence, the closing time of switch SW_s equals to three quarter of the LC_sR circuit period to make sure the voltage of the coil has the same direction with V_t .
- $c \rightarrow d$: SW_s is open while SW_t is closed. C_{0t} received the energy from the coil and V_t is inverted to its opposite extreme. Since the inversion time is short, V_s remains at zero.
- $d \rightarrow e$: All switches are open. V_s and V_t increase. Mechanical energy transfers to the electrical energy again.
- $e \rightarrow f$: SW_s is closed. V_s drops to zero. Note the V_s and V_t have the same sign, thus the closing time equals to quarter of the LC_sR circuit period.
- $f \rightarrow g$: SW_s is open while SW_t is closed. V_t is inverted to its opposite extreme. Note that point g and a are not the same point due to the different transferred energy each time.

3.2 Mathematical modeling in time domain

This section models SSDET technique in time domain by using the state space approach. The system parameters identification are also introduced. The dynamic behavior and observation equations are solved by simulink model to verify the proposed method. Compared with the previous time domain simulation in which the voltage inversion is implemented by a inversion factor, the details during the voltage inversion including the voltages and the current in coil can be observed in this simulation.

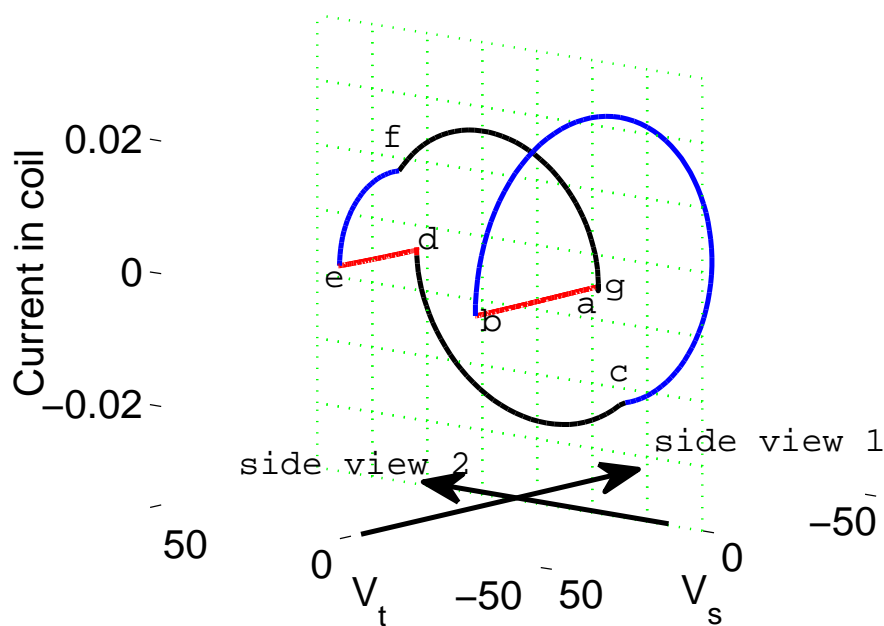


Figure 3.5: Voltages versus current in coil.

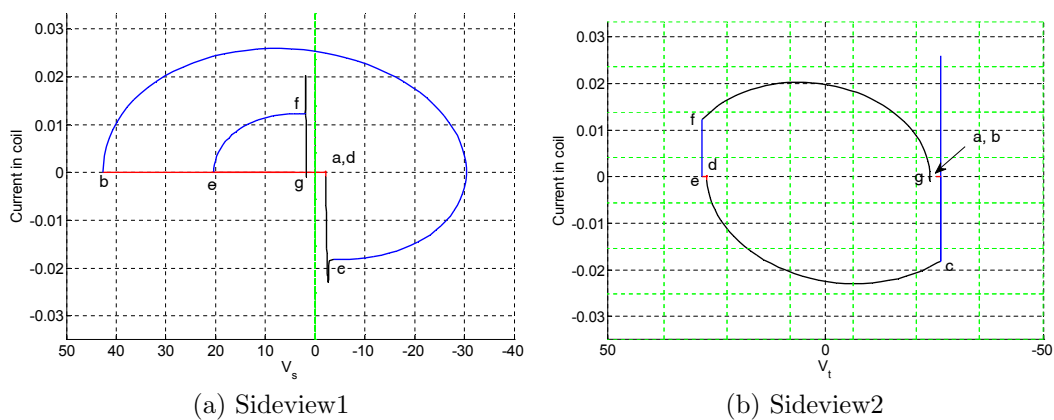


Figure 3.6: Sideviews of Fig.3.5.

3.2.1 Modeling by state space approach

In this section, we proposed an electromechanical coupling equation for SSDET by employing a state space representation. Assuming that there is no mechanical coupling effect between source and target, they can be treated as a standalone system. Therefore, they can be still presented by Eq.(3.3). SSDET circuit can be seen as two LCR oscillators sharing a coil, however, the switches are never closed simultaneously. Thus, the LCR circuit law which is given in Eq.(3.4) could be used to present the circuit SSDET property.

$$\begin{cases} m\ddot{u} + c\dot{u} + k^E u = F - \alpha V \\ i = \alpha \dot{u} - C_0 \dot{V} \end{cases} \quad (3.3)$$

$$V = L \frac{di}{dt} + Ri \quad (3.4)$$

Based on the above equations, the governing equation is represented in terms of a state space formulation (3.5)

$$\dot{\mathbf{x}}(t) = \mathbf{A}\mathbf{x}(t) + \mathbf{B}\mathbf{f}(t) \quad (3.5)$$

Here, the state vector $\dot{\mathbf{x}}(t)$ is chosen as

$$\begin{aligned} \mathbf{x}(t) &= [x_1 \ x_2 \ x_3 \ x_4 \ x_5 \ x_6 \ x_7]^T \\ &= [u_s \ \dot{u}_s \ u_t \ \dot{u}_t \ v_s \ v_t \ i]^T \end{aligned} \quad (3.6)$$

Thus, the derivative of the state vector is (3.7)

$$\dot{\mathbf{x}}(t) = [\dot{u}_s \ \ddot{u}_s \ \dot{u}_t \ \ddot{u}_t \ \dot{v}_s \ \dot{v}_t \ \dot{i}]^T \quad (3.7)$$

The state matrix \mathbf{A} is a 7-by-7 matrix (3.8) and can be divided into four blocks:

$$\mathbf{A} = \begin{bmatrix} \mathbf{A}_1 & \mathbf{A}_2 \\ \mathbf{A}_3 & \mathbf{A}_4 \end{bmatrix} \quad (3.8)$$

$$\mathbf{A}_1 = \begin{bmatrix} 0 & 1 & 0 & 0 \\ -k_s^E/m_s & -c_s/m_s & 0 & 0 \\ 0 & 0 & 0 & 1 \\ 0 & 0 & -k_t^E/m_t & -c_{ts}/m_t \end{bmatrix} \quad (3.9)$$

$$\mathbf{A}_2 = \begin{bmatrix} 0 & 0 & 0 \\ -\alpha_s/m_s & 0 & 0 \\ 0 & 0 & 0 \\ 0 & -\alpha_t/m_t & 0 \end{bmatrix} \quad (3.10)$$

$$\mathbf{A}_3 = \begin{bmatrix} 0 & \alpha_s/C_{0s} & 0 & 0 \\ 0 & 0 & 0 & \alpha_t/C_{0t} \\ 0 & 0 & 0 & 0 \end{bmatrix} \quad (3.11)$$

\mathbf{A}_1 includes only the parameters of mass, damping and short circuit stiffness, and it thus represents the mechanical properties of the coupling system. \mathbf{A}_2 and \mathbf{A}_3 can be seen as electromechanical coupling matrices which reveal the interaction between structures and piezoelectric elements. \mathbf{A}_4 shows the electrical properties of the system and it has different forms under varying control stages.

When both of the switches are open, the current i is zero and \mathbf{A}_4 can be written according to:

$$\mathbf{A}_4 = \begin{bmatrix} 0 & 0 & 0 \\ 0 & 0 & 0 \\ 0 & 0 & 0 \end{bmatrix} \quad (3.12)$$

When SW_s is closed while SW_t is open (step 1), \mathbf{A}_4 could be written as:

$$\mathbf{A}_4 = \begin{bmatrix} 0 & 0 & -1/C_{0s} \\ 0 & 0 & 0 \\ 1/L & 0 & -R/L \end{bmatrix} \quad (3.13)$$

When SW_s is open while SW_t is closed (step 2), \mathbf{A}_4 can be written according to equation

$$\mathbf{A}_4 = \begin{bmatrix} 0 & 0 & 0 \\ 0 & 0 & -1/C_{0t} \\ 0 & 1/L & -R/L \end{bmatrix} \quad (3.14)$$

Considering two external forces $f_s(t)$ and $f_t(t)$ exerted on each structure, the input vector $\mathbf{f}(t)$ can be written according to Eq.(3.15) and the input matrix \mathbf{B} according to Eq.(3.16):

$$\mathbf{f}(t) = [f_s(t) \quad f_t(t)] \quad (3.15)$$

$$\mathbf{B} = \begin{bmatrix} 0 & 1/m_s & 0 & 0 & 0 & 0 & 0 \\ 0 & 0 & 0 & 1/m_t & 0 & 0 & 0 \end{bmatrix}^T \quad (3.16)$$

3.2.2 Introduction of simulink model and configurations

Based on the equations in the previous section, the simulation in time domain is implemented under the Matlab\Simulink[®] environment. The diagram of the simulation model is depicted in Fig.3.7. In this figure, we can see that the system consists of the mechanical part(source and target structure), electromechanical part (PZT on the structures), electrical circuit(LCR oscillators) and control system. It can be noticed that the mechanical part and electrical part are connected by the α factor. The piezoelectric voltage can input to the electrical circuit so as to calculate the output current. The control system detects the extrema of the source displacement to determine the switching timing. The voltage V_s and V_t are used to make a sign relationship judgment in order to set the switching duration.

The simulink model is depicted in Fig.3.8. Since the non-linearity of the system, the state space model can not directly adopted to simulate. Thus, a simulink model with switch components is employed here to solve the equations listed in Eq.(2.7) and Eq.(3.4) in time domain. Since the closing duration of step 2 was variable and the fact that there was no diode in the simulation, the system had to estimate the closing duration in step 2 according to the zero-crossing instant of the current. Once this zero-crossing instant was detected, the SW_t opened immediately. However, the derivative of the current around zero was large, and even a small delay would lead to a large deviation of the current from zero. Hence, a fine step size is required in the simulation to guaranty the simulation accuracy. On the contrary, small step size drastically increases the calculation time. In the section, the time step is set as 3×10^{-6} seconds, which is sufficient when compared to the oscillation period of the circuit. Moreover, the model can achieve SSDI control on target simply by always keeping the SW_s open.

3.2.3 System parameter identification

The parameters identification method for SSD techniques has been mentioned in several literatures[7, 73, 100]. The main parameters which need to be identified are summarized in Tab.3.1. The superscript E and D stand for short circuit and open circuit respectively. However, only several parameters can be obtained from the measurement, the others can be calculated by the equations from Eq.(3.17) to

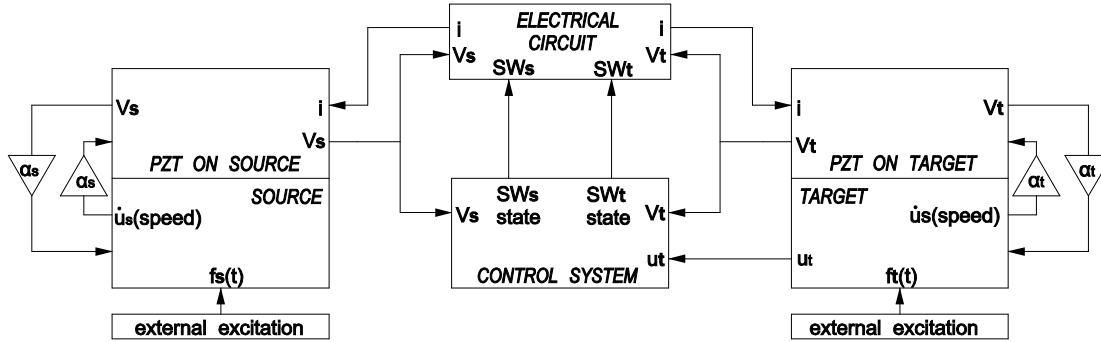


Figure 3.7: A diagram of the simulink model.

Eq.(3.21). λ factor is the proportionality coefficient between voltage and displacement in open circuit. The mechanical quality factor Q_M can be obtained from the half-power bandwidth method [101]. It should be pointed out that the values for the mass, stiffness and damping are those equivalents to their corresponding mode. This parameter identification is available for both the source and target.

Classification	Parameters	notations
<i>Mechanical</i>	Mass	m
	Damping coefficient and damping ratio	c and ζ
	Stiffness	k^D and k^E
	Natural circular frequency	ω^D and ω^E ♣
	Mechanical quality factor	Q_M ♣
<i>Electrical</i>	Resistance	R
	Capacitance	C_0 ♣
	Inductance	L ♣
<i>Electromechanical</i>	Ratio between voltage and displacement	λ ♣
	Force factor	α

The symbol ♣ means this parameter can be directly obtained from measurement

Table 3.1: System parameters in SSD techniques.

$$\alpha = \lambda C_0 \quad (3.17)$$

$$k^E = \alpha \lambda \frac{\omega^{E^2}}{\omega^{D^2} - \omega^{E^2}} \quad (3.18)$$

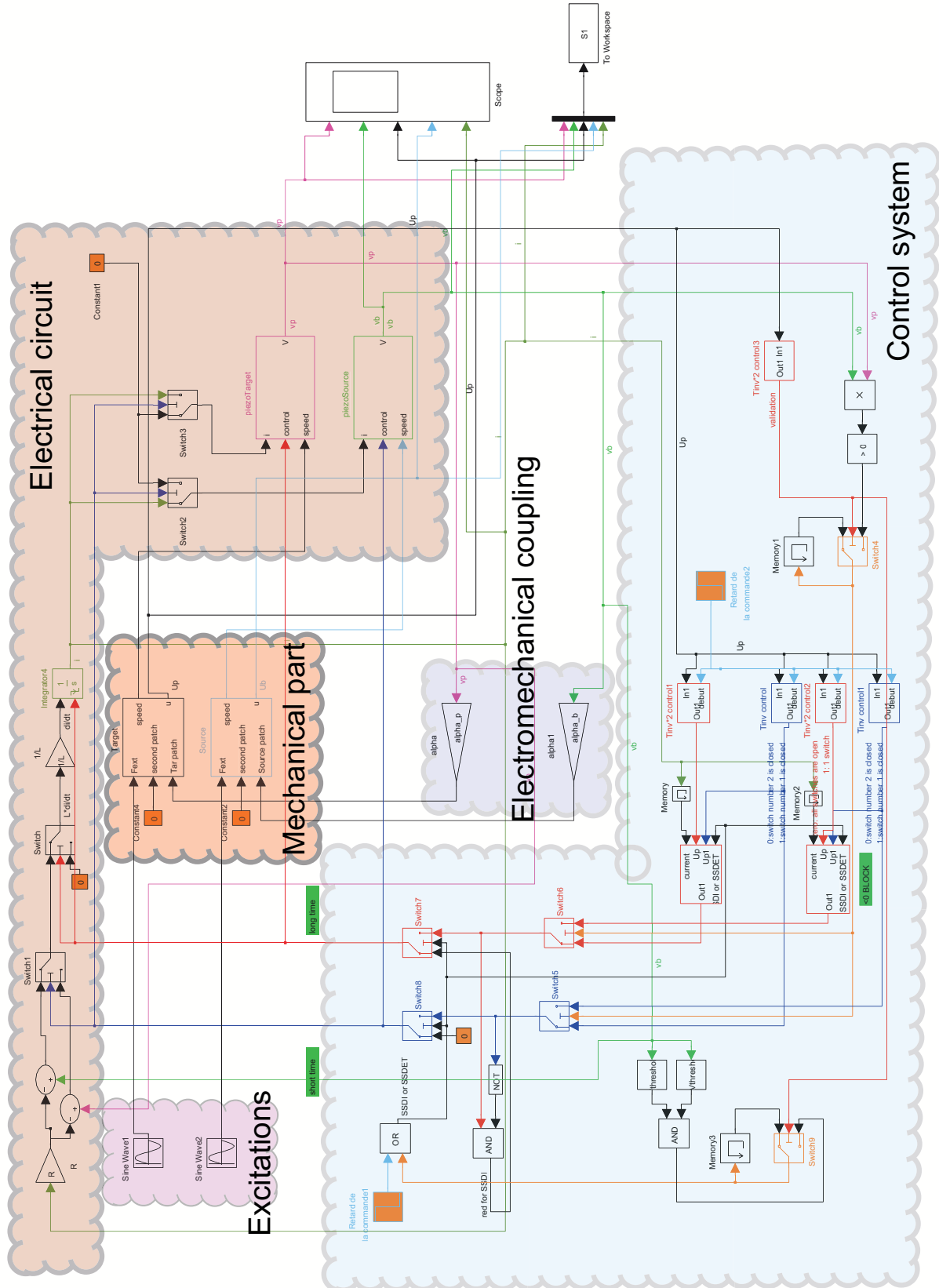


Figure 3.8: Simulink model.

$$m = \frac{k^E}{\omega^{E^2}} \quad (3.19)$$

$$\zeta = \frac{1}{2Q_M} \quad (3.20)$$

$$c = 2\zeta m \omega^D \quad (3.21)$$

Symbol	Value(unit)
L	0.09 H
R	300 Ω
C_{0s}, C_{0t}	44.5 nF , 44.2 nF
ω_s^E, ω_t^E	139.8 rad^{-1} , 318.2 rad^{-1}
ω_s^D, ω_t^D	140.1 rad^{-1} , 318.6 rad^{-1}
m_s, m_t	135.6 g , 98.7 g
k_s^E, k_t^E	2650 Nm^{-1} , 9998 Nm^{-1}
c_s, c_t	0.2584 $Nm^{-1}s^{-1}$, 0.3017 $Nm^{-1}s^{-1}$
λ_s, λ_t	$1.6 \times 10^4 Vm^{-1}$, $2.1 \times 10^4 Vm^{-1}$
α_s, α_t	$7.2 \times 10^{-4} NV^{-1}$, $9.4 \times 10^{-4} NV^{-1}$
Q_s, Q_t	73.9, 103.7
ζ_s, ζ_t	6.8×10^{-3} , 4.8×10^{-3}
t_a, t_b	$9.3688 \times 10^{-5} s$, $1.8738 \times 10^{-5} s$
t'_a, t'_b	$2.9465 \times 10^{-4} s$, $1.8738 \times 10^{-5} s$

Table 3.2: System properties in simulation.

3.2.4 Simulations and results discussions

The simulation is carried out by using the developed simulink mode. The system properties are showed in Tab.3.2. They are obtained from a cantilever beam (energy source) and a four edge clamped plate (target) by employing the proposed identification method.

Considering the equivalent resistance of the coil, the switches and the piezo-electric patches as well as other losses in the circuit, the resistance is empirically

determined to be 300Ω . In the simulation, the energy is transferred from the cantilever beam (source) to the plate (target) so as to suppress the vibration of the plate.

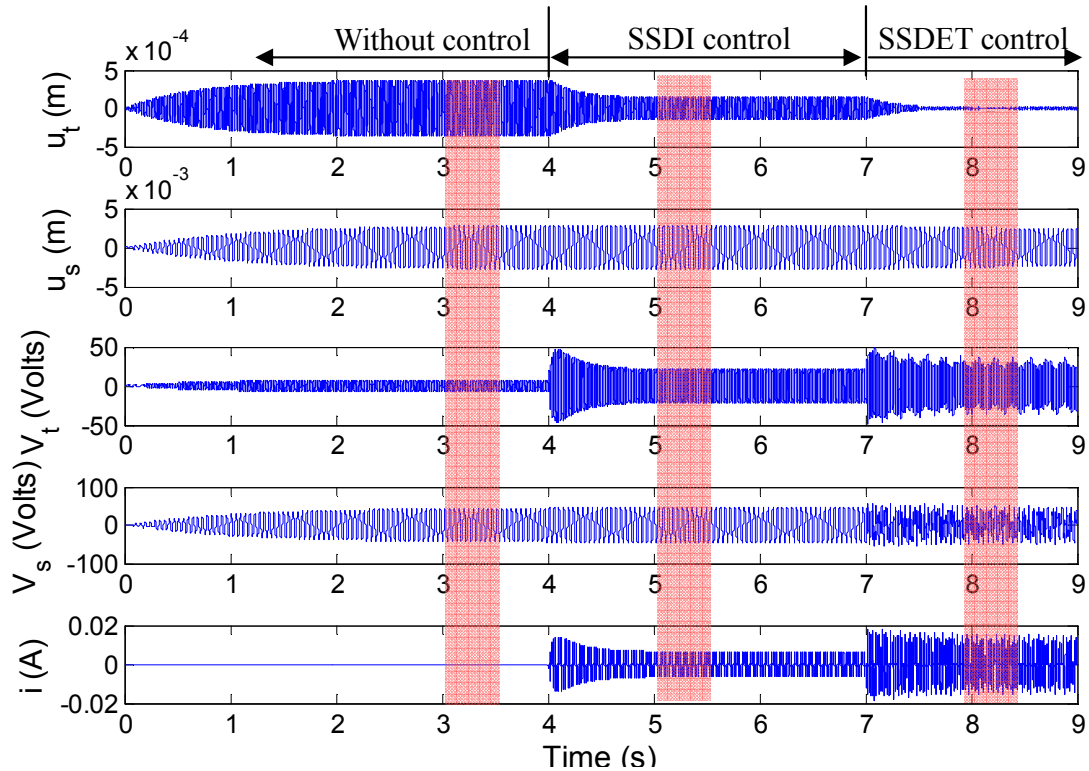


Figure 3.9: Time simulation results.

The excitations for both source and target are sinusoidal with their resonant frequencies. The simulation is running for 9 second with the step size 3×10^{-6} second which is sufficient when compared to the oscillation period of the circuit (4×10^{-4} seconds for both oscillators). Fig.3.9 shows the simulation results including the displacements and piezoelectric voltages of both source and the target as well as the current in the coil of entire time-of-flight. The different control stages are noted on the top of the figure. As shown in Fig.3.9, the simulation is implemented with the following operations .

- 0 – 4 seconds. No control is applied in the system. Both source and target motions and voltages get to a steady response around 4 second.
- 4 – 7 seconds. SSDI control begins. The voltage V_t increases a lot at the very beginning of this stage (switch closing instant). After a short instant, its amplitude decreases and holds on a steady value. This change can be

attributed to the transient effect of the system. This steady amplitude is much larger than that in no control stage. The source voltage is not involved during this stage. Thus, they do not show any changes in this stage. It shows that the current occurs in the coil due to the voltage inversion of the target. Displacement curves shows that the target motion is suppressed. However, since SSDI only reacts to the target, the source is not damped during this stage.

- 7 – 9 seconds. SSDET is conducted. it shows that V_t is enhanced comparing with that of SSDI due to the transferred energy from source. V_s waveform no longer steady since the switch SW_s switches with the frequency of target motion. The current in coil shows a larger amplitude than that in SSDI due to a larger voltage inversion occurs on the target. It is evident that SSDET shows a better damping than SSDI due to a larger voltage inversion.

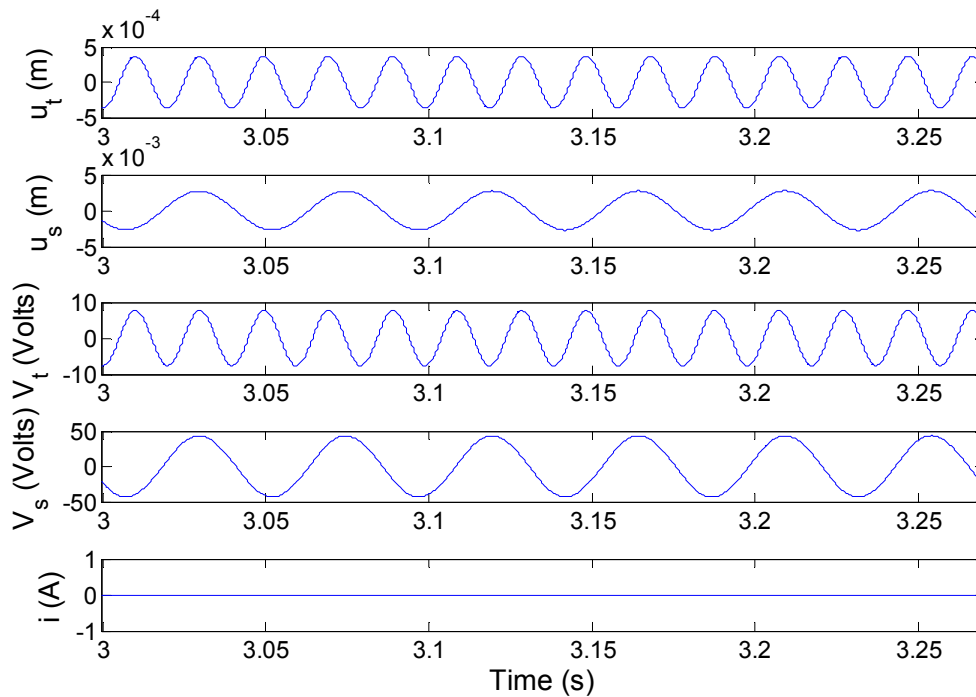


Figure 3.10: Details of the simulation waveform(Without control).

The three portion of Fig.3.9 which is covered by the red shadow are magnified in Fig.3.10, Fig.3.11 and Fig.3.12 in order to show the waveform details.

In Fig.3.10, the waveforms of all displacement and voltages are sinusoidal. It shows that voltages are in-phase with the corresponding displacements. Considering the force induced by the piezoelectric elements F_{piezo} equals to $-\alpha V$, that is

to say this force has a phase deference of 180 degree with the displacement. No damping can be induced for both vibrations.

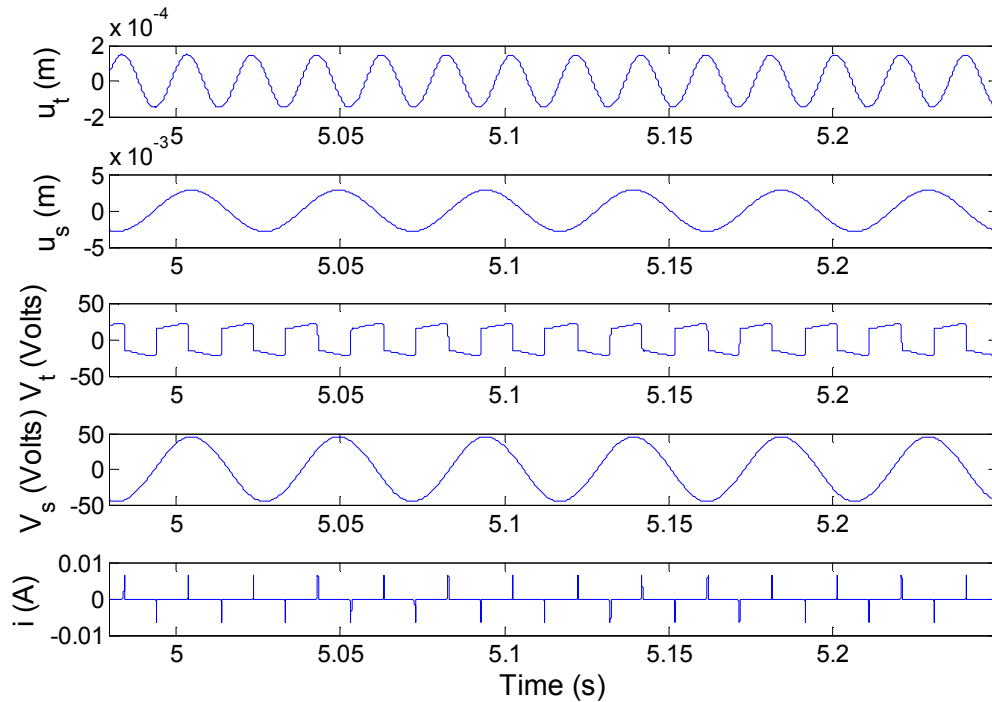


Figure 3.11: Details of the simulation waveform(SSDI).

Fig.3.11 shows waveform details in SSDI control stage. It exhibits that the voltage on target shows a typical SSD voltage waveform. That is the target voltage V_t is inverted at the u_t extrema and always increases its absolute value except the inversions. The current only appears during the inversion. The current signs depend on the sign of V_t at the beginning of the switching. It shows that the current increases at first, and reaches to the extrema value when V_t drops to zero. And it returns back to zero at the end of the inversion when V_t inverts to its opposite maximum. The current is null at the rest of the time due to the switches are open.

SSDET control stage is exposed in Fig.3.12. Due to the control law, it is found that the piezo-voltage of the source V_s is consistently stopped around zero at each switching. It can be seen that the voltage V_t can be also inverted at each switching. However, the inversion factor is not constant owing to the transferred energy is fluctuant. Nevertheless, it shows a greater value than that in SSDI due to the transferred energy. The voltage V_t increases when the switches are open, but this phenomenon is not obvious (it seems like the voltage keeps a constant between two switchings). That is because the voltage is high while the u_t level is very low due

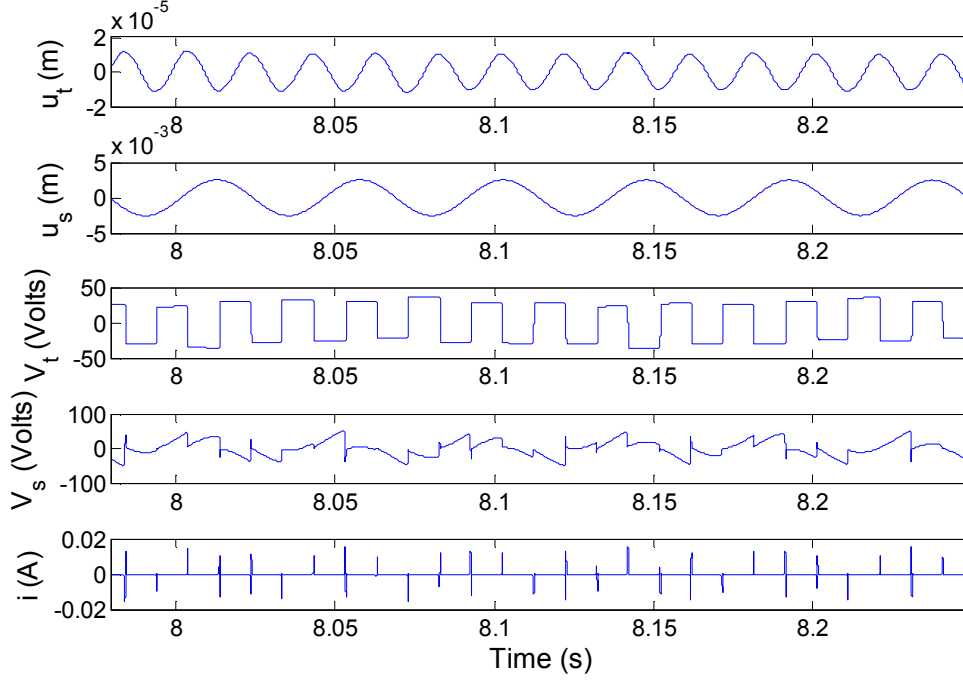


Figure 3.12: Details of the simulation waveform(SSDET).

to a drastic damping. It means a little energy could be extracted from the target between two switchings. On the other hand, It needs more energy to enhance the voltage if the voltage is high because the electrical energy is proportion to the voltage square value. So, such energy is too few to increase the voltage level too much. The current is also enhanced if we observe the y-axis scale ($0.01 \rightarrow 0.02$). That means more energy is dissipated during this control stage. Moreover, the u_s also reduces due to the source motion energy is partly extracted and used to control the target.

The extracted energy from source and target are calculated by $\int V idt$ and plotted in Fig.3.13. Where, V is piezoelectric voltage (V_s and V_t) and i is the outgoing current from the corresponding piezoelectric patch. From 0-4 seconds, no energy is extracted from both vibration. From 4-7 seconds, the mechanical energy is extracted from target due to SSDI control. It can be observed that the slope of the curve which indicates the extracted power, is large at the very beginning and then becomes to a smaller constant. In fact, the extracted energy can be also expressed as $\int F_{piezo} du$, which can be extended as $\int -\alpha V du$. At the very beginning after SSDI is conducted, the velocity of the target is still large and the piezo-voltage is also high that leading to a high extracted power in this duration. After that, the target vibrates under steady state, thus the extracted power should

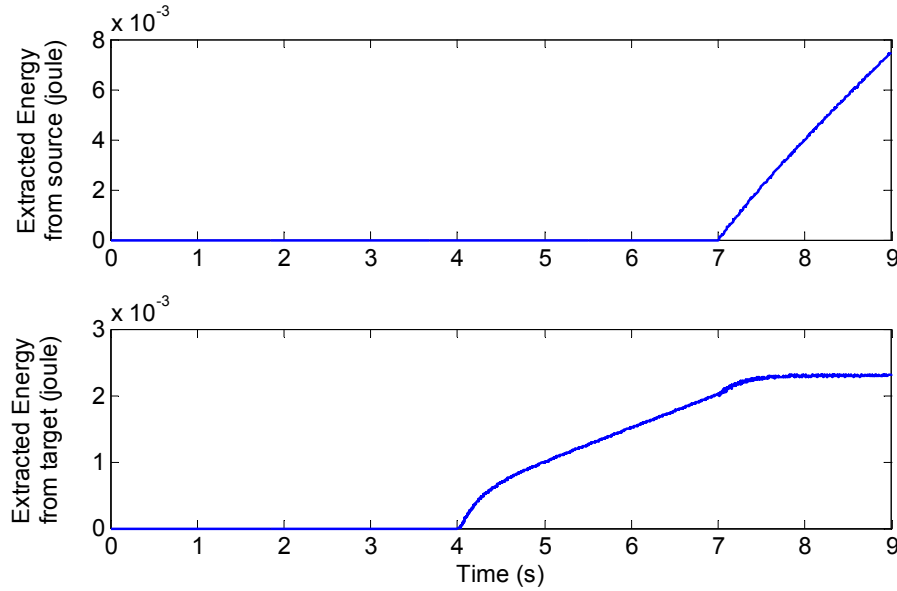


Figure 3.13: Extracted energy from source and target.

be a constant as shown in the figure. From 7-9 seconds, the mechanical energy is extracted from both source and target. The extracted energy from source grows monotonously and its curve slope is constant because the source vibrations is not damped too much. The curve of the extracted energy from target also have a large slope at the beginning, but then the slope is nearly zero. That means little energy is extracted from the target after 8 second. That is because the target vibration level is too low due to the damping effect, thus it is impossible to extract much energy from target vibration.

Due to the sign relationship between the source voltage and target voltage as we discussed in Eq.(3.1), the current will have four representative waveforms which are illustrated in Fig.3.14. We can see that the current direction at the end of step 1 is always same with that of the following process. That ensures the transferred energy always enlarges the current in the step 2, which images a greater voltage inversion on the target piezo-voltage.

3.3 Mathematical modeling in frequency domain

In this section, SSDET model is established in the frequency domain. The transfer function is derived when the target vibrates at its resonant. Numerical simulation is carried out to testify the damping effect with several parameters.

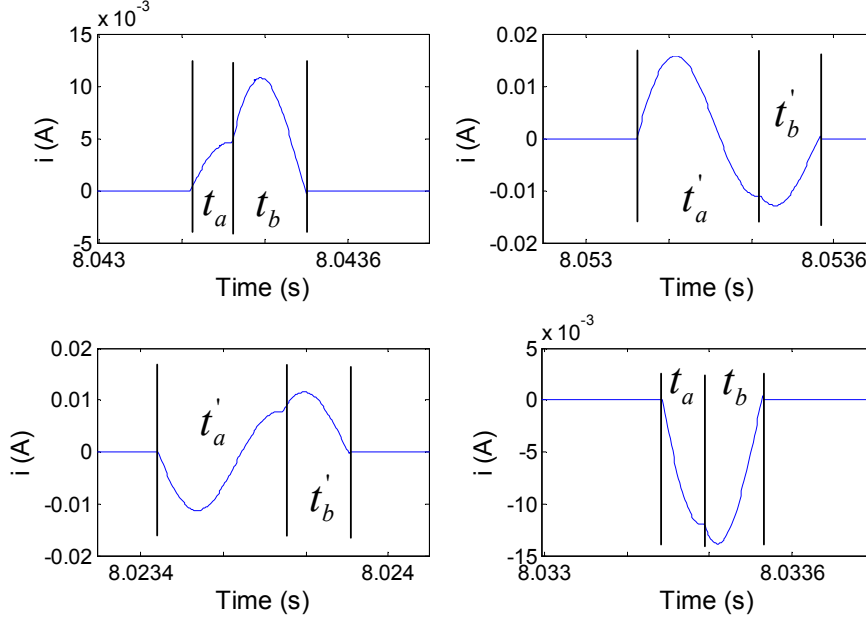


Figure 3.14: Representative current waveforms in SSDET.

3.3.1 Mathematical modeling

The voltage and displacement typical waveforms of both source mode and target mode are shown in Fig.3.15. It is assumed that the displacement of the target mode under SSDET control is sinusoidal as shown in Eq.(3.22). Concerning with the typical SSDET technique, the energy transfer happens at each peak of the target displacement extreme, thus two transfers would be conducted during one period of the target mode at its maximum and minimum displacement instant. If the operation time is T and the vibration frequency of the target mode is f_t , the transferred times n can be obtained by Eq.(3.23)

$$u_t(t) = u_{Mt}^{ssdet} \sin(\omega_t t + \phi_t) \quad (3.22)$$

$$n = \lfloor 2f_t T \rfloor \quad (3.23)$$

As shown in Fig.3.15(b), the voltage on the target mode relates to the transferred energy from the source. Generally, the V_t would have a big inversion when transfer energy is large *i.e.* the V_s is large at the transferring instant. However, it is evident that V_t is not a periodical function as SSDI due to the aperiodic transferred energy, that makes impossible to get a precise function to depict V_t . The statistic approach is used here to address such problem.

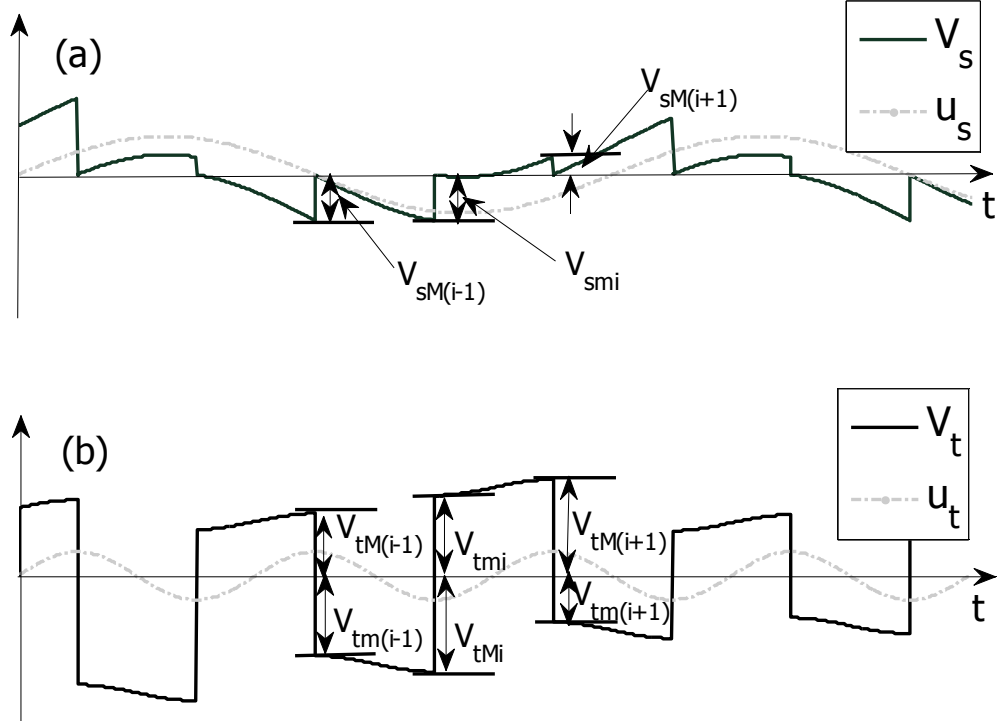


Figure 3.15: Voltage waveforms under SSDET technique.

For the target mode, the voltages before and after inverted are defined as V_{tMi} and V_{tmi} respectively as shown in Fig.3.15(b), where the subscript i stands for the order of the transfer *i.e.* i_{th} transfer. Thus, two equivalent voltages, which are before inverted \tilde{V}_{tM} and after inverted \tilde{V}_{tm} , can be defined by using the root mean square value in Eq.(3.24) and Eq.(3.25). In the same way, the equivalent voltage of the source mode before switching \tilde{V}_{sM} can also be defined in Eq.(3.26).

$$\tilde{V}_{tM} = \sqrt{\sum_{i=0}^n V_{tMi}^2/n} \quad (3.24)$$

$$\tilde{V}_{tm} = \sqrt{\sum_{i=0}^n V_{tmi}^2/n} \quad (3.25)$$

$$\tilde{V}_{sM} = \sqrt{\sum_{i=0}^n V_{sMi}^2/n} \quad (3.26)$$

Thus, the total transferred energy from the source mode E_s can be calculated by Eq.(3.27), and the extracted power from source P_s can be written as Eq.(3.28).

$$E_s = \frac{1}{2}C_{0s} \sum_{i=0}^n V_{sMi}^2 = n \cdot \frac{1}{2}C_{0s}\tilde{V}_{sM}^2 \quad (3.27)$$

$$P_s = \frac{E_s}{T} = C_{0s}f_t\tilde{V}_{sM}^2 \quad (3.28)$$

As known, the mechanical energy is extracted from the structure and finally dissipated as heat in SSD technique, so the energy losses for SSD technique can be only considered in the transfer process. At the beginning of the first step of SSDET, the piezoelectric voltages are \tilde{V}_{sM} on source mode and \tilde{V}_{tM} on the target mode, thus the total energy stored in the circuit equals to $\frac{1}{2}C_{0s}\tilde{V}_{sM}^2 + \frac{1}{2}C_{0t}\tilde{V}_{tM}^2$ at this instant. Here, $\frac{1}{2}C_{0s}\tilde{V}_{sM}^2$ and $\frac{1}{2}C_{0t}\tilde{V}_{tM}^2$ stand for the energy stored on the piezoelectric patches for source mode and target mode respectively. At the end of this transfer, the voltages are zero on source mode and \tilde{V}_{tm} on target mode. So the rest of the energy in circuit is $\frac{1}{2}C_{0t}\tilde{V}_{tm}^2$ which only stored in the piezoelectric element on target mode. The total dissipated energy $E_{dissipated}$ during one transfer cycle can be easily obtained by Eq.(3.29), and the dissipated power of all system can be given as Eq.(3.29)

$$E_{dissipated} = \underbrace{\frac{1}{2}C_{0s}\tilde{V}_{sM}^2}_{\substack{\text{Extracted energy} \\ \text{from source mode}}} + \underbrace{\frac{1}{2}C_{0t}\tilde{V}_{tM}^2 - \frac{1}{2}C_{0t}\tilde{V}_{tm}^2}_{\substack{\text{Extracted energy} \\ \text{from target mode}}} \quad (3.29)$$

$$P_{dissipated} = 2f_t E_{dissipated} \quad (3.30)$$

An efficiency factor η is defined in Eq.(3.31) by the stored energy in the circuit before and after energy transfer.

$$\eta = \frac{\frac{1}{2}C_{0t}\tilde{V}_{tm}^2}{\frac{1}{2}C_{0s}\tilde{V}_{sM}^2 + \frac{1}{2}C_{0t}\tilde{V}_{tM}^2} \quad (3.31)$$

If \tilde{V}_{sM} is null *i.e.* the transferred energy is zero, SSDET turns into a pure SSDI technique, and then η reduces to Eq.(3.32), where γ is the inversion factor which reflects the voltage ratio before and after inversion in SSDI technique.

$$\eta = \frac{\tilde{V}_{tm}^2}{\tilde{V}_{tM}^2} = \gamma^2 \quad (3.32)$$

In general case, the equivalent voltage \tilde{V}_t for the target mode can be expressed as the sum of two functions as shown in Eq.(3.33), one is proportional to the displacement and another one is a piecewise constant function \tilde{V}_0 .

$$\tilde{V}_t = \frac{\alpha_t}{C_0} u_t + \tilde{V}_0 \quad (3.33)$$

Considering the electric period is much shorter than the mechanical period, \tilde{V}_{tM} and \tilde{V}_{tm} can be seen to occur at the same instant that displacement u_t gets to its extreme u_{tM}^{ssdet} . They can be expressed in Eq.(3.34) and Eq.(3.35).

$$\tilde{V}_{tM} = |\tilde{V}_0| + \frac{\alpha_t}{C_t} u_{tM}^{ssdet} \quad (3.34)$$

$$\tilde{V}_{tm} = |\tilde{V}_0| - \frac{\alpha_t}{C_t} u_{tM}^{ssdet} \quad (3.35)$$

By inserting Eq.(3.34) and Eq.(3.35) into Eq.(3.31), the $|\tilde{V}_0|$ can be obtained as Eq.(3.36).

$$|\tilde{V}_0| = \frac{\alpha_t u_M^{ssdet} (1 + \eta) + \sqrt{4\eta\alpha_t^2 u_M^{ssdet^2} + 2\eta E_s C_t (1 - \eta)/n}}{C_t (1 - \eta)} \quad (3.36)$$

Since the \tilde{V}_0 always has the same sign with the velocity, thus it could be expressed in Eq.(3.37). \tilde{V}_0 is also periodic and can be expanded as Fourier series as shown in Eq.(3.38).

$$\tilde{V}_0 = |\tilde{V}_0| \cdot \text{sign}(\dot{u}) \quad (3.37)$$

$$\tilde{V}_0 = |\tilde{V}_0| \cdot \left(\sum_{n=0}^{\infty} \left(\frac{4}{\pi(2n+1)} \cos((2n+1)\omega_t t + \phi) \right) \right) \quad (3.38)$$

Combining Eq.(2.7) and Eq.(3.38), the excitation force F on target mode can be written as Eq.(3.39)

$$F = m_t \ddot{u}_t^{ssdet} + c_t \dot{u}_t^{ssdet} + \left(k_t^E + \frac{\alpha^2}{C_{0t}} \right) u_t^{ssdet} + \alpha_t \tilde{V}_0 \quad (3.39)$$

Since the displacement is assumed to remain sinusoidal during SSDET control, only the first harmonic of the piecewise constant can be considered. Thus the excitation force F can be expressed in frequency domain as (3.40), where j is the imaginary unit.

$$\tilde{F} = (-m_t \omega_t^2 + j c_t \omega_t + k_t^E + \frac{\alpha_t^2}{C_{0t}}) \tilde{u}_t^{ssdet} + \frac{4\alpha_t}{\pi} \left| \tilde{V}_0 \right| j \quad (3.40)$$

It is assumed that the force F and the speed are still in phase at the resonant frequency after the control is performed. Combining the Eq.(2.18) and Eq. (3.40), SSDET damping can be expressed by the ratio of the displacement (before control) and (after control) in Eq.(3.41).

$$\frac{u_{tM}^{ssdet}}{u_{tM}^E} = \left| W - X \sqrt{Y \cdot \frac{P_s}{(u_{tM}^E)^2} + Z} \right| \quad (3.41)$$

$$\begin{aligned} \text{where } W &= \frac{A \cdot (4\alpha_t^2(\eta+1) - (\eta-1)(A+j \cdot \alpha_t^2\pi))}{(\eta-1)(\alpha_t^2\pi^2 - 16\alpha_t^4 - A \cdot (A+j \cdot 2\alpha_t^2\pi)) + 8\alpha_t^2(\eta+1)(A+j \cdot \alpha_t^2\pi)} \\ X &= \frac{4\alpha_t}{(\eta-1)(\alpha_t^2\pi^2 - 16\alpha_t^4 - A \cdot (A+j \cdot 2\alpha_t^2\pi)) + 8\alpha_t^2(\eta+1)(A+j \cdot \alpha_t^2\pi)} \\ Y &= \frac{2\pi\eta C_t}{\omega_{0t}} \{ (\eta-1)(\alpha_t^4\pi^2 - 16\alpha_t^4 - A \cdot (A+j \cdot 2\alpha_t^2\pi)) + 8\alpha_t^2(\eta+1)(A+j \cdot \alpha_t^2\pi) \} \\ Z &= 4\alpha_t^2\eta \cdot A^2 \quad \text{and } A = \pi c_t \omega_{0t} C_t \end{aligned}$$

It can be observed that the parameters W , X , Y and Z are determined by the properties of the structure and piezoelectric elements. Thus, such damping is only the function of the extracted power P_s and the displacement before control u_{tM}^E .

3.3.2 Simulations and discussions

From the target damping Eq.(3.41), we know that the control effect of SSDET technique is determined by several parameters. In this section, we focus on three parameters which are extracted power from the source P_s , resonant frequency ω_{0t} and efficiency factor η . A numerical simulation is carried out based on the derived Eq.(3.41) and the results are plotted in Fig.3.16. In this simulation, the target displacement without control is set to one. All other parameters are normalized to their maximum value.

As shown in Fig.3.16a, the target displacement decreases when the extracted power increases. The damping effect with SSDI is also calculated by setting the extracted energy as zero and plotted in the figure. It is evident that SSDI damping is a constant value if no energy is injected into the target.

Fig.3.16b shows the the damping effect will be worse if the target resonant frequency is high. Since the vibration amplitude without control is set as one for all simulation cases, the vibration with higher frequency surely possesses larger mechanical energy, that makes it harder to suppress when the extracted power from source is constant. Meanwhile, SSDI damping is also effected by the structural

resonant frequency. Fig.3.16c shows the efficiency factor η effect. Larger efficiency factor means greater voltage inversion on the target thus bringing better damping. The point ($\eta = 0$) corresponds SSDI control effect. Three other target properties are considered in the simulation which are the force factor α_t , damping coefficient c_t and the capacitance C_t . From Fig.3.16d, we know that SSD technique performs better to the structure with low damping coefficient. Fig.3.16e and Fig.3.16f indicate that increasing the force factor α can increase the damping on the target. However, the α is directly proportional to the capacitance, and increasing the capacitance will decrease the damping which is shown in 3.16f.

3.4 An enhanced SSDET control law based on a threshold setting

As mentioned in the previous section, the extracted power P_s is related to the voltage of the source mode and can not be changed by employing the classical SSDET technique if the vibrating level of the source mode keeps constant. In this section, a threshold for the source mode voltage is presented to increase such extracted power under constant vibration amplitude of the source mode. A simple simulation is designed by using Matlab[®] to verify its effectiveness and to find the best threshold configuration.

3.4.1 Threshold setting principles

For a typically SSDET control, the switch SW_s is closed when u_t gets to its extremes in order to transfer the energy to the inductor and then the voltage V_s dropped to zero at the switch SW_s reopening instant(the end of the first step). In fact, such operation on source mode is similar with a newly developed SSD technique, so called *blind switch damping on short circuit* (BSDS) technique [17]. In BSDS, the shunt circuit switches under a random frequency for canceling the electrical charge on the piezoelectric elements. Therefore, the piezoelectric voltage returns back to zero after each switching and the electrical energy dissipates in the circuit as heat during this charge neutralization. In SSDET, the operation of step 1 achieves the same effects, the only difference is that the electrical energy is not dissipated but stored in the inductor for transferring. Hence, the analysis for BSDS technique could also be adopted for the source mode of SSDET technique. The expression of the attenuation of the BSDS technique is defined in Eq.(3.42)

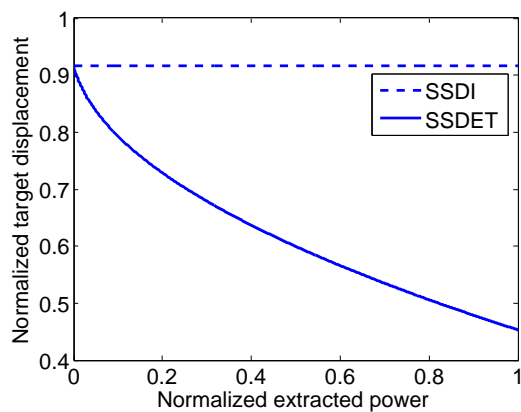
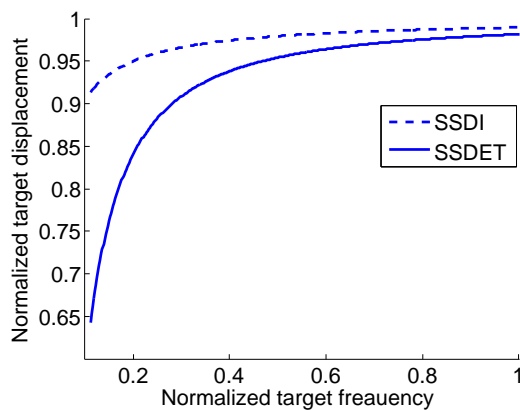
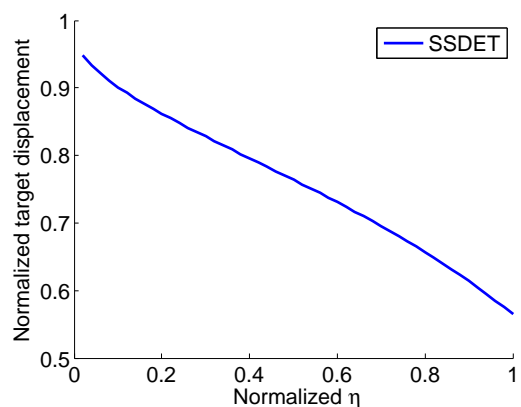
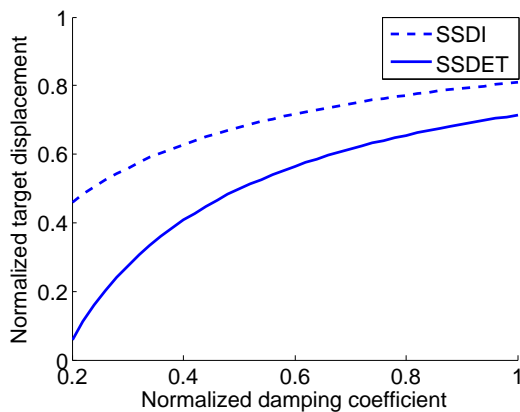
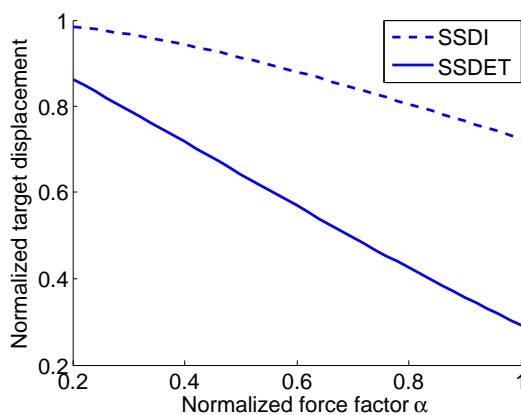
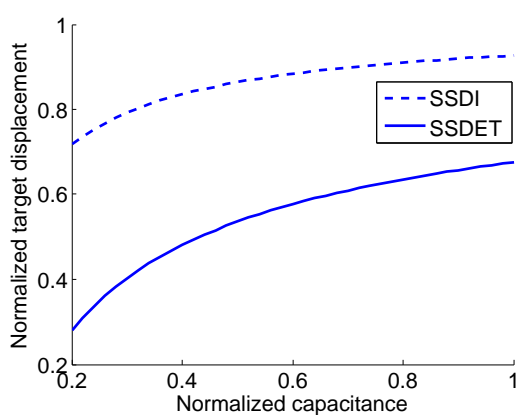
(a) Target displacement versus extracted power P_s (b) Target displacement versus target frequency f_t (c) Target displacement versus η (d) Target displacement versus damping coefficient c_t (e) Target displacement versus force factor α_t (f) Target displacement versus capacitance C_t

Figure 3.16: Target displacement versus several parameters.

$$A_{BSDS} = \frac{1}{1 + \frac{1}{c} \frac{\alpha^2 T'}{C_0 \pi p}} \quad (3.42)$$

Where T' is the vibration period of the structure and p is the number of switching per period. This equation reveals that the smaller switching times could elevate the control effect. That is to say the extracted energy from structure could be increased by adjusting the transfer times. In fact, such point also appears in [92] but no prove had been given. In this section, a simple prove is made by numerical simulation. From the equation (3.41), the damping effect is related to the extracted power, greater extracted power usually results in better damping before the system loses its stability. This conclusion implies that the damping for the torsion mode could be improved by reducing the switching times on source mode.

Consequently, a threshold setting for the piezoelectric voltage of the source mode is defined in the control law to realize such goal. Being different with the original SSDET control law, the proposed SSDET control law always compares the absolute value of the voltage V_s with the threshold when the extremes of u_t occur. The switch SW_s will be closed if the V_s is larger than the preset threshold at this moment. Otherwise, only SW_t will be closed for doing a pure SSDI on target structure. As a matter of fact, the threshold setting decreases the number of transfer times but increases the transfer energy of each time. However, the transfer energy power can be increased though there is tradeoff between these two factors which will be demonstrated in the following part.

3.4.2 Simulation validation

According to Eq.(3.28), the extracted power from source mode is proportional to the square of the equivalent source voltage \tilde{V}_s at the switching instant. Therefore, a simple time-domain simulation was designed under Matlab[®] environment to show the voltage V_s with different threshold. The flow chart of the simulation is illustrated in Fig.3.17. It should be pointed out that the damping on source mode does not take into account for the sake of simplicity. Moreover, it could be noticed that the displacement of u_s is set with an offset u_{sM} . Such configuration aims at a higher threshold even up to twice of the V_s amplitude under open circuit condition which equals to $\frac{\alpha_s}{C_{0s}} u_{sM}$. Fig.3.18 shows the normalized voltage and the displacement of the source mode under different normalized threshold. The normalized values are obtained by equations (3.43)-(3.45).

$$u_s^{normalized} = \frac{u_s}{u_{sM}} \quad (3.43)$$

$$V_s^{normalized} = \frac{V_s}{\frac{\alpha_s}{C_{0s}} u_{sM}} \quad (3.44)$$

$$threshold^{normalized} = \frac{threshold}{\frac{\alpha_s}{C_{0s}} u_{sM}} \quad (3.45)$$

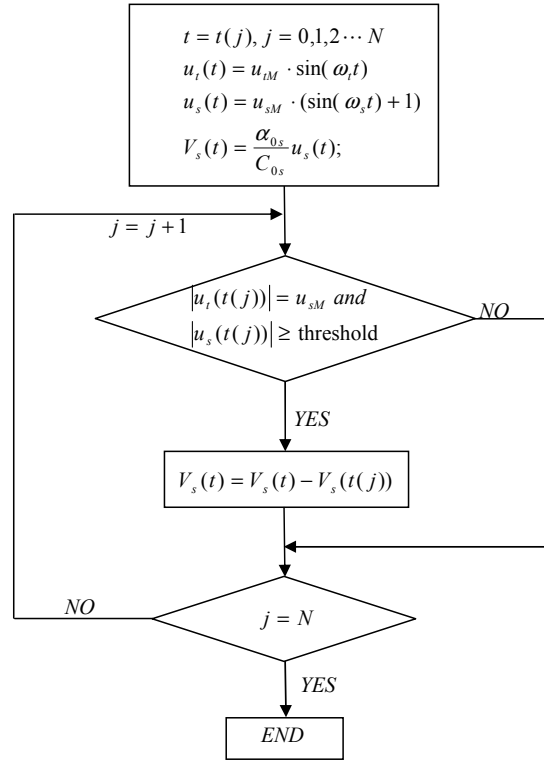


Figure 3.17: Flow chart.

From Fig.3.18, it showed that the higher threshold could decrease the transfer times meanwhile increase the voltage at the transfer instant. Particularly, when the $threshold^{normalized}$ was set to 1.8, the $V_s^{normalized}$ could increase most of the time but only drop to zero when $u_s^{normalized}$ closed to its maximum or minimum. This indicates the energy transmission path is unidirectional which is from mechanical energy (structure) to electrical energy (piezoelectric patches).

Thus, the power of the extract energy can be calculated by Eq.(3.25) and Eq.(3.28). Fig.3.19 shows that a larger threshold could obviously lead to a larger extract energy power. (Here, the power is normalized to its maximum value.) However, it could be noticed that the threshold effect is also affected by the frequency

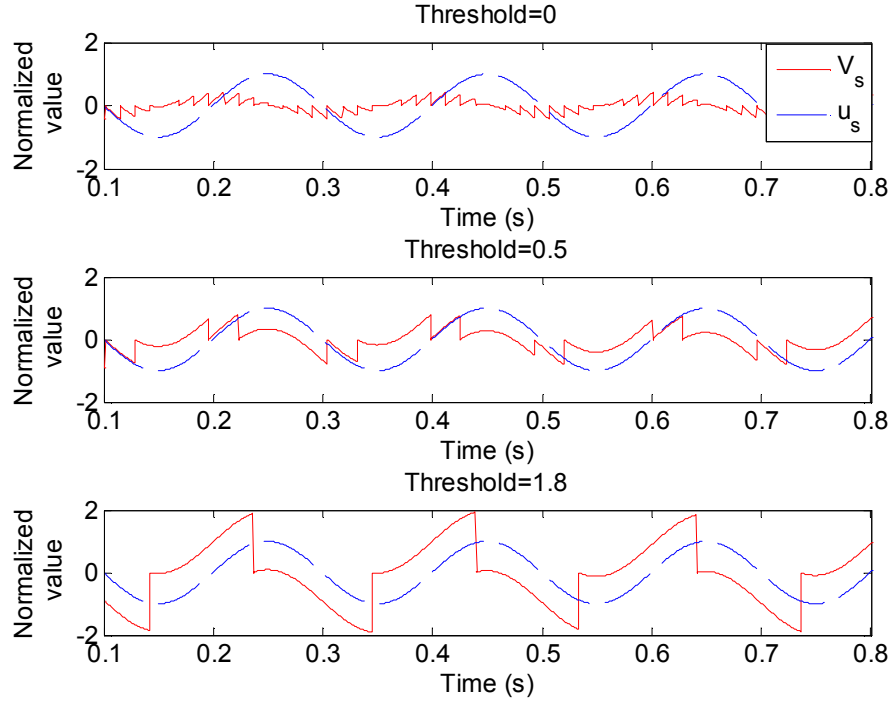


Figure 3.18: Normalized values under different normalized threshold.

ration f_t/f_s . It can be seen that the threshold could have a better performance of increasing the extract energy power at a larger frequency ratio. It is not hard to image that the extracted power should be null if such ratio approaches to infinite while the threshold is set to zero. That is because the SW_s could always be closed like short circuit condition resulting no energy can be extracted from the source structure. The simulation results also showed that whatever the threshold is, the extract power always keeps the maximum when this ratio equals to one (when both source and target are synchronized with their extrema). It could be explained that the displacements u_s and u_t would simultaneously get their extremes in this case, thus the SW_s will always be closed at the moment of the extremes u_s that leads to the maximum of the displacement difference between two consecutive switching, which image the maximum V_s could be reached at the switching instant. Such results denote that the maximum extracted power from source mode could be obtained when the switch SW_s is closed at its extremes displacement.

3.5 Conclusion

In this chapter, we present the principles of SSDET techniques in three main aspects.

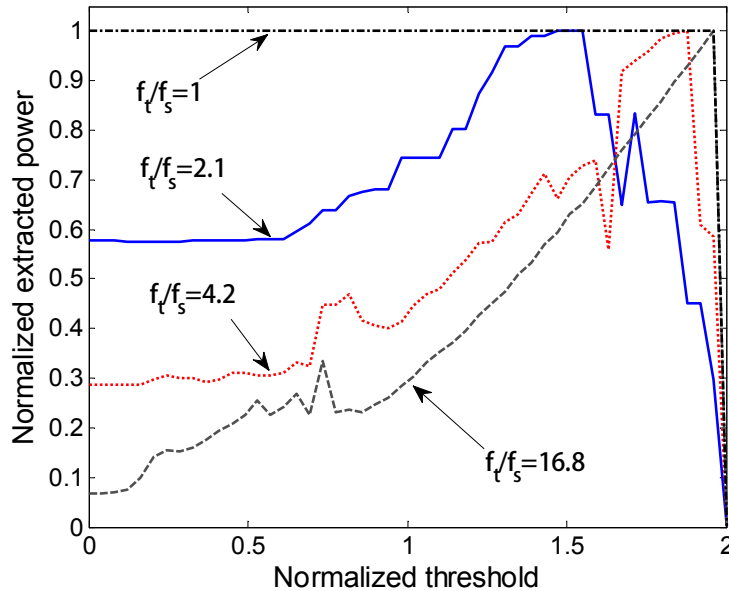


Figure 3.19: The extract energy power versus threshold with each frequency ratio.

- First, the goal of SSDET technique is introduced in which we expect damp the motion of a target by using the energy from a source. Moreover, the source is not a man-made power source but a vibrating structure or one of its vibration mode. A simple electric circuit is proposed then for delivering the energy between source and target. It reveals that the energy is transferred by a shared coil. The corresponding control law is carried out by two steps: storing the energy to the coil and transferring it to the target. Voltages cycle clearly indicates SSDET can dissipate more energy in the circuit resulting to a better daping on the target.
- Second, The mathematical models are built in both time domain and frequency domain. In time domain modeling, the state space representation is adopted to show the system behavior in different control stages. The simulation in time domain shows SSDET can increase the damping comparing with SSDI by means of greater voltage inversion. Meanwhile, the source can also be damped due to the extracted energy. Frequency domain modeling considers the relationship between the extracted power from source and the damping on the target. The transfer function of the target is obtained by mathematical means at the its resonant. the damping versus several

parameters are simulated. In addition, the system identification is briefly introduced.

- Third, an enhanced control law is developed based on the derived equations. The proposed control law can increase the extracted power form source by decreasing the switch times. Comparing with the original control law, numerical simulation results show that the enhanced control law can show a great improvement when the frequency ratio is large.

Chapter 4

SSDET experiments and discussions

In this chapter, three experiments are designed to verify the SSDET techniques. In these experiments, SSDET is conducted between different structures as well as vibration modes in one structure. A control law based on the electrical energy amount for multi-source-single-target system is tested in an experiment. The experimental results demonstrate that the SSDET can evidently improve the control effect comparing with SSDI technique. Moreover, the threshold setting can effectively increase the extracted power of the source improving the control. The stability of the SSDET control is also discussed based on the experimental results.

4.1 Introduction of the control system

A general view for SSDET experiments can be depicted in Fig.4.1. The working principle of the experimental system can be briefly described as follows. At first, the piezoelectric patches bonded on the structures are connected with the SSDET circuit which contains pulse-controlled switches (MOSFET). Then, the control system which built in Simulink environment (as shown in Fig.4.2) is written into a dSPACE ds1104 board. Finally, the sensed signals by the sensors are input to the dSPACE board for generating pulse signals to on/off the corresponding switches at the desire timing. A user interface is designed in Controldesk software (as shown in Fig.4.3) to control the whole system and observe the signals (displacements, voltages, switches on/off states).

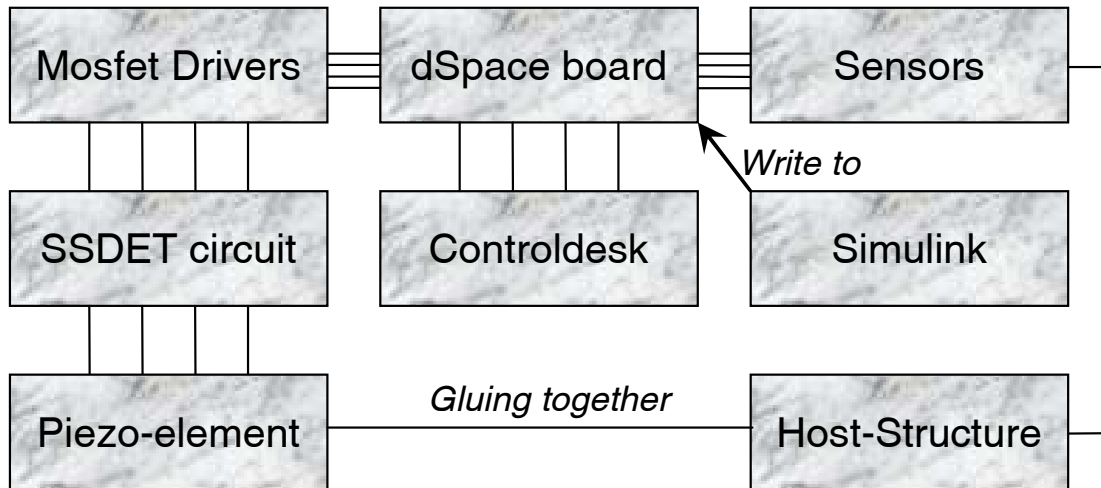


Figure 4.1: A schematic diagram of the experimental system.

The control system plotted in Fig.4.2 is the its Simulink scheme. It mainly contains six blocks: voltages input block, displacements input block, bit-out output block, voltage signs judgment block, max/min detector block and switches control block. I/O blocks consists of the A/D and D/A converters. They are used to receive the voltage signals from the instruments and generating pulse signals to control the MOSFET switch. Voltage signs judgment block is used to judge the voltage signs of both the source and target which determines the switching duration of two steps. Max/min detector is used to find the extrema of the target displacement and generate a pulse signal whose pulse width equals to one sample time. Base on the preliminary pulse signal and the voltage signs judgment, the switches control block generates a switch control pulse sequence for controlling the different switches with proper pulse widths corresponding to the control law.

4.2 Energy transfer between different structures

4.2.1 Experimental setup

The schematic diagram of the experiment is shown in Fig.4.4. The energy source structure was the cantilever beam clamped on a rigid structure shown in Fig.4.5, and the target structure was a four-edge clamped plate. Both of the two structures were made of steel. Eight piezoelectric patches (PZT) were bonded at the root of the beam with a parallel connection and their equivalent capacitance was 44.5 nF. A commercial piezoelectric patch (ACX Quickpack QP10N, PZT) with a

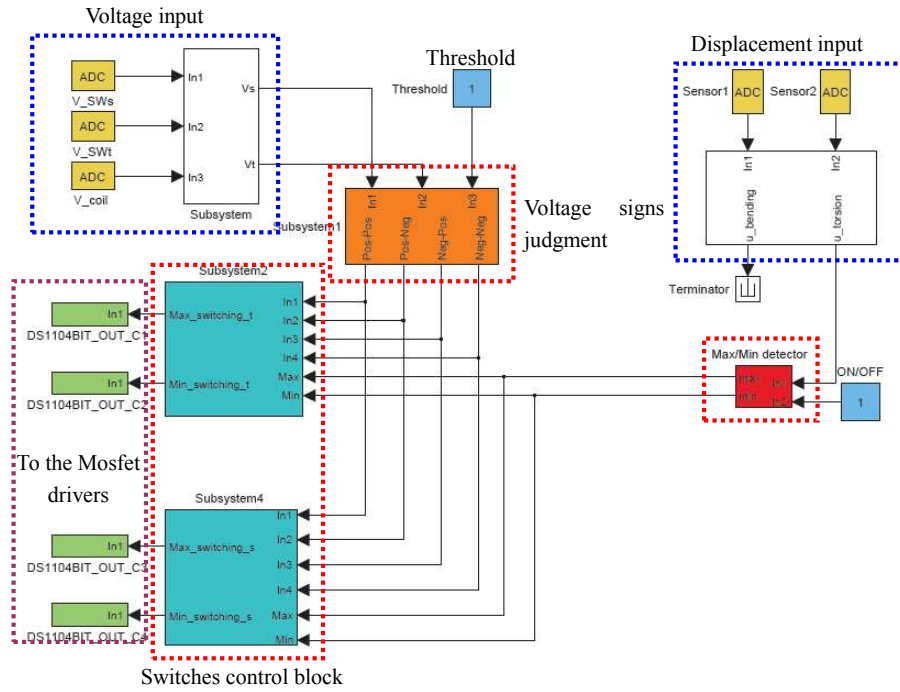


Figure 4.2: Control system designed in Simulink.

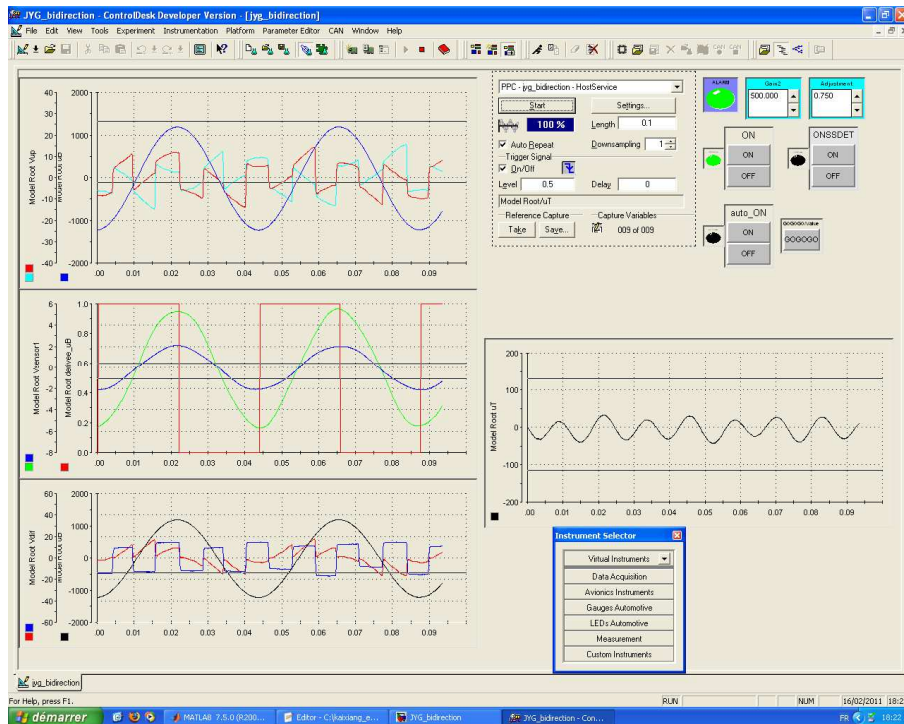


Figure 4.3: Control user interface designed in ControlDesk.

capacitance of 44.2 nF was bonded on the plate near the clamped edge in order to receive the transferred energy and damp the plate. The poling direction of all the piezoelements was perpendicular to the structure surface. The electrical circuit was simply composed of two switches (dual-MOSFETs with diodes) and a tunable inductor. The displacement of the plate was measured at its geometric center by an inductive proximity sensor. The geometric characteristics of the structures and piezoelectric elements are summarized in Tab.4.1.

The structures were driven by an electromagnet under their first-mode natural frequencies which were 22.3 Hz for the beam and 50.7 Hz for the plate. A dSPACE system was used to control the switches and store the sensed signatures. The switching control platform was developed by the simulink/dSPACE system, as shown in Fig.4.7, to detect the extremes of the plate displacement and generate a timing pulse to control the switches. From the control law Eq.(3.1), the signs of piezoelectric voltage led to two switching strategies, and it was thus necessary to detect the voltage sign of the piezoelectric patches simultaneously on both beam and plate to determine which strategy should be implemented. It should be pointed out that the switching strategy was only determined by the sign relationship between V_t and V_s at the very beginning of the step 1, and it should not be changed during the whole switching period. Thus, a holder was designed in the control system to hold the sign judgment during one switching period (both step 1 and step 2) to avoid any mis-estimating due to the voltage sign changing.

The switching duration t_a in step 1 could be precisely set since it was constant and equals to 1/4 (voltages with same sign) or 3/4 (voltages with different signs) circuit period. However, t_b was difficult to set accurately since it was a function of the initial voltage of the PZT on the plate and the current of the inductor as shown in Eq.3.1. Detecting a precise current value is not possible since it needs an extremely fine step size in the control system, leading to a heavy memory space. Moreover, the noise in the current generated during the switching instant could easily result in false current detection. Fortunately, the current direction cannot be changed, even when the switching time is larger than the precise time t_b or t'_b (in Eq.3.1). Since the diode in the switch can stop the current from another direction, this could ensure the holding of the voltage at its extremes for a certain period of time after the current drops to zero. In practice, the switching duration for SW_s was set to the half period of the RC_sL circuit, which is always larger than t_b .

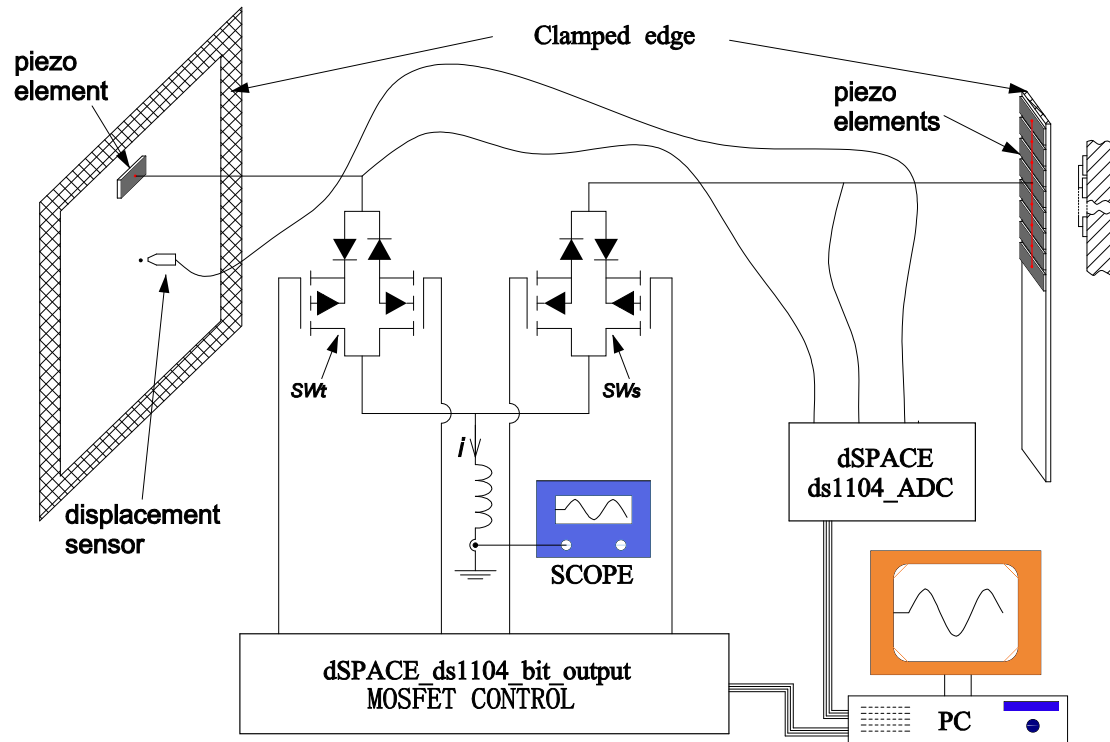


Figure 4.4: A schematic diagram of the experiment (SSDET between different structures).

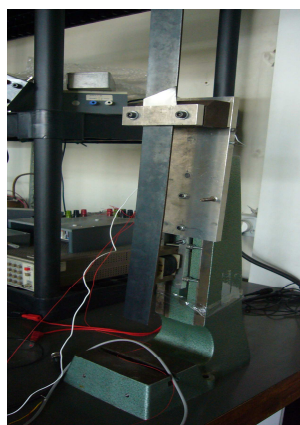


Figure 4.5: Energy source structure: A cantilever beam. Figure 4.6: Energy target structure: A four edge clamped plate.

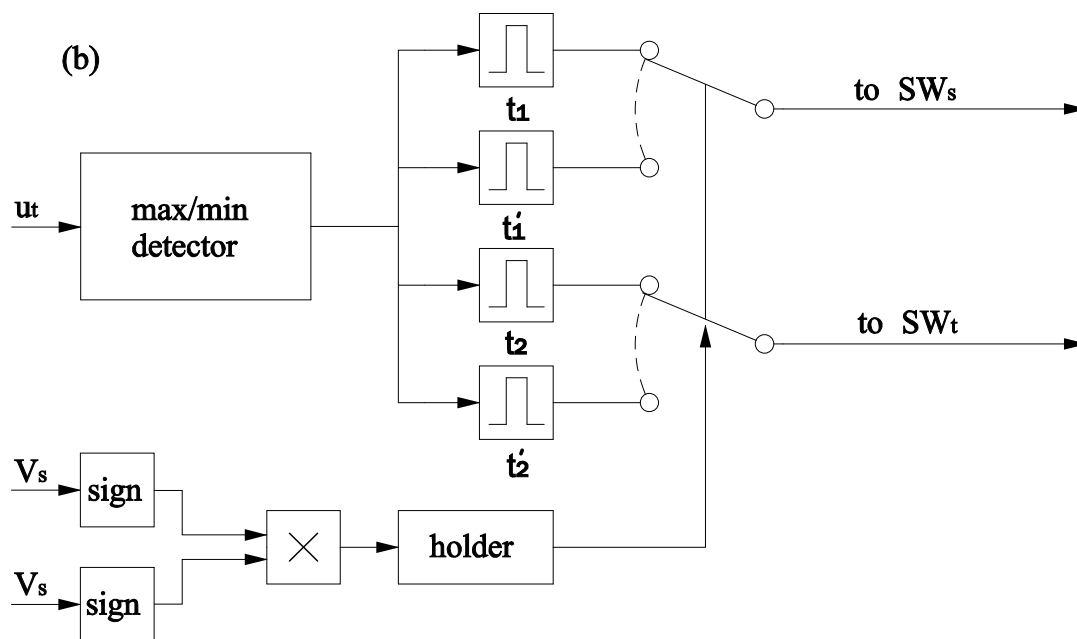


Figure 4.7: The switching control scheme.

	length(mm)	width(mm)	thickness(mm)
beam	345	4.00	2.50
plate	400	300	0.5
PZT on beam	40.0	20.0	1.00
PZT on plate	50.0	25.0	0.37

Table 4.1: Geometric characteristics.

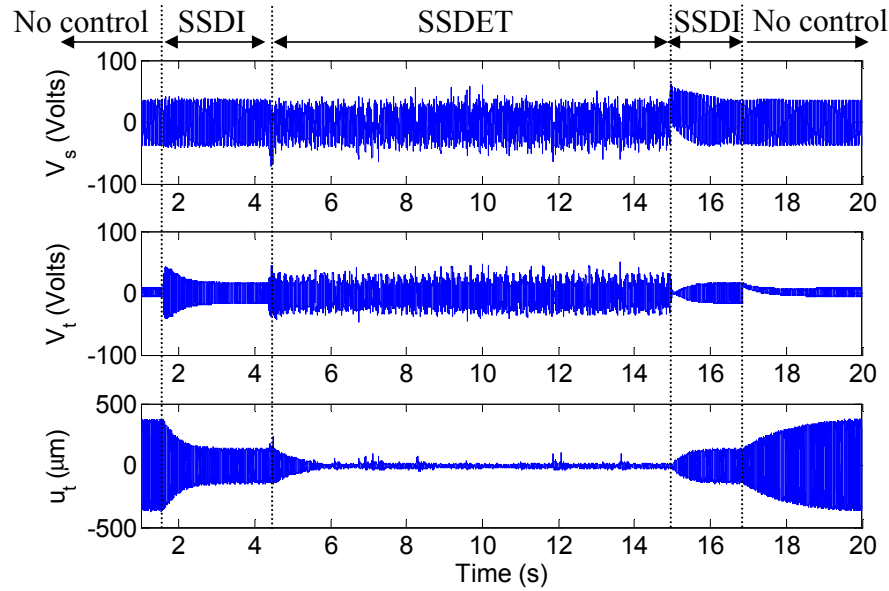


Figure 4.8: The damping of the plate by SSDI and SSDET.

4.2.2 Results and discussion

Fig.4.8 shows the damping effect of the plate by both the SSDI and SSDET techniques. The experiment demonstrated that the SSDET method gave rise to a better damping effect than the SSDI technique. At first, both structures vibrated under their first mode. The SSDI performed from 1.7 s, and the plate vibration consequently decreased in this period. When the vibration of the plate reached the stable state at 4.7 s, the SSDET approach performed the energy transfer from the vibrating beam to the piezoelectric patch on the plate and enhanced the damping effect. From 15.4 s, the SSDET was stopped and only the SSDI remained active. Finally, all the controls were stopped and the amplitude of the beam returned back to its original value after 16.8 s.

The simulation and experimental results were compared in order to confirm the mathematical model. The procedure of the simulation was the same as that in the experiment. Fig.4.9 shows the comparisons between the experiment and the simulation in various control stages. At first, two structures were subjected to a harmonic excitation at their resonance frequencies, as shown in Fig.4.9a. Subsequently, the SSDI control was performed according to Fig.4.9b, and it was found that the simulation results coincided well with those of the experiment. During each closing instant, a tiny fluctuation of the piezoelectric voltage on the beam was observed in the experiment, as can be seen in the magnified image in Fig.4.9b. It was attributed to the parasitic capacitance. Finally, SSDET control was conducted

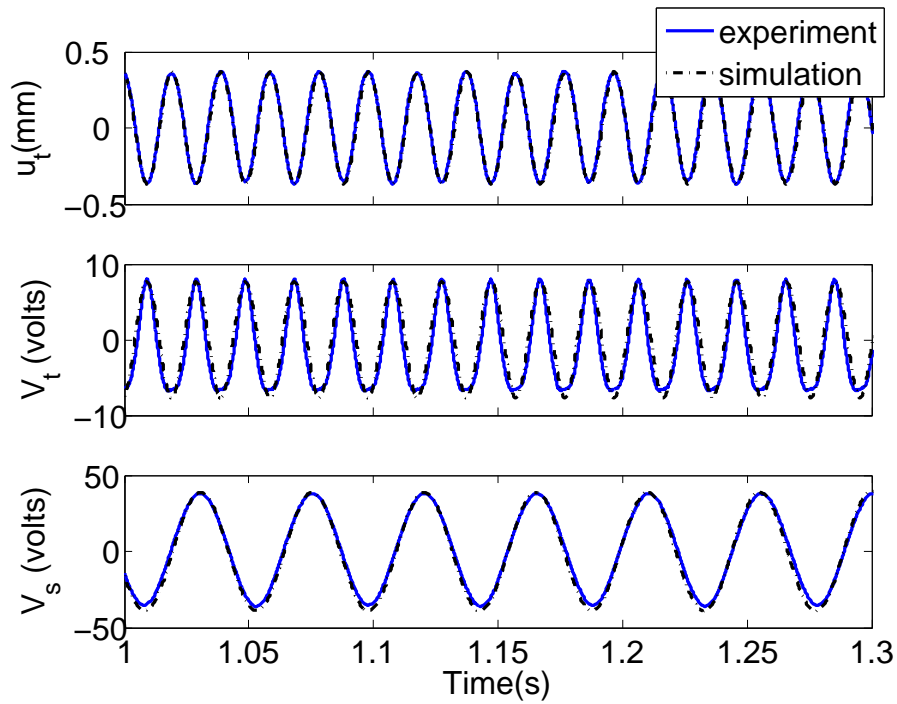
Symbol	Value(unit)
L	0.09 H
R	300 Ω
C_{0s}, C_{0t}	44.5 nF , 44.2 nF
ω_s^E, ω_t^E	139.8 rad^{-1} , 318.2 rad^{-1}
ω_s^D, ω_t^D	140.1 rad^{-1} , 318.6 rad^{-1}
m_s, m_t	135.6 g , 98.7 g
k_s^E, k_t^E	2650 Nm^{-1} , 9998 Nm^{-1}
c_s, c_t	0.2584 $Nm^{-1}s^{-1}$, 0.3017 $Nm^{-1}s^{-1}$
λ_s, λ_t	$1.6 \times 10^4 Vm^{-1}$, $2.1 \times 10^4 Vm^{-1}$
α_s, α_t	$7.2 \times 10^{-4} NV^{-1}$, $9.4 \times 10^{-4} NV^{-1}$
Q_s, Q_t	73.9, 103.7
ζ_s, ζ_t	6.8×10^{-3} , 4.8×10^{-3}
t_a, t_b	$9.3688 \times 10^{-5} s$, $1.8738 \times 10^{-5} s$
t'_a, t'_b	$2.9465 \times 10^{-4} s$, $1.8738 \times 10^{-5} s$

Table 4.2: System characteristics in simulation.

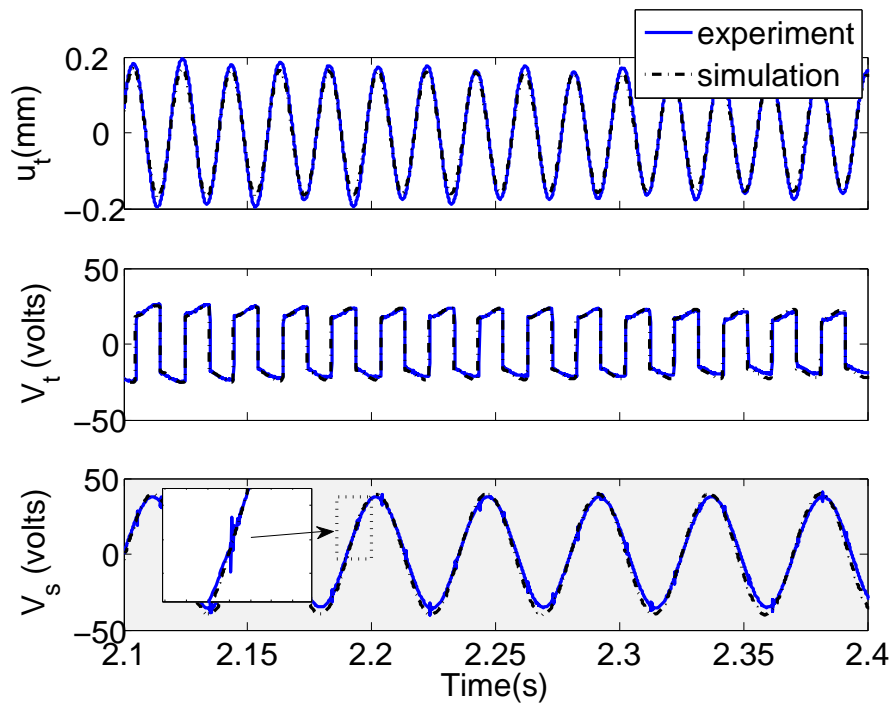
as demonstrated in Fig.4.9c. It was found that the voltage of the piezoelements on beam was consistently stopped around zero at the moment SW_s reopened (which was also when the current was at a maximum) and the voltage of the plate was consistently enhanced by the initial current during each transfer both in experiment and simulation. Consequently, the control strategy could be confirmed. It was also found that the damping was better in the simulation than that in the experiment. The voltages in simulation were larger than in experiment despite a trend that was similar to that of the experimental data. This was attributed to the max/min detector detecting a more precise extreme causing the inversion to occur at a higher voltage in the simulation as opposed to in the experiment.

4.2.3 Stability analysis

The stability of SSDET was confirmed both experimentally and through simulation. In this test, the plate was driven at its first natural frequency and was under the control of SSDI in the very beginning. The excitation of the beam was continuously increased until unstable control occurred on the plate. Fig.4.10 shows the damping effect by SSDET beyond SSDI technique. The damping effect (y -axis) is defined in Eq.4.1. Here, δ is the root mean square of the plate displacement.

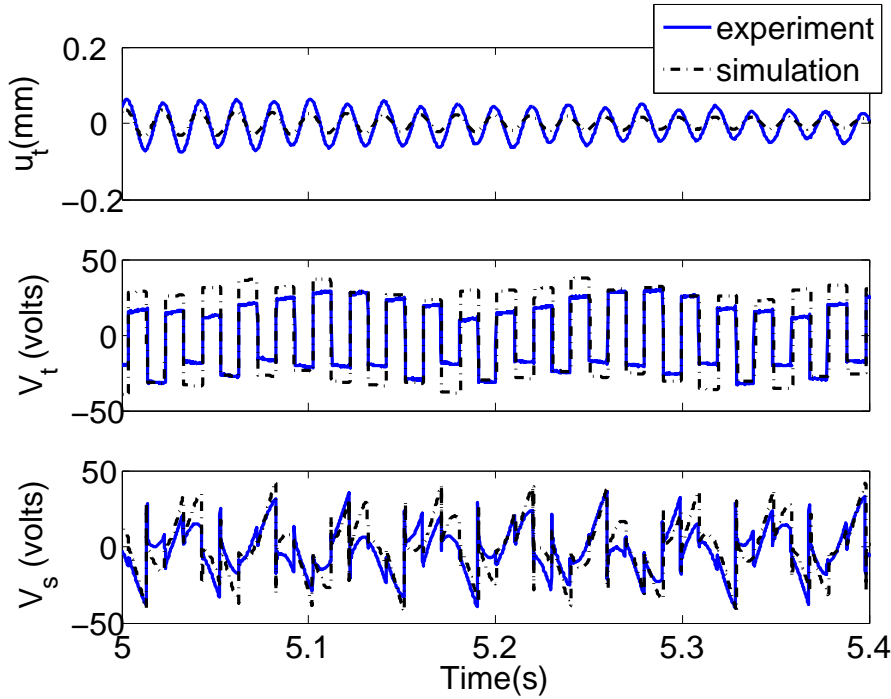


(a) Without control



(b) SSDI control

Figure 4.9: A comparison between experiment and simulation.



(c) SSDET control

Figure 4.9: A comparison between experiment and simulation.

$$damping = -20 \log_{10} \frac{\delta_{SSDET}}{\delta_{SSDI}} \quad (4.1)$$

It is clear that the damping effect increased with the beam displacement when this displacement was not too large. From the point of view of the transferred energy, it could be easily understood that more external energy was injected into the controlled structure leading to a higher inverted voltage of the PZT patches on the plate, and thus to a better damping effect. Nevertheless, as a semi-active vibration control, SSDET technique might generate instabilities. The damping effect was unable to increase monotonously when the beam vibrated with high amplitude. It was observed that the damping effect on the plate became destabilize when the tip displacement of the beam was larger than 1.8 mm in the experiment, and it even sharply decreased in simulation. One reason was that the displacement of the plate became too attenuated and was no longer sinusoidal, especially in simulation, thus resulting in an erroneous switching timing. Moreover, SSD technique, which sharply changes the stiffness of the structure, induces the residual modes which also disturb the max/min detector. This phenomenon could not be simulated by

employing an SDOF model. In fact, even though the residual mode was not excited; the displacement of the plate would still be destabilized when its vibration is low while the transferred energy would remain high as in the classical SSDV control[7].

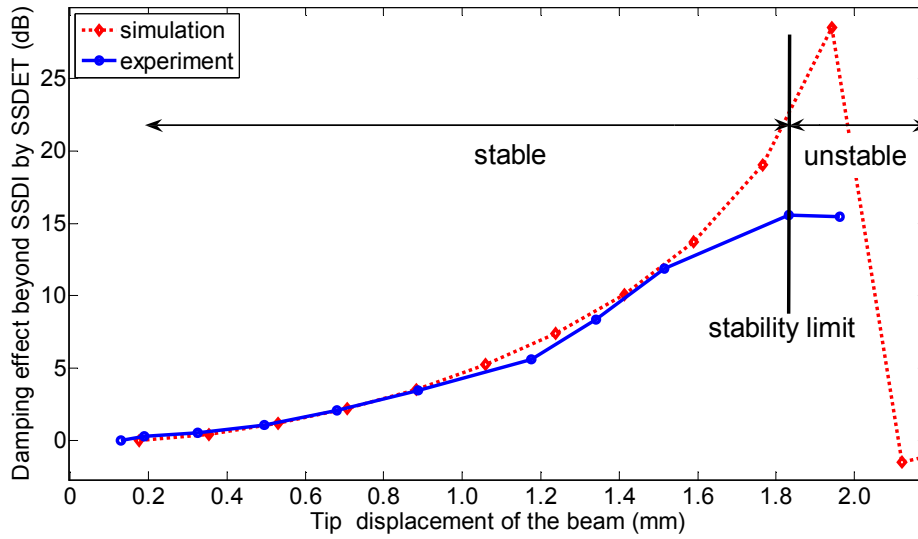


Figure 4.10: The theoretical and experimental damping effect of SSDET beyond SSDI versus the displacement of the energy-source structure.

In order to reveal the frequency components of the plate displacement, the displacement of the plate from experiment under SSDI and SSDET control was transferred to the frequency domain presented in Fig.4.11. The frequency component under SSDI was mainly the excited frequency, i.e., the first mode natural frequency of the plate. When SSDET was conducted, the first mode frequency of the beam appeared in the plate motion, which signified that the vibration frequency of the energy source structure could also affect the target structure while energy was being transferred. The experiment showed that the amplitude of this component was larger when the beam vibration level was higher, thus giving rise to a 'beating' phenomenon of the plate displacement.

4.3 Energy transfer in one structure between different modes: Harmonic response

This section aims at experimentally verifying SSDET technique on a cantilever plate. In this test, the energy is transferred from its first bending mode (source

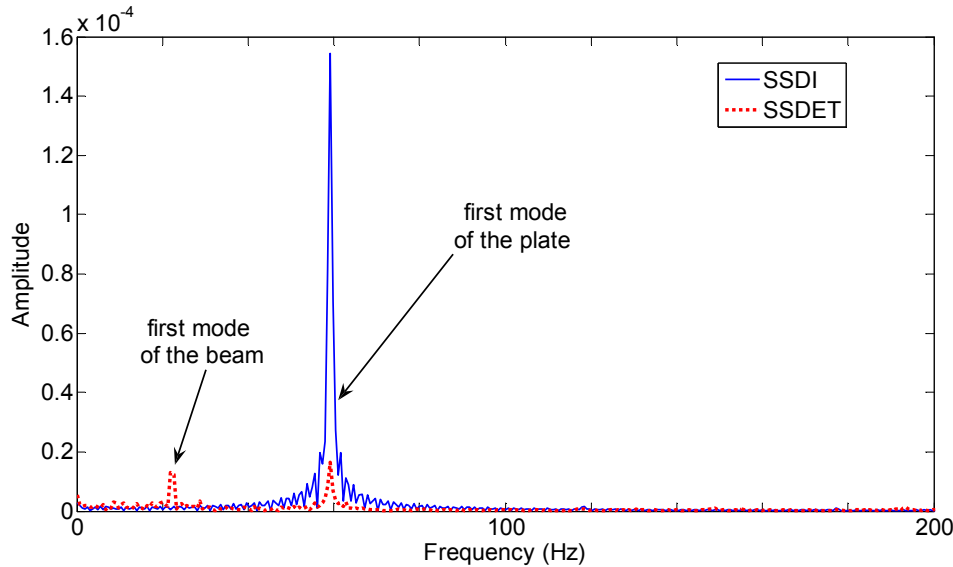


Figure 4.11: A spectrum comparison between experimental SSDI and SSDET.

mode) to the first torsion mode (target mode) so as to damp the latter. The control strategy with threshold setting was applied in experiment for sake of better damping effect.

4.3.1 Experimental setup

The experiment was carried out on a printed circuit board with one edge clamped as shown in Figure.4.12 and the schematic experimental setup was illustrated in Fig.4.13(a). The frequencies of its first bending mode and first torsion mode are 23.7 Hz and 82.5 Hz under open circuit condition. Their mode shapes are shown in Fig.4.14. As shown in Fig.4.12 and Fig.4.13(a), the plate was clamped on a rigid support and excited under a two-wave mixing signal by an electromagnet in order to simultaneously excite the first bending and first torsion mode. Two groups of piezoelectric elements (PZTs) were bonded on the plate surface close to the clamped edge as shown in Fig.4.12. The induced charge was also shown in Fig.4.14. Note that the charge show different polarities between different modes. Hence, the PZTs of group 1 can only extract the bending mode energy, and the PZTs of group 2 can only extract the torsion mode energy by connecting the PZTs of group 2 in parallel. The displacement was measured by two laser sensors at two points which were symmetric to the static line of the torsion mode. Assuming that the measured global displacements were u_1 and u_2 , thus the bending displacement

u_s equals to $\frac{u_1+u_2}{2}$ and torsion displacement u_t equals to $\frac{u_1-u_2}{2}$. Such sensing method has the same function with the *model observer* as mentioned in chapter 2.

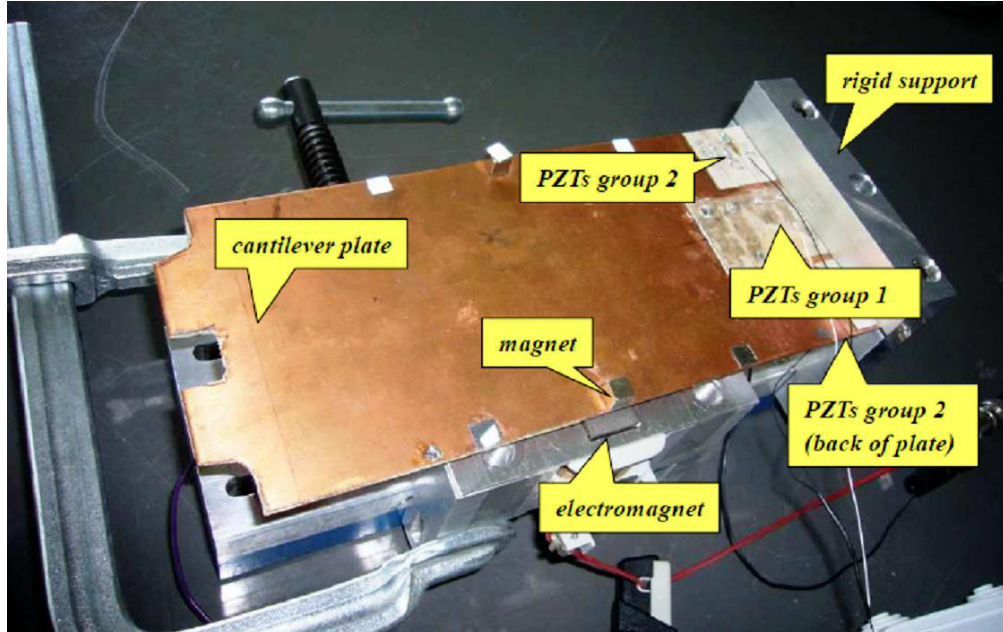


Figure 4.12: A cantilever plate with the bonded PZTs.

A switching control system, which is showed in Fig.4.13(b) was designed by Matlab/Simulink/dSPACE scheme to control the MOSFET switches. From this scheme, it could be known that switch SW_t will be always closed once u_t reaches to its extremes. However, switch SW_s could be closed when two conditions are met at the same instant. One is u_t gets to its extremes. Another one is that the absolute value V_s is greater than the preset threshold.

4.3.2 Results and discussion

The control effects are shown in Fig.4.15. The threshold is set to 5V in the experiment. The experiment was carried out as following steps. At first, the structure was excited under both bending and torsion mode without any control. And then, SSDI control was conducted on the torsion mode from 5 seconds to 10 seconds, which damped the torsion motion. During this time range, the bending mode kept its amplitude since no operation was acted on it. From 10 seconds to 17 seconds, SSDET control was conducted, and it caused obvious damping to the torsion mode. The source mode was also suppressed because its energy was extracted and transferred during this period.

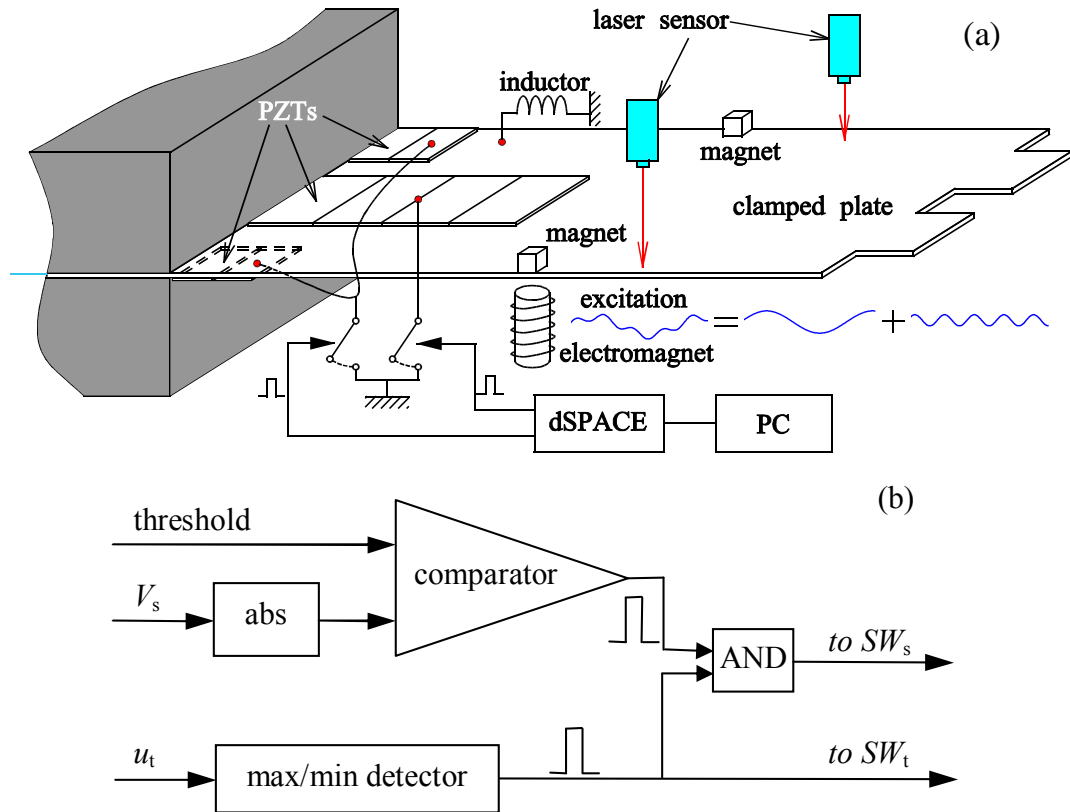


Figure 4.13: A schematic diagram of the experiment. (a) The experimental setup. (b) The switching control scheme.

The details of the displacements and voltages under different control stage are shown in Fig.4.17. A slight coupling effect could be observed from global displacement in Fig.4.17(a) and in the piezoelectric voltage of torsion mode. Such voltage waveform represented a clear SSDI waveform under SSDI operation in Fig.4.17(b). Fig.4.17(c) detailed the waveforms with SSDET control. Thanks to the threshold setting, the bending mode energy was transferred when the voltage V_s was larger than the predetermined threshold value. Otherwise, only SSDI is conducted on the torsion mode. Fig.4.16 shows the transfer function under no-control case and several SSDET with different threshold as well as SSDI control. The bandwidth range covers the torsion mode (target mode) frequency. Larger threshold would increase the damping, meanwhile the transfer function curve became not smooth any more. In fact, the system would lost its stability if the threshold is larger than a certain value which approximately equals to half of the source voltage amplitude under open circuit condition. Because the fact of threshold setting is to accumulate more energy on the source. However, it is inevitable to decrease the transfer times

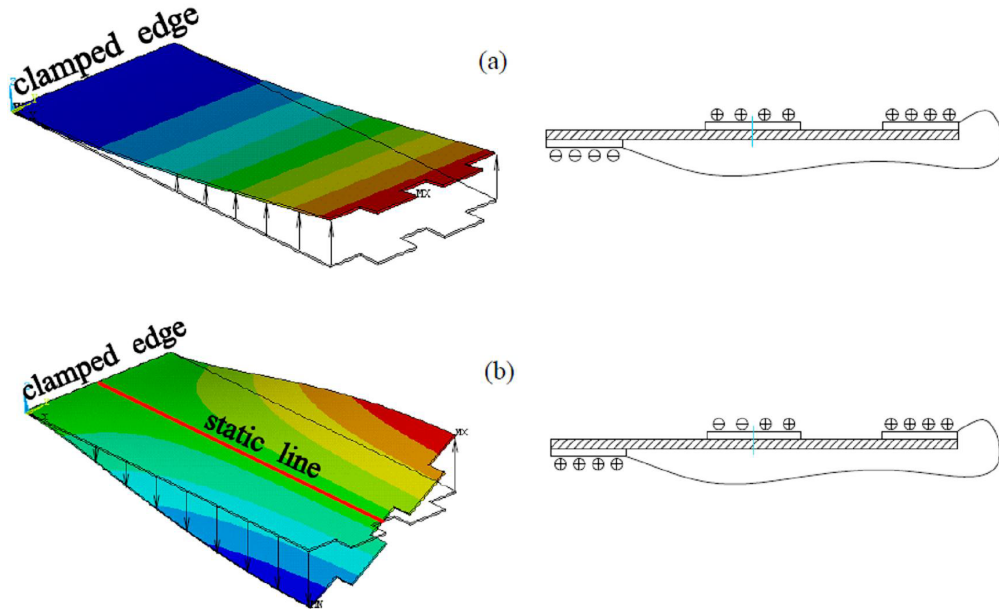


Figure 4.14: Mode shapes of the plate. (a) the first bending mode shape ($f_s=23.5\text{Hz}$) and the electrical charge distribution (b) the first torsion mode ($f_t=81.7\text{Hz}$) and the electrical charge distribution.

as we discussed before. If the threshold is set too high, there will be a long time interval between two switching which images unsteady piezoelectric force exerting on target. Moreover, the strong energy transfer leads to a great voltage inversion on the target would excite the residual modes of the structure[80].

4.3.3 Comparison between the experiment results and mathematical predictions in frequency domain

This section presented two test patterns in order to exhibit the relationship between the extract power from the bending mode and the damping of the torsion mode. The simulation, which was presented in section 3.4, was also carried out to predict the transfer times and the extracted power from the source. Moreover, the theoretical displacement of torsion mode was calculated by the Eq.(3.41) which was presented in chapter 3. These predicted values were compared with the experimental results so as to validate the proposed model. The structural properties are identified based on the methods introduced in section 3.2.3. The superscripts E and D stand for the piezoelectric elements being short-circuited and open-circuited, respectively. The mechanical quality factor Q_M was obtained from the half-power bandwidth method. λ is the proportionality coefficient between

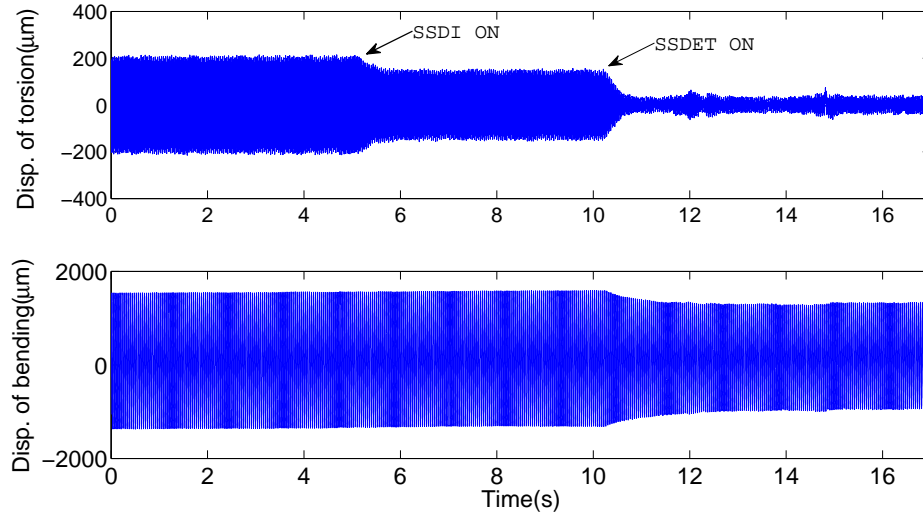


Figure 4.15: Control effect in time domain.

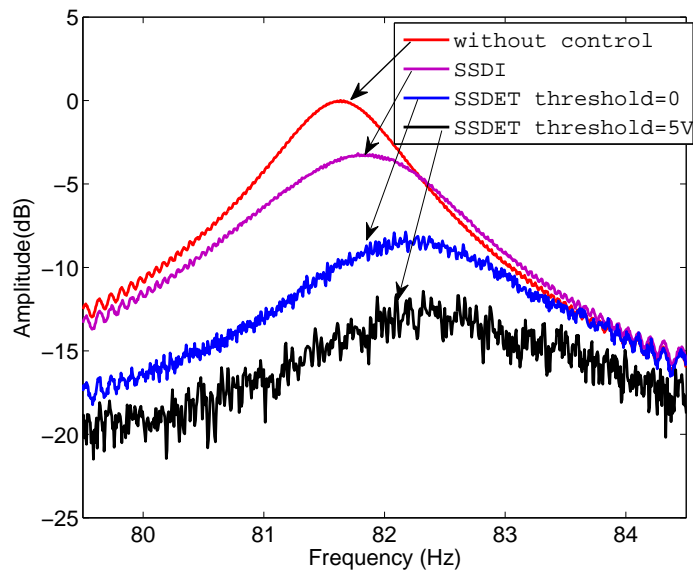


Figure 4.16: Transfer function of the plate with different control strategies.

voltage and displacement in open circuit, and ζ is the structural damping ratio. The mass, stiffness and damping are those equivalents under modal coordinate.

- Test pattern 1 (Increasing bending vs. damping on torsion)

In this test, the amplitude of the bending mode was continuously increased from 0 to 1.2 mm by turning up its excitation for the sake of larger source mode energy. As shown in Figure.4.18(a), the transfer times constantly

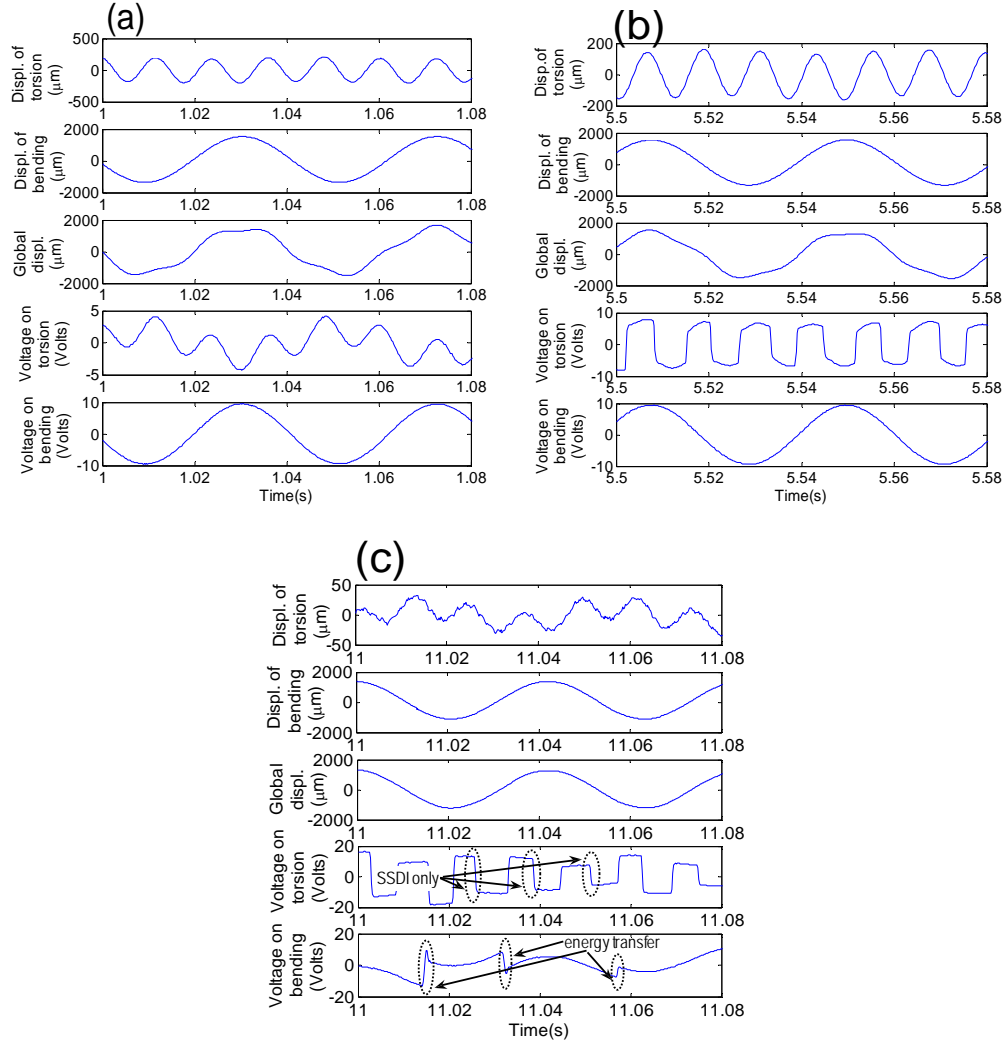


Figure 4.17: Details during different control stage. (a) Without control (b) SSDI control (c) SSDET control.

symbol	value (unit)
C_{0s}, C_{0t}	116 nF, 28.4 nF
f_s^E, f_t^E	23.7 Hz, 81.7 Hz
m_t, k_t, c_t	30.1g, 8213Nm ⁻¹ , 0.087Nm ⁻¹ s ⁻¹
α_s, α_t	3.9×10^{-4} NV ⁻¹ , 37.6×10^{-4} NV ⁻¹
Q_s, Q_t	103.7, 105.7
ζ_s, ζ_t	6.8×10^{-3} , 4.8×10^{-3}

Table 4.3: System parameters of the clamped plate.

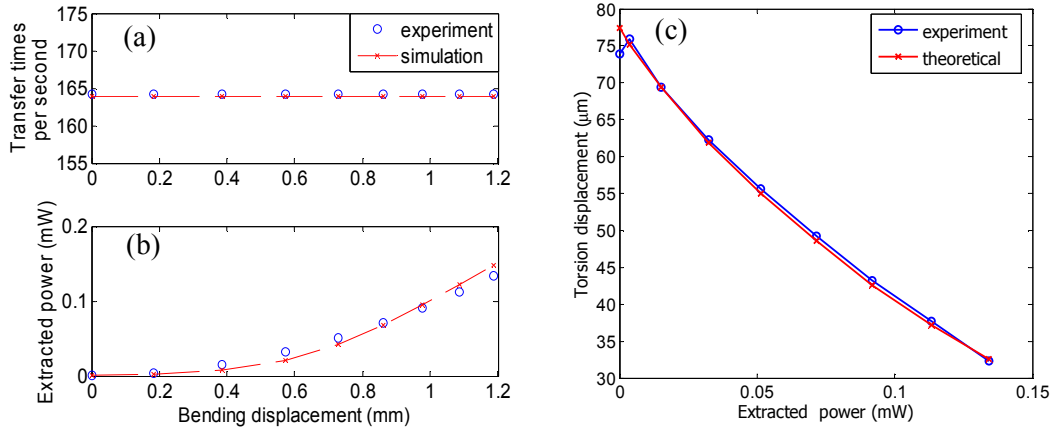


Figure 4.18: The comparison between the experiment and prediction (Increasing bending case). (a) Transfer times per second vs. bending displacement (b) Extracted power vs. bending displacement (c) Torsion displacement vs. extracted power.

equals to double of the torsion mode frequency due to the threshold was set to zero. It is clear that extracted power increased with the increasing of the bending mode displacement as shown in Figure.4.18(b). Such increasing power also brought an increasing damping shown in Figure.4.18(c). The simulation for the extract power and theoretical predictions for the torsion displacement are in a good agreement with the experimental results.

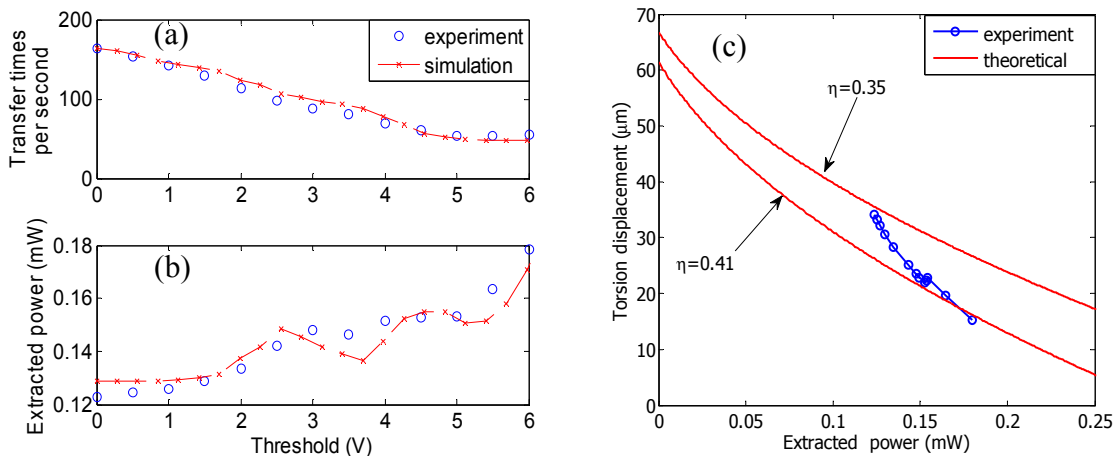


Figure 4.19: The comparison between experiment and prediction (Increasing threshold case). (a) Transfer times per second vs. threshold (b) Extracted power vs. threshold (c) Torsion displacement vs. extracted power.

- Test pattern 2 (Threshold vs. damping on torsion)

In this test, the amplitude of the bending displacement was 1.2 mm all the

time, which corresponded to the last point of the test pattern 1. The threshold was tuned from 0 to 6 volts with a step of 0.5 volts. Figure.4.19(a) showed that the transfer times per second were decreased by increasing the threshold, and the extracted power could increase up to 50% comparing with the initial point as plotted in Figure.4.19(b). Eq.(3.41) was employed to obtain the theoretical torsion displacement which was compared with the experimental results as shown Figure.4.19(c). It is shown that the theoretical prediction do not fit the experimental value very well. That is because the efficiency η changed with different threshold values. It could be observed from measurement that η decreased when the threshold increased. However, a constant efficiency was used in the theoretical calculation, which explains such difference.

4.4 Energy transfer in one structure between different modes: Impulse response

Previous SSDET work was usually carried out under the circumstance that both of the source mode and the target mode are excited under their nature frequency. This section exhibited the performance of SSDET technique for transient case. The objective of these tests is to transfer the energy from the bending mode to the patches bonded on the torsion mode so as to get better damping on torsion. Three test patterns were implemented as below.

- Impact on torsion mode when structure vibrates under its bending mode,
- Impact on bending mode when structure vibrates under its torsion mode,
- Impact on both bending mode and torsion mode.

4.4.1 Experimental setup

The transient experiment is carried out on the one edge clamped plate as we used before (shown in Fig.4.12). As listed above, the impact for the first two cases should occur when structure is vibrating under one nature mode. Thus, it is impossible to use a force hammer to excite another mode. That is because the excitation has the influence to the vibrating harmonic, and it can not be guaranteed that each impact occurs at the same phase of the harmonic (that means the same effect to the harmonic). That makes the results incomparable.

In order to handle this problem, an excitation system is designed for achieving an identical excitation under such situation. As shown in Fig.4.20, two electromagnets are placed at P1 and P2 under the plate. Meanwhile, two permanent magnets are placed on the plate corresponds the upper electromagnets. The electromagnets can be controlled in the control system which is designed by simulink. Therefore, the impact can be generated at a very precise timing which is determined by the harmonic displacement (e.g., the peak or zero-crossing instants of the harmonic motion). Such impact would be perfect for impacting the bending when structure is vibrating under its torsional mode. The impact location is just at the static line of the torsion mode. So, theoretically, only bending mode can be induced by such excitation. However, it is hard to impact the torsion mode while keeping none influence to the bending mode. For impacting both bending and torsion modes, we still use a force hammer to implement at the point P3.

In this section, It should be pointed out that all displacements and voltages are normalized to the their maximum values under open circuit case (without control).

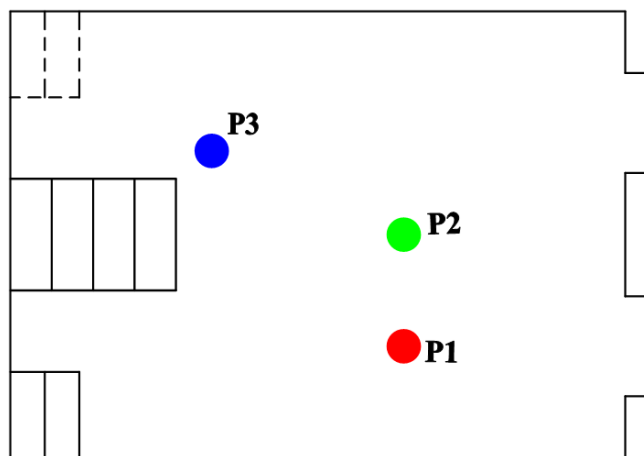


Figure 4.20: An experimental scheme of transient case (top view).

4.4.2 Impulsing torsion motion while the structure vibrates under its bending mode

In this experiment, the plate is vibrating under its bending mode by the excitation of the electromagnet under P1 at the very beginning. When the displacement of the bending mode gets to its equilibrium, a pulse signal is generated by the control device and used to drive the other electromagnet under P1. Therefore, both bending and torsion transient response could be excited. The decays of the

torsional displacement(u_t) with SSDI control and SSDET control are compared with that of open circuit case as shown in Fig.4.21. Evidently, SSDET control performed a better control compared with SSDI technique. Their voltage are also plotted in Fig.4.22. The torsion voltage(V_t) does not show an obvious enhancement comparing with that of without control. Due to the transferred energy, V_t with SSDET control showed a much higher amplitude than that in SSDI control thus leading to better damping. Meanwhile, the displacements and voltages of the bending mode under different control strategies are also exhibited in Fig.4.23 and Fig.4.24. Since the bending mode energy was partially extracted, the decay speed performs faster than that of without control. Fig.4.24b showed the energy transfer began at 0 second and finished at around 0.25 second. The length of the energy transfer duration is determined by the preset threshold. If the V_s is less than such threshold, SSDET control will be stopped.

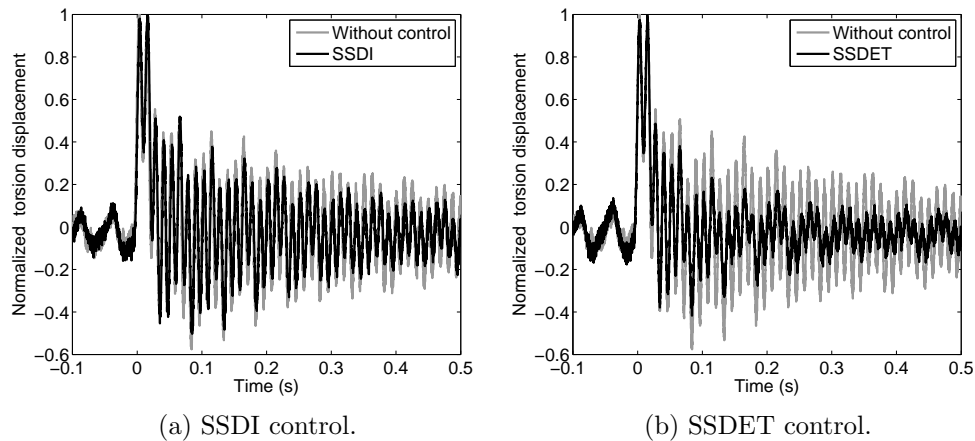


Figure 4.21: Torsion displacement as the function of time for the impulse experiment.(Impact on torsion while bending is under harmonic excitation).

4.4.3 Impulsing bending mode while the structure vibrates under its torsion mode

In this test, the plate is continuously excited by the electromagnet under P1 with the nature frequency of its torsion mode. When torsion displacement gets to its maximum, a pulse signal was generated and used to drive the electromagnet under P2 for the sake of inducing its bending mode. Fig.4.25 shows the torsional displacement after the impact on P2. P2 is on the static line of the torsion mode.

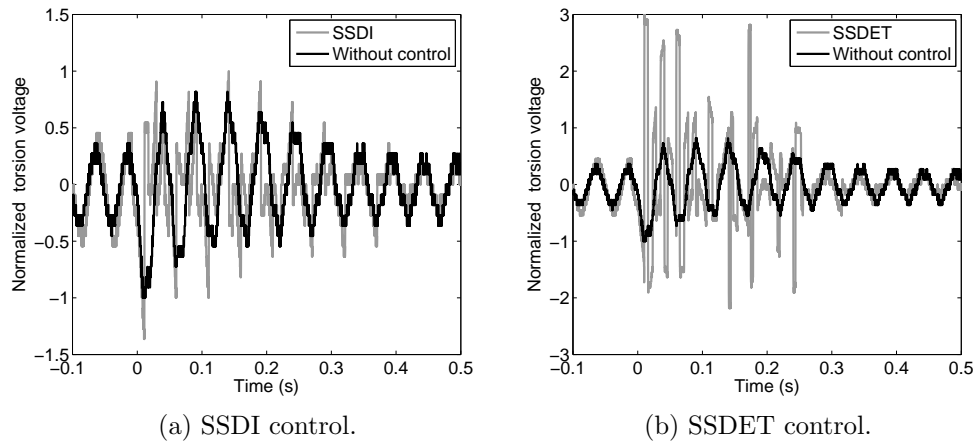


Figure 4.22: Torsion voltage as the function of time for the impulse experiment. (Impact on torsion while bending is under harmonic excitation).

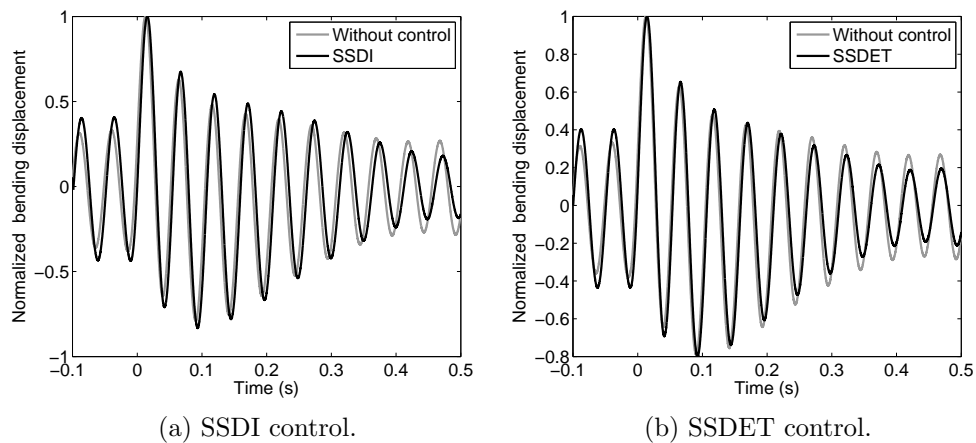


Figure 4.23: Bending displacement as the function of time for the impulse experiment. (Impact on torsion while bending is under harmonic excitation).

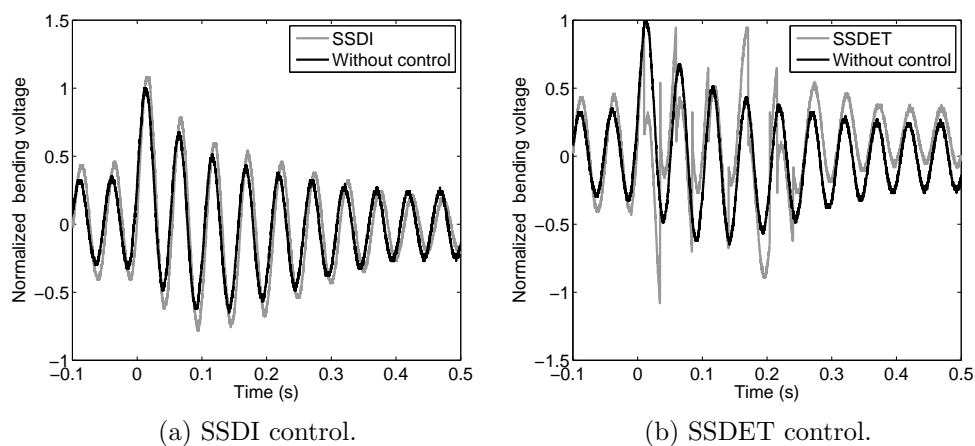


Figure 4.24: Bending voltage as the function of time for the impulse experiment. (Impact on torsion while bending is under harmonic excitation).

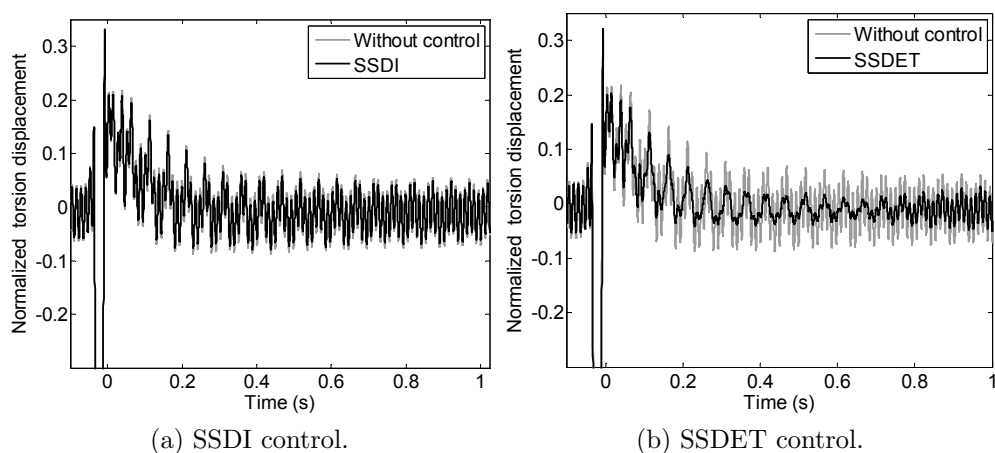


Figure 4.25: Torsion displacement as the function of time for the impulse experiment. (Impact on bending while torsion is under harmonic excitation).

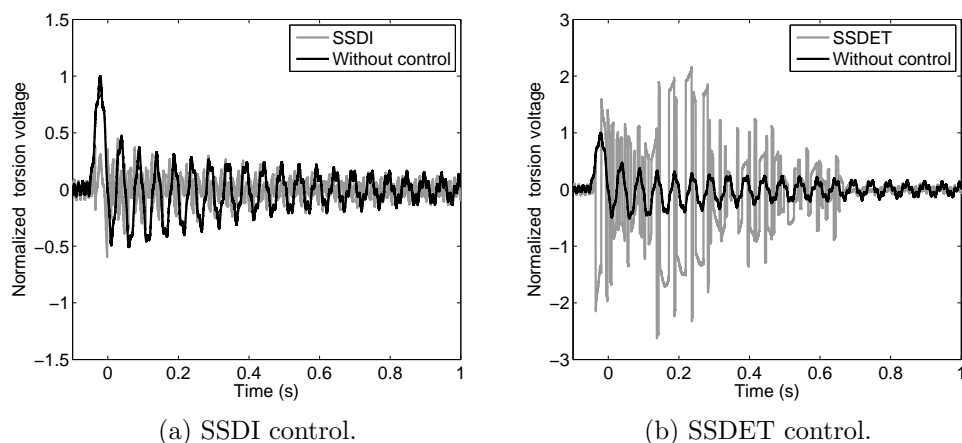


Figure 4.26: Torsion voltage as the function of time for the impulse experiment. (Impact on bending while torsion is under harmonic excitation).

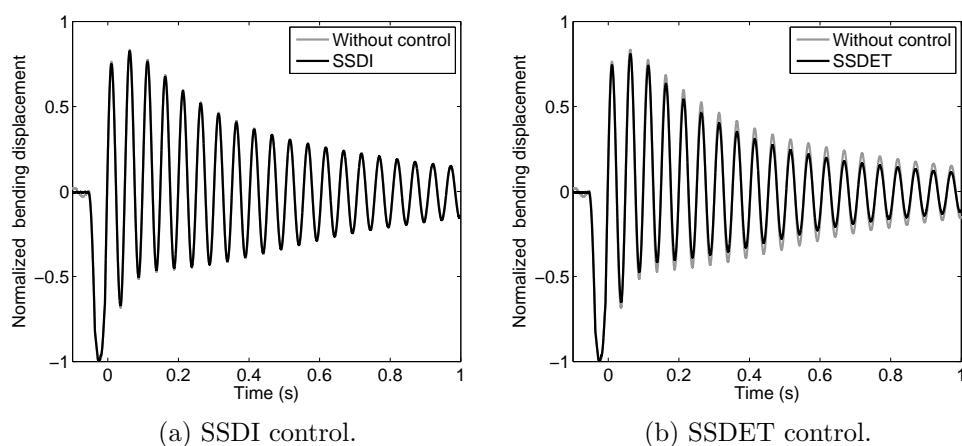


Figure 4.27: Bending displacement as the function of time for the impulse experiment. (Impact on bending while torsion is under harmonic excitation).

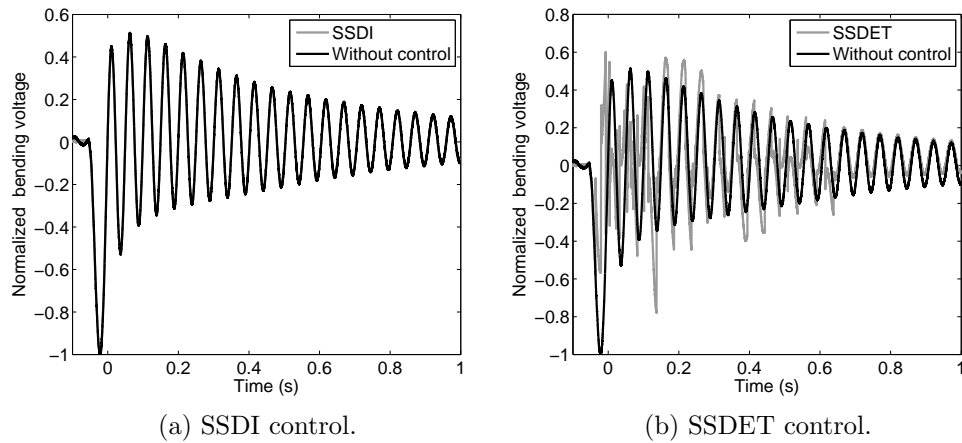


Figure 4.28: Bending voltage as the function of time for the impulse experiment. (Impact on bending while torsion is under harmonic excitation).

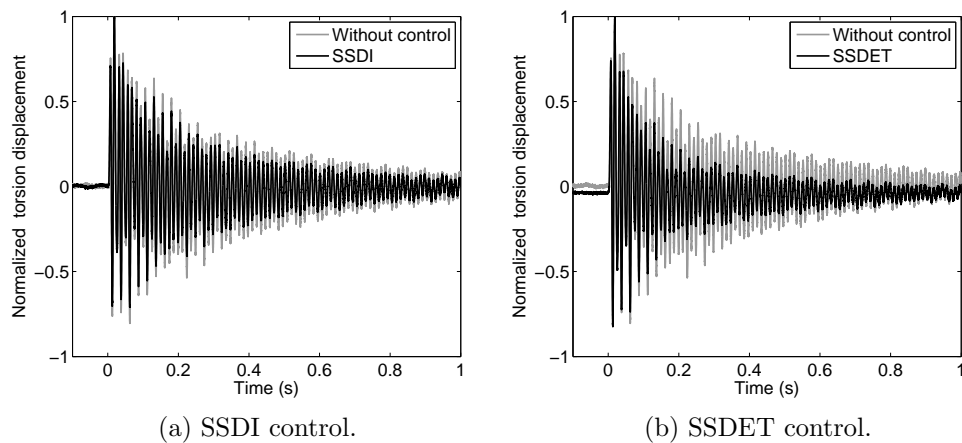


Figure 4.29: Torsion displacement as the function of time for the impulse experiment. (Both of bending and torsion mode are impacted by a force hammer).

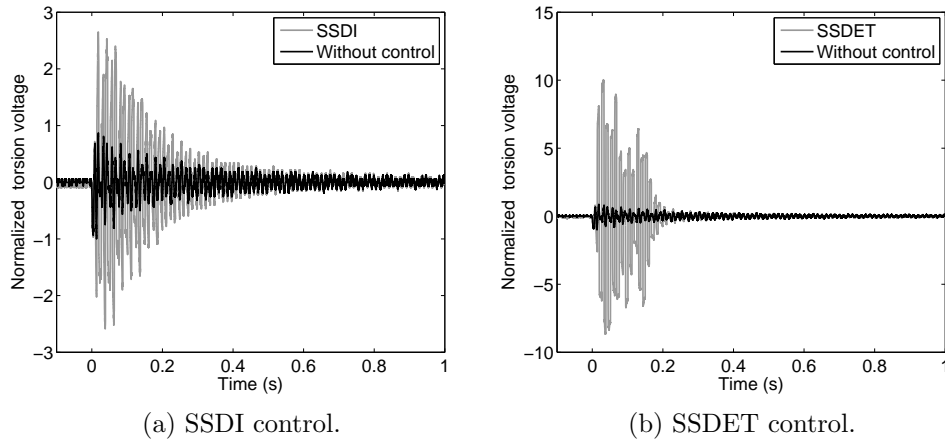


Figure 4.30: Torsion voltage as the function of time for the impulse experiment. (Both of bending and torsion mode are impacted by a force hammer).

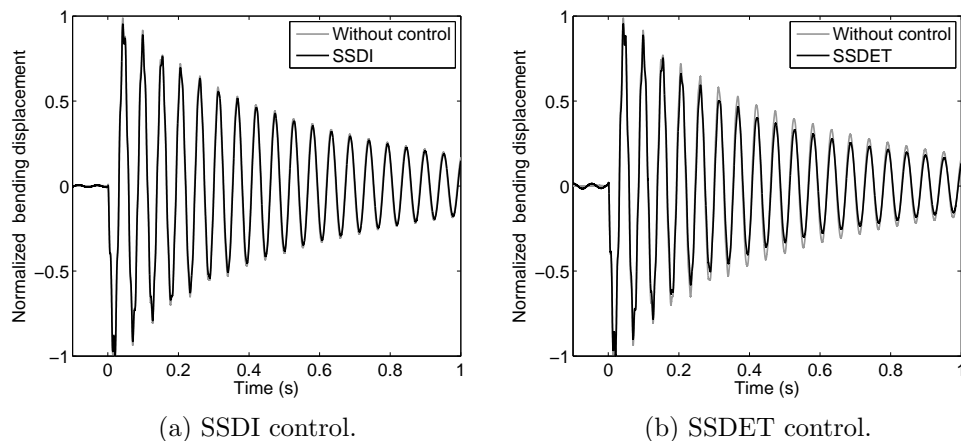


Figure 4.31: Bending displacement as the function of time for the impulse experiment. (Both of bending and torsion mode are impacted by a force hammer).

Theoretically, any excitation on this point would not disturb its torsion displacement. Nevertheless, we find that this line shift a little from where it should be. From Fig.4.25, both of bending and torsion motion can be observed after the impact though the bending ingredient is very small. It is shown that the torsion mode motion is attenuated to a very low level in Fig.4.25b during 0-0.6 seconds due to SSET control. The torsion voltages are also showed in Fig.4.26. It is evident that the torsion voltage under SSET is much larger than that under SSDI control which leads to the damping effect.

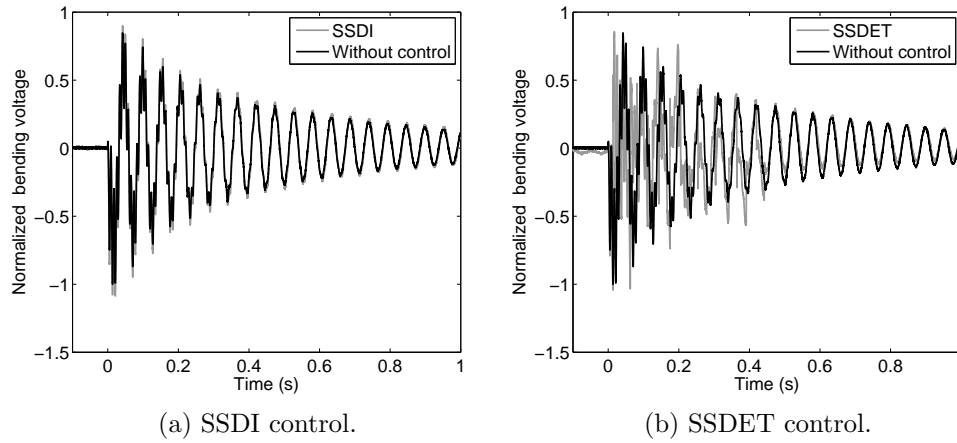


Figure 4.32: Bending voltage as the function of time for the impulse experiment. (Both of bending and torsion mode are impacted by a force hammer).

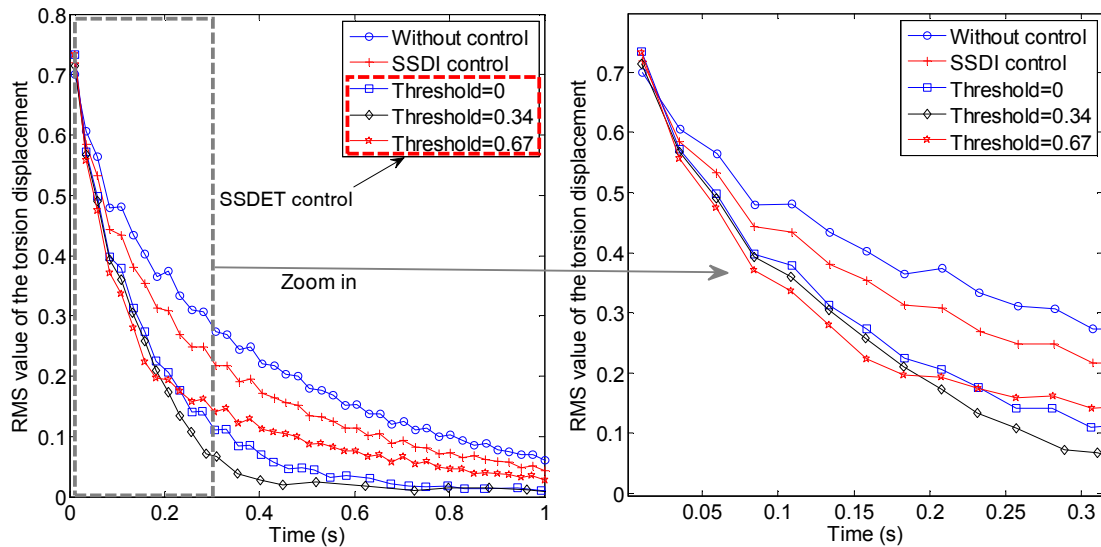


Figure 4.33: The envelope of the torsion displacement with different control strategies.

4.4.4 Impulsing both the bending and torsion mode at the same time

In this test, a force hammer is used to impact the plate at the point P3 in order to induce the bending and the torsion mode simultaneously. Compared with the first two tests, such impulsion is more close to the practical circumstance. The force signal was also recorded to make sure that each impact had almost the same

amplitude. Fig.4.29 to Fig.4.32 show the torsion displacement, torsion voltage, bending displacement and bending voltage respectively. It can be seen that SSDET can show much better damping than that of SSDI for the torsion mode motion.

The root mean square (RMS) envelopes of the torsion displacement with different control strategies are plotted in Fig.4.33. Here, the threshold value is normalized to the maximum bending voltage under open circuit condition. From Fig.4.33, it illustrated that that large threshold (Threshold=0.67) can not always bring a better control performance. In the enlarge window, it can be noticed that the decay (when threshold=0.67) is the largest at the very beginning after the impact. However, this control can not last long due to the decrement of the bending voltage. Hence, SSDET will be stopped once the bending voltage is smaller than the threshold. Overall, the setting(Threshold=0.34) shows the best performance which indicates that the threshold configuration gets to a good balance between transfer duration and extracted power.

4.5 Energy transfer between multi piezoelectric patches

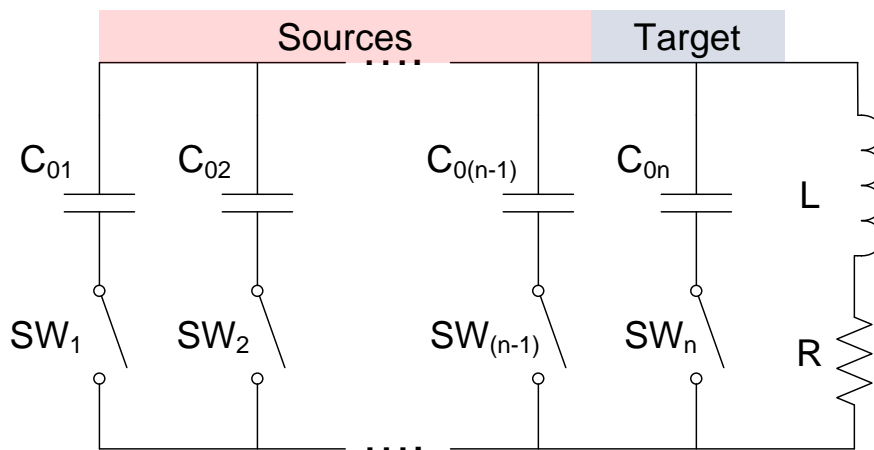


Figure 4.34: SSDET circuit for multi piezoelectric patches.

In the previous experiments, the energy is usually transferred between two piezoelectric groups. In this section, we present a system with multi piezoelectric patches. Among these piezoelectric patches, one of them is set as the target motion need to be damped, the rest are treated as energy sources. Compared with the enhanced control law (transferring the energy only at a high voltage level), the

control law for SSDET in multi-patches are similar with traditional control law which transfers the energy at every extrema of the target. However, the energy transferring is selective. Only the patch with maximum energy would be connected into SSDET circuit for transferring.

Fig.4.34 depicts the electrical circuit scheme for SSDET of multi patches. A switches controller is designed in Simulink/dSPACE system. When the target reaches to its displacement extrema, the controller calculates the electrical energy amount stored on each patch which equals to $\frac{1}{2}C_{0i}V_i^2$, where $i = 1, 2 \dots (n-1)$. Then, a timing-pulse signal will be generated to enable the switch which is connected with the patch with maximum energy. Thus, the energy transfer will occur only between the target and one patch with maximum energy each time. Comparing with traditional SSDET, the transfer energy per-time can be enhanced due to the multi sources; Comparing with SSDET with enhanced control law which decrease the transfer times, the transfer frequency with such control strategy always equals to double frequency of target vibration .

4.5.1 Experimental setup

An experiment is established for validating SSDET in multi-patches. The experimental setup is depicted in Fig.4.35. As shown in this figure, three mechanical motion forms are involved, which are bending mode motion of a steel cantilever beam and the bending and torsional modes of a one-edge clamped plate. These structures are excited under their nature frequencies. In the experiment, we set the torsional mode as the target mode, and the bending mode of the cantilever beam and that of clamped plate as two energy sources. They are named as source 1 and source 2 respectively and noted at the superscript. The control law is designed in simulink environment and built into the dSPACE board. When the torsional mode gets to its displacement extrema, a comparison will be implemented by the control system. The source which stored higher electrical energy on corresponding piezoelectric patches will be connected into SSDET circuit for energy transfer. This energy at the transferring instant equals to $\frac{1}{2}C_{0s}V_s^2$. The basic system properties are summarized in Tab.4.35. The capacitance and inductance values are used to calculate the switching closing duration based on the control law equations. It has to be mentioned that the resistance is not taken into account since small resistance has little effect to the period of the LCR oscillator.

Symbols	Values (unit)
$C_{0s}^1, C_{0s}^2, C_{0t}$	28.9 nF, 116 nF, 28.4 nF
f_s^1, f_s^2, f_t	22.2 Hz, 23.7 Hz, 81.7 Hz
L	0.09 H

Table 4.4: System properties in multi-patches SSDET experiment.

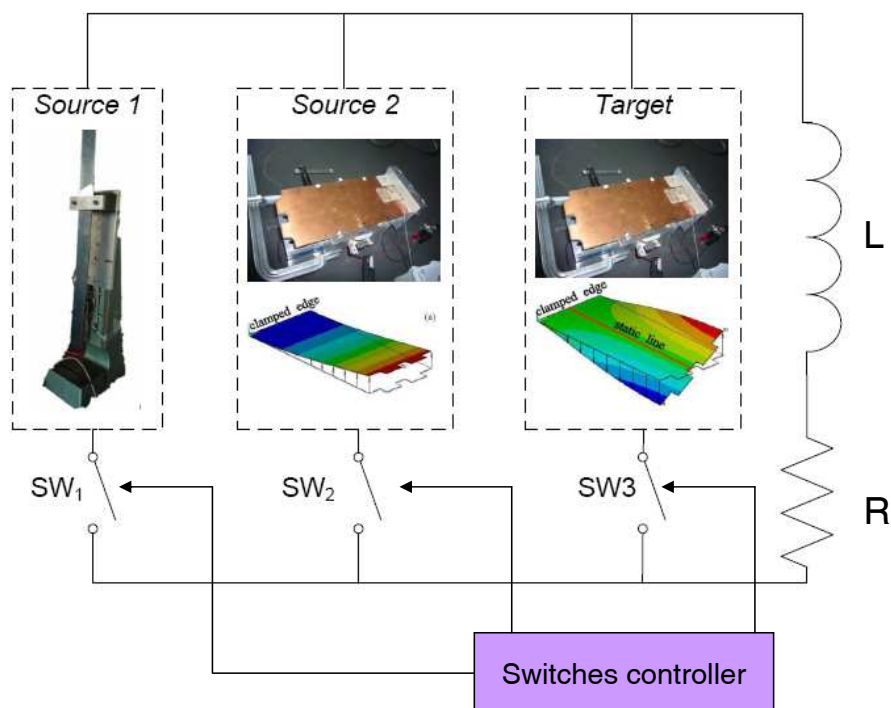


Figure 4.35: Experimental setup for multi-patches.

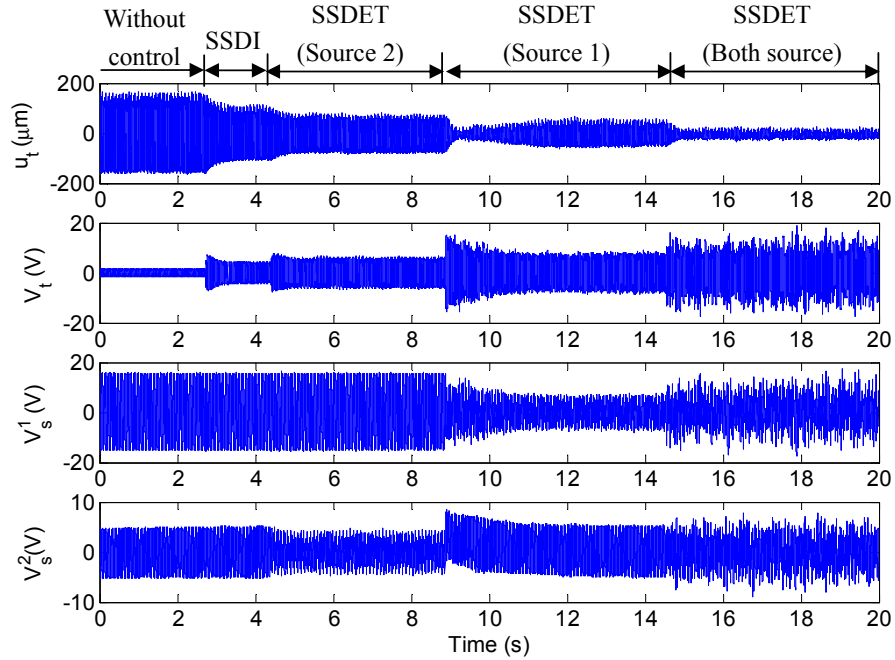


Figure 4.36: Experimental results in time domain.

4.5.2 Results and discussion

In order to compare the different control strategies, the experiment is performed in five stages as shown in Fig.4.36. In this figure, the displacement of the target (torsional displacement of the plate) and the voltages of the target and two energy sources are plotted. At first, all controls are shut down. Then, only SSDI control is conducted on the target (from 2.7s to 4.4s). It can be noticed that the voltage V_t increases compared with that of no-control. From 4.4s to 8.8s, SSDET control is running. The energy is transferred from the source2 (the bending of the plate) to the target. Thus, it shows a better damping effect on the target than that of SSDI control. After that, we did SSDET only from the source1 (the bending of the beam) to the target. Due to a higher vibration level of the source2, the damping performance can be still increased compared with the previous stage. Finally, we enable SSDET in multi-patches. It can be noticed in voltage signatures that both two sources are used as energy sources during this stage. However, only one of them are connected into SSDET circuit at each transferring depending on the its electrical energy amount. Consequently, the best damping on the target is obtained due to the largest transferred energy.

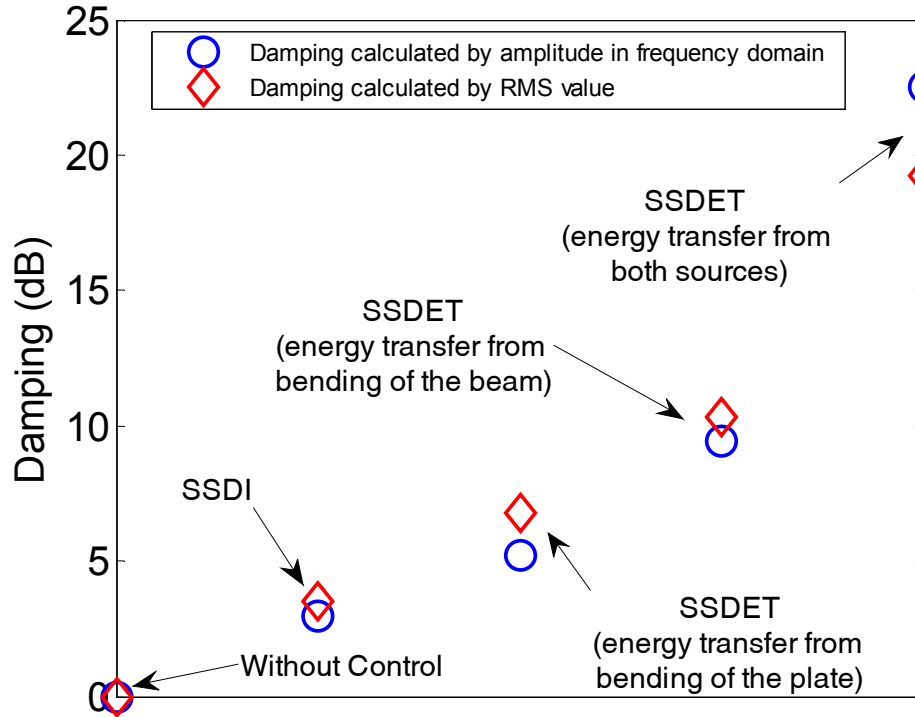


Figure 4.37: Damping during different control stages.

$$damping = -20 \log_{10} \frac{\delta_{ControlOn}}{\delta_{ControlOff}} \quad (4.2)$$

Fig.4.37 shows the damping effect during the five control stages. The damping in each control stage is calculated by two means. One is the RMS method introduced in Eq.4.2. Another is used the amplitude of the target motion in frequency domain. It shows that they nearly same during the first four stages but show a big difference at the fifth stage (SSDET in multi-patches). That could be explained that the frequency component of the source can be brought into the target which has been analyzed in SSDET between structures. And strong energy source can excited the residual modes of the target as well. Thus, the damping calculated by RMS value can describe the global control effect more precisely especially when the transferred energy is large.

4.6 Conclusion

In this chapter, we focus on demonstrate SSDET technique by experiments. Three different SSDET experiments are implemented to test this technique. They can be summarized as follows:

In this chapter, we focus on demonstrating SSDET technique by experiments. Three different SSDET experiments are implemented to test this technique. They can be summarized as follows:

- First, SSDET experiment is carried out between two structures: a cantilever beam and a four edge clamped plate. This case should be a good test bench for SSDET because there is no mechanical coupling effect between two structures. In the experiment, we transfer the energy from the 1st bending mode of the beam (as the source) to the plate (as the target) which is also vibrating under its 1st mode (1-1 mode). The results show that SSDET can obviously increase the damping on the plate comparing with that of SSDI. Moreover, the experimental results show a good agreement with the time domain simulation. The experiment also reveals that higher vibration level of the source (which indicates larger transferred energy) can bring better damping on the target.
- Second, SSDET experiment is done on a one edge clamped plate between its bending and torsion modes. Due to the motion coupling between the bending and torsional mode, the bonded piezoelectric patches are divided into two groups and distributed at the optimized place in order to extract the energy from their corresponding mode. The energy transfer path is from the bending mode (as the source) to the torsional mode (as the target). The results verify SSDET technique in this circumstance and also the effectiveness of the threshold settings. The experimental results are compared with that of mathematical model in frequency domain. The extracted power also compared with that of the numerical simulation for the threshold. It shows that the experimental results fit well with the analytical predictions. A SSDET experiment is carried out for attenuate the transient motion as well on this structure.
- Third, we use SSDET between multi group patches. In this experiment, three vibration modes of two structures are involved. The target is still the torsional mode of the one edge clamped plate, but the source could be alternatively a steel beam or the bending mode of the plate. Only the one

with higher electrical energy is connected into the circuit as the source at the transferring instant. With such control strategy, it results in a higher transferred energy to control the target.

- In addition, SSDET stability is discussed in these experiment. It is found that the frequency component of the source motion appears in the target. When the source structure vibrates under a high level, this component become obvious. We also found that the system may lose its stability when the transferred power is too large. We attribute it to two reasons: (a) The displacement is no longer a sine wave with drastic damping effect. Thus, the max/min detector can not detect the extreme instant correctly. (b) Large energy transfer also induces residual modes of the structure.

Chapter 5

Bidirectional SSDET: A preliminary research

In the previous sections, the proposed SSDET technique pumps the mechanical energy and transfers it between different structure or modes to damp one motion. In this technique, the piezoelectric patches can only extract the energy from corresponding mode and the energy transfer patch is always from source patches to target patches. However, there are kinds of connections if multi patches are distributed on the structure. In this chapter, we introduce four different connections between two patches and simulate their dynamic behaviors by Matlab/Simulink. Base on a bending-torsion coupling vibrating structure, we also propose a bidirectional SSDET method in which every piezoelectric patch can extract all modes energy and the energy transfer path is bidirectional between two patches. Experimental results demonstrate that the bidirectional SSDET can achieve a best damping on both bending and torsion motion among all proposed connections.

5.1 A bending-torsion coupling vibration case

The bending-torsion vibrating clamped plate is employed to illustrate the principles bidirectional SSDET as shown in Fig.5.1. As shown in this figure, there are two groups of piezoelectric patches bonded on the upper and lower surface of the clamped plate, and they are not connected together at first. In the scheme, we still have the energy source mode which is bending mode and the target mode which is torsion mode. Our goal is to damp the target mode motion by using the bending

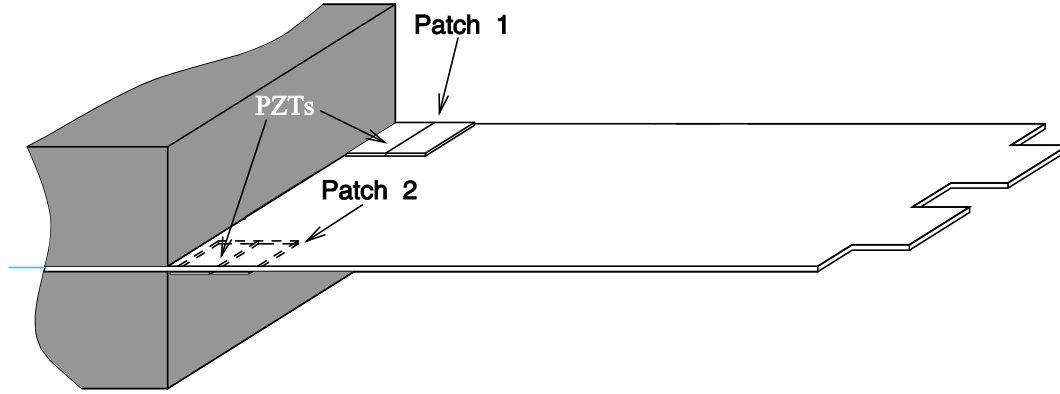


Figure 5.1: A bending torsion coupled vibrating plate.

mode energy as well. It is assumed that the bending mode frequency f_s is less than the torsion mode frequency f_t .

Because the induced piezoelectric voltage can be attributed to both bending and torsion motion, it could not be always enhanced due to the vibration frequency difference between bending and torsion motion if we only implement simple SSDI technique. This can be demonstrated in the following sections. Bi-directional SSDET is developed to solve such problems. That is to keep all voltages being enhanced though bidirectional energy transfer.

If the bending and the torsion motion can be written as Eq.(5.1), then their voltages can be defined as V_1 and V_2 in Eq.(5.2) under open circuit condition.¹ Where, the subscripts s and t stand for bending mode (source) and torsion mode (target). From this equation, we know that the voltage can be represented as the sum of two parts: torsion induced voltage and bending induced voltage. Moreover, the torsion induced voltage are is always in-phase and the bending induced voltages are opposite phase. Fig.5.2 shows the displacement and voltage waveforms. No matter how we connect the two patches, the piezoelectric forces exert on bending mode F_s and torsion mode F_t can be calculated in Eq.(5.3).

$$\begin{aligned} u_s &= A_s \sin(\omega_s t + \varphi_s) \\ u_t &= A_t \sin(\omega_t t + \varphi_t) \end{aligned} \quad (5.1)$$

¹Here, we consider the global displacement can be uncoupled as the bending motion and torsion motion.

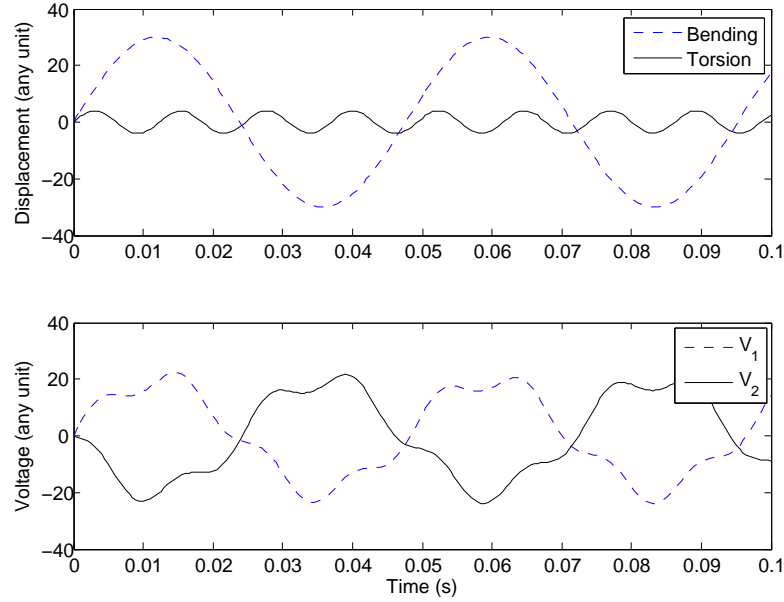


Figure 5.2: Displacement and voltage waveforms when structure vibrates under bending and torsion modes.

$$\begin{aligned} V_1 &= \frac{\alpha_t}{C_1} u_t + \frac{\alpha_s}{C_1} u_s \\ V_2 &= \frac{\alpha_t}{C_2} u_t - \frac{\alpha_s}{C_2} u_s \end{aligned} \quad (5.2)$$

$$\begin{aligned} F_s &= \alpha_s (V_1 - V_2) \\ F_t &= \alpha_t (V_1 + V_2) \end{aligned} \quad (5.3)$$

5.2 Damping behavior comparisons between four connections with SSDI control

Before we introduced bidirectional SSDET technique, four electrical circuits are employed to implement the SSDI technique when the structure is vibrating under its bending and torsion modes. Their dynamic behaviors are simulated under Matlab/Simulink environment.

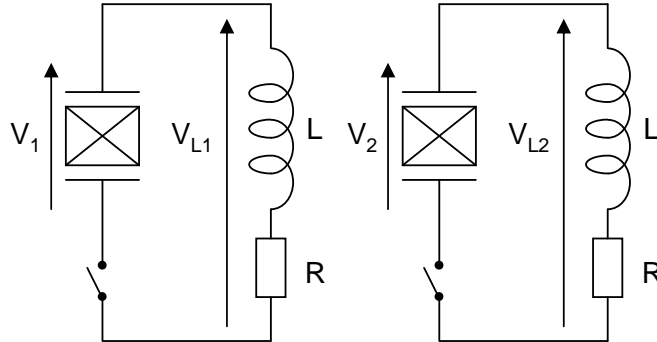


Figure 5.3: Electrical scheme for two electrically separated SSDI control (Case-A).

5.2.1 Case-A: Each patch is connected into a standalone SSDI circuit

In this part, the two patches are connected into two SSDI circuits separately as shown in Fig.5.3. The main control target is the torsion mode (target). The control law is to close both two switches during one half of the oscillation period of the LCR circuit when torsional displacement extrema occur.

Fig.5.4 shows the simulation results under such control. These values are normalized to their maximum in this time window. From this figure, we know that V_1 and V_2 do not exhibit a periodical waveform. However, we can calculate the forces which are exerted on bending mode and on torsion mode respectively from Eq.(5.2). Since the switching is not synchronized with the bending mode motion, the F_s (force in bending mode) waveform is irregular and do not always opposite to the bending mode velocity. However, if we treat $F_s \dot{u}_s$ as a stationary random process and the integration of this item in time domain $\int_0^t F_s \dot{u}_s dt$ should be small, it would have a little damping effect to the bending mode². The force exerted on the torsion mode shows a typical SSD waveform. That is the force F_t always anti-phase with the torsional velocity. Therefore, the torsional motion can be reduced.

5.2.2 Case-B: Two patches connected in parallel

The connection in parallel is common used when multi-patches are bonded on the host structure. Because one electrode of each piezoelectric patch will be inevitably connected together when their electrodes are exposed and the host structure is

²We consider the poor correlation between F_s and \dot{u}_s . Because the switches are on-off synchronously with the torsion peaks but not the bending ones. The damping on bending can be attributed to the loss during the switching.

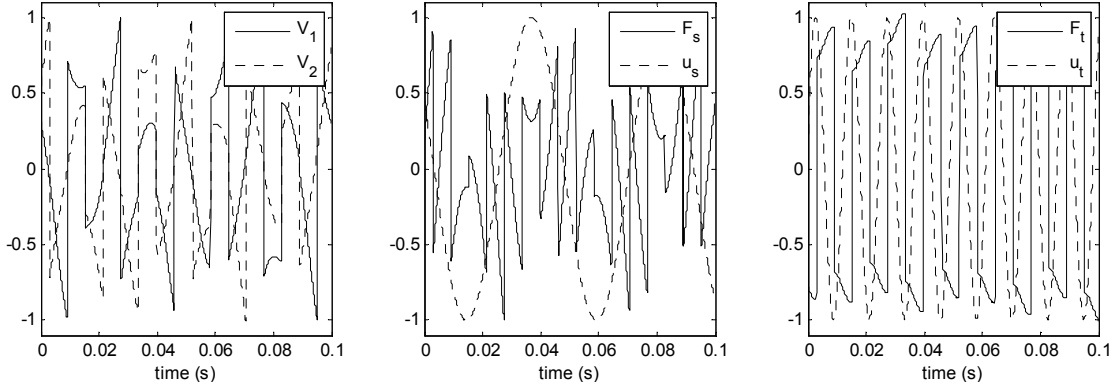


Figure 5.4: Normalized voltages, piezoelectric forces and displacements for two separate SSDI control (Case-A: simulation results).

conductive. If we connect the rest electrodes together, that makes the electrical circuit given in Fig.5.5. As shown in this figure, only one inductor is used in the circuit. The control law is still to close the switch for one-half period of the LCR circuit at the torsional displacement extrema.

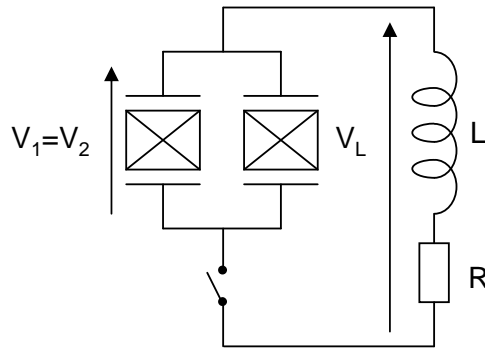


Figure 5.5: Electrical scheme for the SSDI control with two patches in parallel (Case-B).

Fig.5.6 shows the waveforms in simulation. Because they are connected in parallel, their voltages are always same as shown in the figure. Both their voltages show a steady SSD waveform in which they are inverted at each extrema of the torsion displacement. It can be seen that force F_s exerted on the bending is null. Because the bending induced charge will be canceled all the time if they are connected in parallel. That indicates the bending energy can not be extracted at any moment. However, this electrical scheme is equivalent to short-circuit condition for the bending mode. It results a shift of the mechanical transfer function around

the bending nature frequency. The force F_t still shows a typical SSD waveform, that is the force always has a different direction with the torsional velocity.

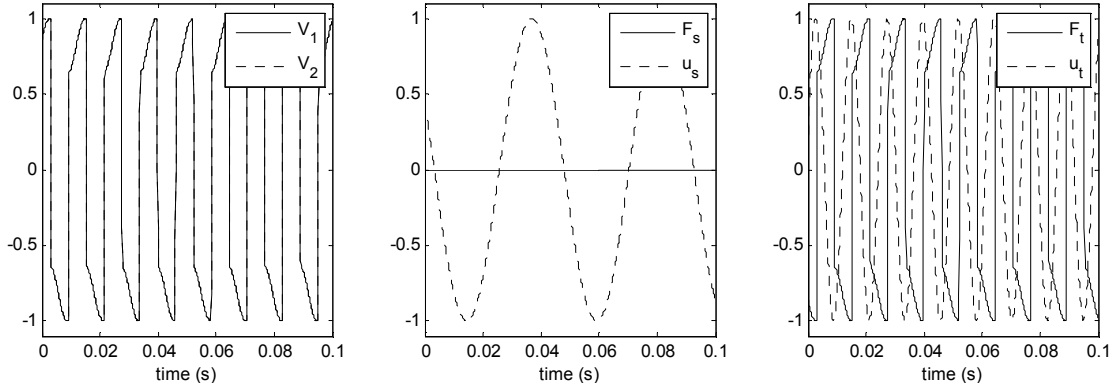


Figure 5.6: Normalized voltages, piezoelectric forces and displacements with SSDI control of two patches in parallel (Case-B: simulation results).

5.2.3 Case-C: Two patches connected in series

Connecting the two patches in series is another connection type. Fig.5.7 shows its electrical scheme in which two patches are connected in series with an inductor, a resistor and a switch. The control law for this circuit is to close the switch at the torsional displacement extrema as we used in the previous connections.

Fig.5.8 shows the waveform under the simulation. It can be noticed that the voltages V_1 and V_2 do not show a same waveform which is different from they are connected in parallel. However, the force F_s shows 180 degree delay to displacement u_s . Thus, this connection is equivalent to open-circuit condition of the source. That is to say the bending mode can not be damped at all by such connection. Being same with the previous two cases, the F_t show a steady waveform and always anti-phase with velocity \dot{u}_t .

5.2.4 Case-D: Two patches with two switches sharing an inductor

In this part, each patch is connected with a switch and then connected in parallel with an sharing inductor as shown in Fig.5.9a. Each switch is composed of a couple transistors (N-MOSFET,P-MOSFET and diode) as shown in Fig.5.9b.³ Usually,

³Most of the published SSD techniques adopt this kind of switch in the circuit. Such switch scheme can prevent the current changing its direction in one switching duration.

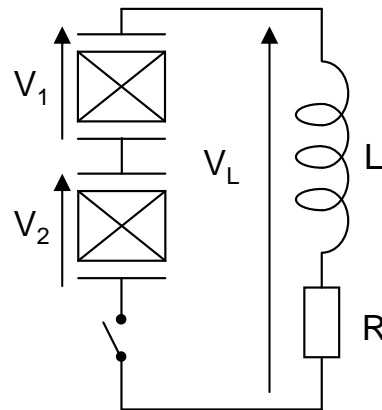


Figure 5.7: Electrical scheme for the SSDI control with two patches in series (Case-C).

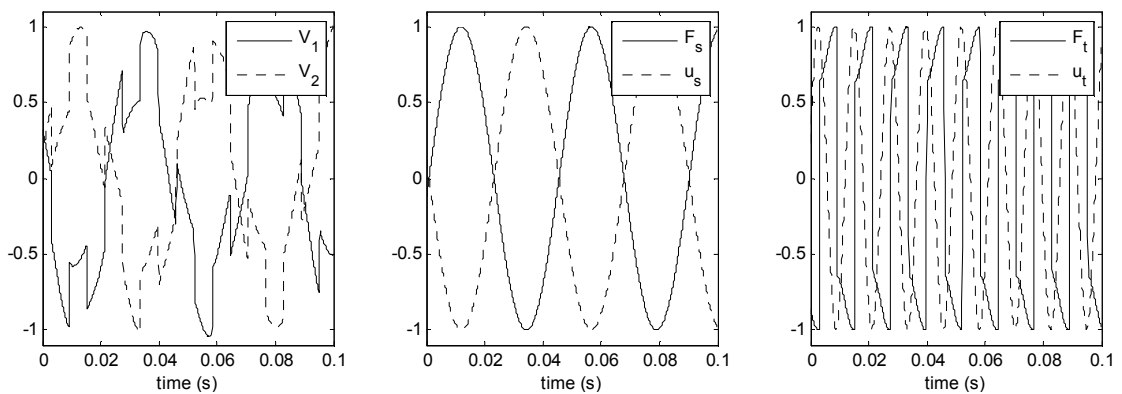


Figure 5.8: Normalized voltages, piezoelectric forces and displacements with SSDI control of two patches in series (Case-C: simulation results).

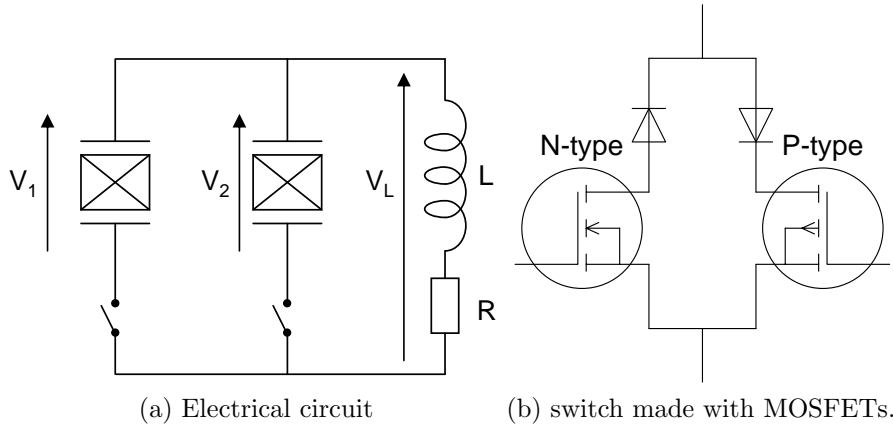


Figure 5.9: Electrical scheme for the SSDI control with two patches sharing an inductor (Case-D).

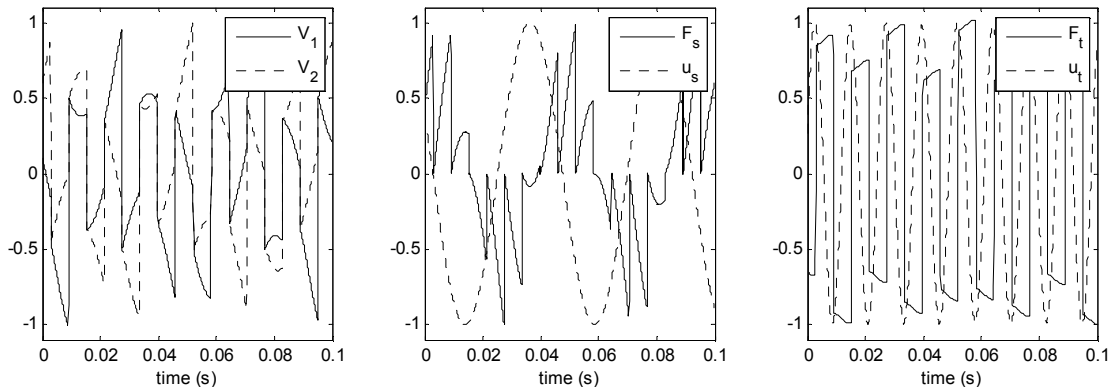
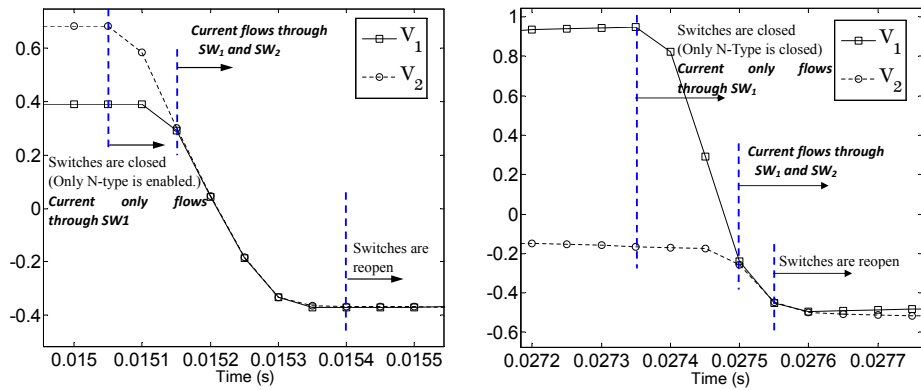


Figure 5.10: Normalized voltages, piezoelectric forces and displacements with SSDI control of two patches sharing one inductor with two switches (Case-D: simulation results).

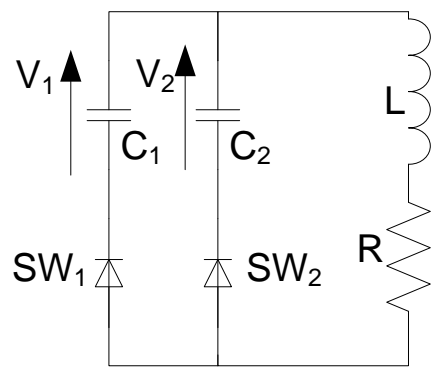
we only close one of them at each switching instant. Therefore, the current can only flow in one direction. Actually, this circuit is identical with that of traditional SSDET. However, the control law is to simply enable one MOSFET when u_t reaches to its extrema as mentioned before.

Fig.5.10 shows the waveforms in simulation. It shows that both V_1 and V_2 will be inverted at the switching instant if they have the same sign. Otherwise, only the voltage on one patch whose sign is opposite to that of the coming \dot{u}_t , will be inverted. Considering only one type MOSFET switch is closed at each transfer, their voltage must be same when switches are re-open as shown in the figure. In order to explain this phenomena, two representative switching durations are selected to show the voltage details in Fig.5.11. These two events occurs when u_t

gets to its maximum. So, only P-type MOSFET is enabled. As shown in Fig.5.11a, V_1 and V_2 are positive at the beginning of the switching. When switches are closed (P-type is enabled), the electrical circuit can be equivalent as in Fig.5.11c. Thus both V_1 and V_2 will be inverted and possess the same voltage after inversion. Otherwise (V_1 is positive and V_2 is negative as shown in Fig. 5.11b, V_1 can be inverted at first. However, V_2 will keep its value due to the diode in the switch until V_1 decreases to the same value with it. After this instant, there will be current flowing through SW_2 . Namely, C_2 is charged and V_2 is enhanced. At the end of the transferring, V_1 and V_2 have the same value since the two patches can be considered as connecting in parallel.



(a) V_1 and V_2 have the same sign at the beginning of switching (b) V_1 and V_2 have the different signs at the beginning of switching



(c) Equivalent circuit scheme (Only P-type MOSFET is enabled).

Figure 5.11: Voltage waveforms during the transferring and the equivalent circuit scheme.

After the re-opening of the switches, the voltage on one patch will increase and the other one must decrease. This can be explained from the Eq.(5.2). The torsion induced voltage ingredient is identical on both patch 1 and patch 2. However, such

ingredient induced by bending are opposite between the patch 1 and patch 2. If we consider the bending induced voltage ingredient is the dominant ingredient (that is common in a bending-torsion coupled vibration). Therefore, the patch whose two ingredients have the same sign, its voltage will be enhanced namely its absolute value (ABSV) increasing. On the contrary, the voltage ABSV on the other patch will decrease. Such decreasing indicates the electrical energy returns back to the mechanical energy namely driving the structure.

The simulation results are plotted in Fig.5.10. It can be seen that the force exerted on bending mode F_s almost always performs an opposite direction with \dot{u}_s and its waveform is similar with that in BSDS control[17]. Let us consider a time span between two switchings. As shown in Fig.5.10, the force F_s ABSV increases at the beginning after the previous switching. That is to say the ABSV of $(V_1 - V_2)$ increases namely the bending energy is extracted and stored on the patches before the next switching. When the extrema of \dot{u}_t occurs, $(V_1 - V_2)$ drops to zero. However, the extracted energy from bending mode does not be dissipated but re-distributed between these two patches. At the end of the switching, V_1 equals to V_2 and their induced force on torsion F_t which equals $\alpha(V_1 + V_2)$ will against the \dot{u}_t . Since V_1 and V_2 which image the stored energy on the patches, partially come from the extracted energy from bending mode during this time span, that is we use the bending energy to damp the torsion mode. This control strategy would show a better damping on torsion comparing with previous three schemes. Moreover, it can also reduce the bending mode motion as that in BSDS. In addition, the waveforms of the voltages are similar with these in SSDET. But the control law in Case-D is easier to implement

Based on the analysis above, the damping ability on bending and torsion modes can be summarized in Tab.5.1. In the table, we also show whether there is energy transfer between two modes. In these techniques, it can be concluded that the more energy extracted from bending, the better damping can be obtained on torsion mode.

5.3 Principle of bidirectional SSDET

In this section, we present the principles of bidirectional SSDET especially its control law. It shows that the bidirectional control law allows a decent control effect both on the bending mode (source) and torsion mode (target).

	Damping on bending	Damping on torsion	Energy transfer?
Case-A	😞	😄	😞
Case-B	😞	😄	😞
Case-C	😞	😄	😞
Case-D	😄	😄	😄

😞-Not at all; 😞- A little; 😄-Good ; 😄- Very good.

Table 5.1: A comparison of the damping between different electrical schemes.

5.3.1 Idea of bidirectional SSDET

SSDET proposed in previous sections deals with reducing the higher mode motion in such a bimodal vibration. In this technique, the vibrating modes are divided as energy source mode and target mode. It also needs two group piezoelectric patches to extract the energy from these modes respectively. These two groups of patches are never connected together but transfer their electrical energy by a sharing inductor for the sake of extracting more energy from target mode. Therefore, the transferring path is always from the source patches to the target patches. It should be also pointed out that each group can only extract the energy from the corresponding mode due to their particular bonding position. However, Such configuration makes the piezoelectric patches lose its extracted energy ability from other modes.

In order to retrieve the energy extraction ability from all vibrating modes by every piezoelectric patches, we propose a new SSDET scheme in which the energy can transfer in both direction. In this technique, there are still source modes and target modes. However, each group of patches will not constantly extract the energy from one mode but all modes. In addition, the control target is set to be the higher mode motion. However, the damping of lower mode is also got a farthest consideration.

5.3.2 Control law of the bidirectional SSDET

The bidirectional SSDET circuit is shown in Fig.5.12 which is same with that in classical SSDET. However, the control law is quite different from that of classical SSDET. The energy transfer still occurs at the moments of the target displacement extrema, but the transfer direction is alternatively patch 1 \rightarrow patch 2 or patch 2 \rightarrow patch 1 which is determined by the sign relationship between \dot{u}_t and \dot{u}_s . Tab.5.2 shows the transfer direction under four circumstances. It can be briefly concluded

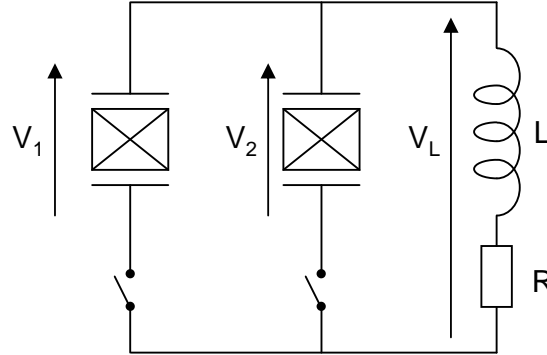


Figure 5.12: Bidirectional SSDET circuit.

that the energy will transfer from patch 1 \rightarrow patch 2 if the \dot{u}_t and \dot{u}_s have the same sign when u_t reaches to its extrema. Otherwise, the transfer direction will be from patch 2 \rightarrow patch 1. The transfer direction can be controlled by adjusting the switching order of two switches. For instance, if the transfer direction is patch 1 \rightarrow patch 2, the SW_1 should be firstly closed and *vice versa*. Therefore, the transfer direction is unique at each transferring instant. By doing so, the voltage of one patch which transfers its energy to another will drop to zero after the transferring. On the other hand, the patch which receives the transferred energy will increase its voltage ABSV due to the transferred energy and extract both bending and torsion energy after the transferring moment until the next switching (because the \dot{u}_s and u_t have same sign), that is to say the voltage will still increase before the next switching. Here, the voltage ABSV increasing between two switching (energy transfer) is attributed to both the source and target mode motion. The force induced by this voltage is anti-phase to the velocity of the target, that means we use the source mode energy to damp the target.

	$\dot{u}_s > 0$	$\dot{u}_s < 0$
u_t maximum \dot{u}_t will < 0	Patch 1 \rightarrow Patch 2 first SW_1 then SW_2	Patch 2 \rightarrow Patch 1 first SW_2 then SW_1
u_t minimum \dot{u}_t will > 0	Patch 2 \rightarrow Patch 1 first SW_2 then SW_1	Patch 1 \rightarrow Patch 2 first SW_1 then SW_2

Table 5.2: Direction of the energy transfer in bidirectional SSDET technique.

The control law of directional SSDET can be summarized in Tab. 5.3 which is an expansion of Tab.5.2. We can see that one circumstance in Tab.5.2 can be detailed in four cases depending on the signs of V_1 and V_2 . In fact, the control can

still be implemented by two continuous steps. First step is to choose one switch between SW_1 or SW_2 for t_a or t'_a . This choice is unique and can be determined from Tab. 5.2 and Tab.5.3. Second step is to close another switch for t_b or t'_b . So, only one switch is closed in one step forming a LCR oscillator. In Tab.5.3, only the duration for the first switch is listed. The switching duration for the second step always equals to one half period of the oscillator in second step. Thanks to the diode in the switch, this time can be set a constant value as long as it is larger than any of t_2 or t'_2 . The diode can prevent the current changing its direction. That is the voltage of the patch which receives the transferred energy, do not decrease its voltage ABSV in step 2 regardless of the switching duration. The closing duration can be calculated from Eq.(5.4). Here, $\beta = \frac{R}{2L}$. U_0 is the initial voltage of the piezoelectric patch which receives the transferred energy at each transfer and i_0 is the initial current in the inductor at the beginning of step 2⁴, ω_a and ω_b are the resonant circular frequency of the LCR oscillators in each steps. They can be calculated from Eq. 5.4. C_{01} and C_{02} are the capacitance of the patch 1 and patch 2 respectively. In fact, the t_a and t'_a equal to 1/4 and 3/4 period of the corresponding LCR oscillator.

$$\begin{aligned} t_a &= \frac{1}{\omega_a} \arctan\left(\frac{\omega_a}{\beta}\right), & t_b &= \frac{1}{\omega_b} \left[\arctan\left(\frac{-i_0 \omega_b L}{U_0 - i_0 \beta L}\right) + \pi \right] \\ t'_a &= \frac{1}{\omega_a} \left[\arctan\left(\frac{\omega_a}{\beta}\right) + \pi \right], & t'_b &= \frac{1}{\omega_b} \left[\arctan\left(\frac{-i_0 \omega_b L}{U_0 - i_0 \beta L}\right) + \pi \right] \end{aligned} \quad (5.4)$$

$$\begin{aligned} \text{If patch1} \rightarrow \text{patch2}, & \omega_a = \sqrt{\frac{1}{LC_{01}} - \left(\frac{R}{2L}\right)^2}, & \omega_b &= \sqrt{\frac{1}{LC_{02}} - \left(\frac{R}{2L}\right)^2} \\ \text{If patch2} \rightarrow \text{patch1}, & \omega_a = \sqrt{\frac{1}{LC_{02}} - \left(\frac{R}{2L}\right)^2}, & \omega_b &= \sqrt{\frac{1}{LC_{01}} - \left(\frac{R}{2L}\right)^2} \end{aligned} \quad (5.5)$$

With the control law, the voltage of the patch which is chosen as the source patch in one transfer, drops to zero at the first step. However, the voltage of the patch which is chosen as the target in one transfer, is not always be inverted during step2. Tab.5.3 shows the voltage changes in step 2 whether it is inverted or not. Where, the capital letter I stands for *Inverted* and NI stands for *Not Inverted*.

In order to make a clear explanation for Tab.5.3, the case ($u_s > 0$ and u_t at its maximum) is selected to show their waveforms around the switching. We plot waveforms under four possibilities around the switching (energy transfer) moment

⁴ U_0 and i_0 are only used for theoretical calculation. In practice, we never measure these values since the precise duration of step 2 is not necessary.

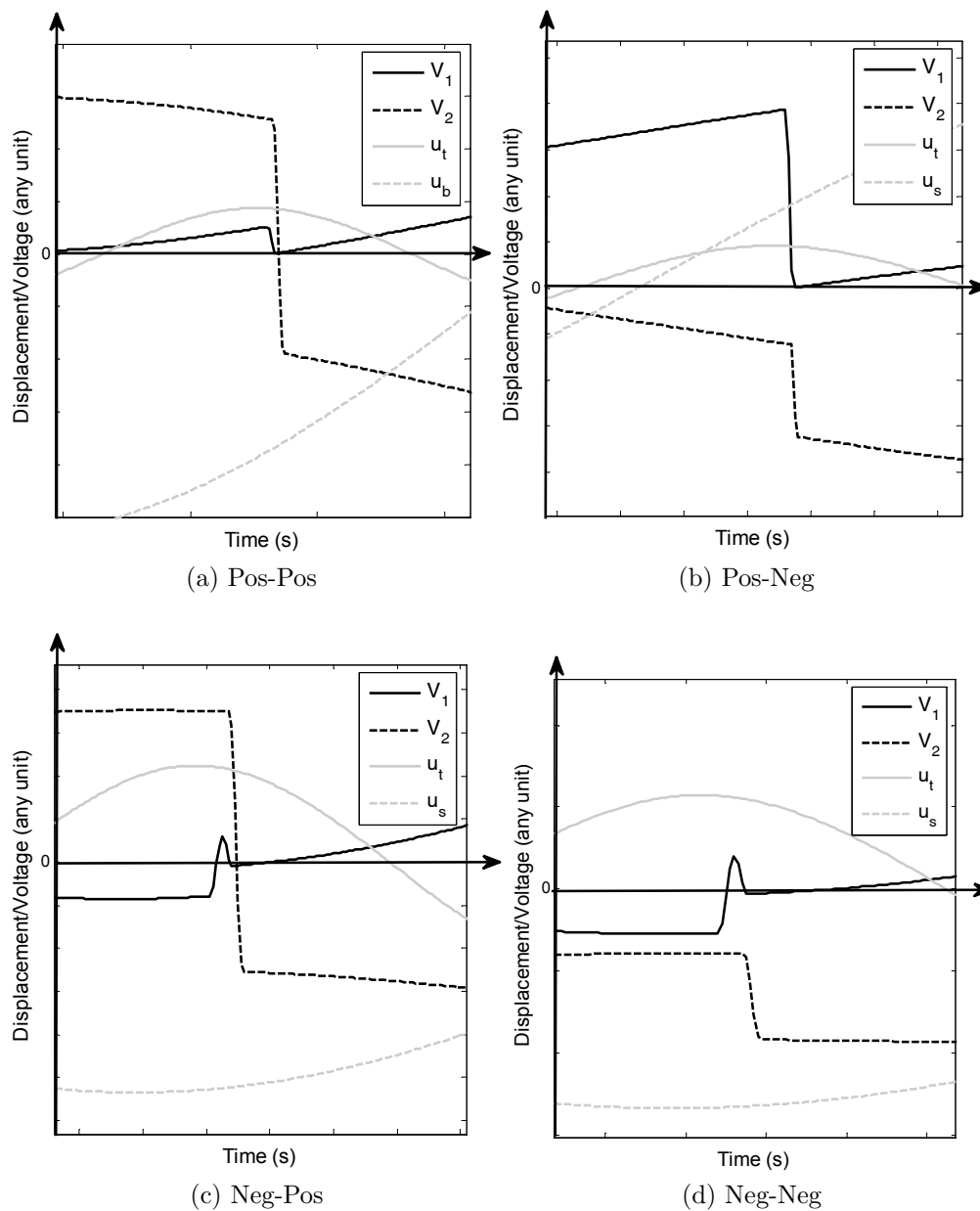


Figure 5.13: Waveforms of displacements and voltages under case $\dot{u}_s > 0$ and u_t at its maximum.

		$\dot{u}_s > 0$		$\dot{u}_s < 0$	
		V_1			
		Positive	Negative	Positive	Negative
V_2					
u_t maximum	Positive	t_a, V_2 I	t'_a, V_2 I	t_a, V_1 I	t_a, V_1 NI
\dot{u}_t will < 0	Negative	t_a, V_2 NI	t'_a, V_2 NI	t'_a, V_1 I	t'_a, V_1 NI
u_t minimum	Positive	t'_a, V_1 NI	t'_a, V_1 I	t'_a, V_2 NI	t_a, V_2 NI
\dot{u}_t will > 0	Negative	t_a, V_1 NI	t_a, V_1 I	t'_a, V_2 I	t_a, V_2 I

Table 5.3: Bidirectional SSDET control law.

in Fig.5.13. These possibilities are determined by the signs relationship between V_1 and V_2 . The caption *Neg-Pos* means that V_1 is negative V_2 is positive at the transfer instant. And the rest use the same expression form. The *Pos* and *Neg* are short for positive and negative respectively. The energy transfer in these figures occurs at the moment that $\dot{u}_s > 0$ and u_t at its maximum. As introduced in Tab.5.2, the transfer direction in these cases is patch 1 \rightarrow patch 2.

Thus, V_1 must drop to zero at the end of step 1. The choice of the switch closing time between t_a or t'_a is to make the current direction at the end of step 1 same with that in step 2. That is the transferred energy from patch 1 will enhance V_2 in the step 2. In step 2, the V_2 would be inverted or not which depends on its sign (positive or negative). Considering both events $\dot{u}_s > 0$ and u_t at its maximum (\dot{u}_t will > 0) leads to V_2 decrease. If V_2 is positive at the transfer moment as shown in Fig.5.13a and Fig.5.13c, it should be inverted to negative in order to keep the amplitude of V_2 increasing in the next ($0 T_t/2$) time range.⁵ Otherwise (V_2 is negative), V_2 will not be inverted but still increase its amplitude in negative like charging a capacitor as shown in Fig.5.13b and Fig.5.13d. The operation for making the V_2 inverted or not is to close the N-type or P-type MOSFET of the switch. In this way, the V_2 can keep a higher value and its amplitude could be enhanced before the next transfer. It indicates a larger force can be induced by patch 2 to damp both bending and torsion modes before next switching. At the same time, V_1 will increase from zero until the next switching as shown in these figures.

Meanwhile, we can also explain why we do not transfer the energy from patch 2 \rightarrow patch 1 under such circumstance ($\dot{u}_s > 0$ and u_t at its maximum). That is because if so, V_2 will drop to zero at the end of step 1. V_1 has to be negative at the end of step 2 in order to damp the torsion mode in the coming ($0 T_t/2$). However, the bending motion drives V_1 increasing meanwhile the torsion mode does the opposite. So, the voltage amplitude in this case must be less than that

⁵Because V_2 is negative after inversion. Decreasing V_2 means increasing its amplitude.

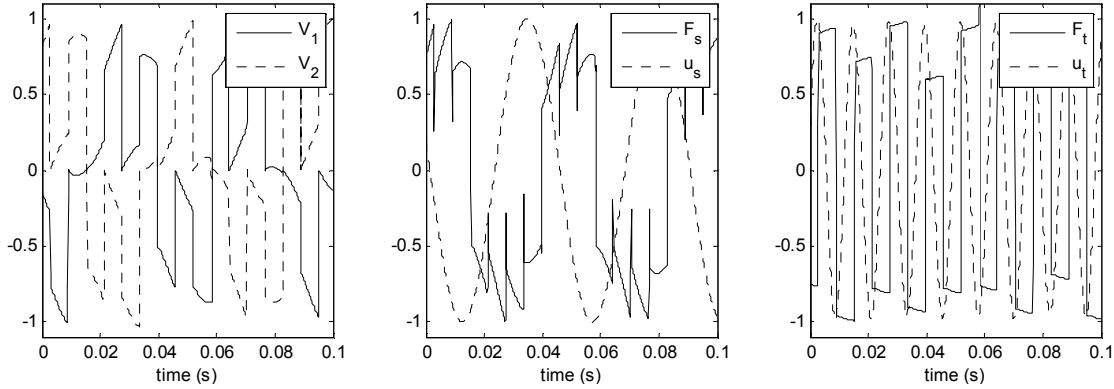


Figure 5.14: Normalized voltages, piezoelectric forces and displacements with SSDI control of two patches sharing one inductor with two switches (simulation results).

in the case which energy is transferred from patch 1 \rightarrow patch 2. Moreover, the induced force by the V_1 will excite the bending mode since the force has the same sign with the bending velocity.

Fig.5.14 shows the simulation results. Besides the switching duration, V_1 and V_2 increase in most cases. It means the energy can only be extracted from the structure but not return them back. The force F_s drops but not to zero at each switching due to the transferred energy. Moreover, it seems like F_s is synchronized with u_s because the \dot{u}_s is taken into account in the control law. So the damping on bending mode can be much better than that in CASE-D. That is also to say that the damping on torsion can also be improved due to the more transferred energy.

5.4 Experimental validation

In this section, an experiment is carried out on an one-edge clamped plate to verify the bidirectional SSDET technique. Meanwhile, some other experiments (CASE B and D) are also implemented in order to compare with the bidirectional SSDET.

5.4.1 Experimental setup

The experimental setup is plotted in Fig.5.15 which is the same structure we used in chapter 4. Two patches are bonded on the upper and lower surface of the plate. Since the surface of piezoelectric patches and the structure are both conductive, one of their electrodes of each patch is connected together. The other electrodes are directly connected with the switches which on/off states are controlled by dSPACE. An inductor is connected between the ground and the surface of the plate (one

electrode of the patches). One electromagnet is placed under the plate near the free edge as shown in Fig.5.15. The plate is excited under its first bending and torsional nature modes. The frequencies are 21.3Hz for bending mode and 81.7Hz for torsion mode. Two laser sensors are used to sense the displacement of two points. Due to the symmetric relation, the bending mode motion can be expressed as one-half of their difference value and the bending mode motion equals to one-half of their sum value.

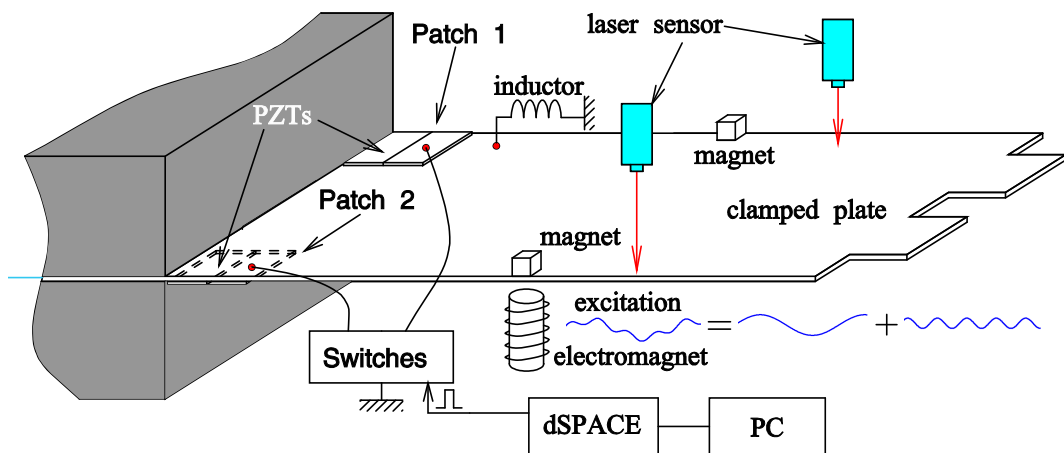


Figure 5.15: Experimental setup.

5.4.2 Results and Discussions

- No control results: Two patches are open circuit.
In this case, the piezoelectric patches are open circuit. Fig.5.16 shows the waveforms of the forces, voltages and the displacements. Because the bending motion is the dominant component in the structure motion, the torsion component is not obvious in the voltages of each patch. There is a 180 degree phase delay between the Force F_s and displacement \dot{u}_s as well as F_t and u_t . No damping occurs neither on bending nor torsion under open circuit condition.
- CASE-B results: Two patches are connected in parallel.
In the experiment, the electrical circuit shown in Fig.5.5 are employed. The control law is to close the switch simply when displacement u_t reaches to its extrema. The experimental waveforms shows a good agreement with our simulation ones. That is the two voltages are always same due to the parallel

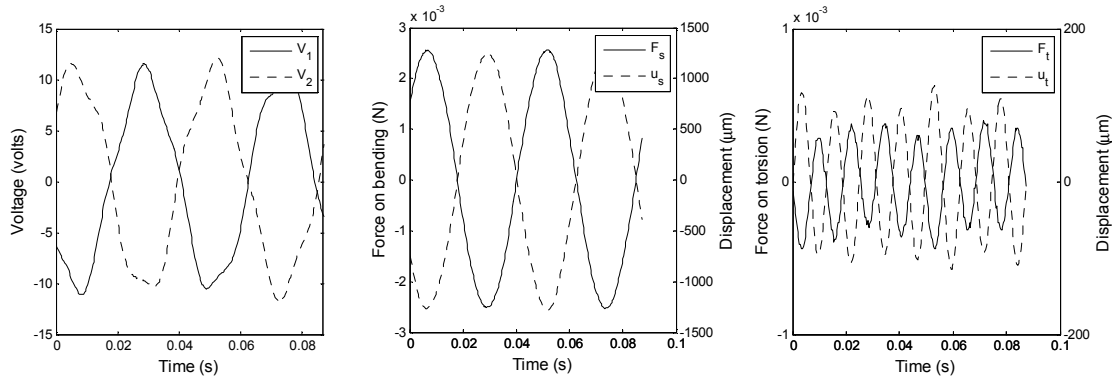


Figure 5.16: Experimental waveforms (Without control).

connect. The force exerted on bending F_s is zero all the time. Only torsion mode can be damped under this case.

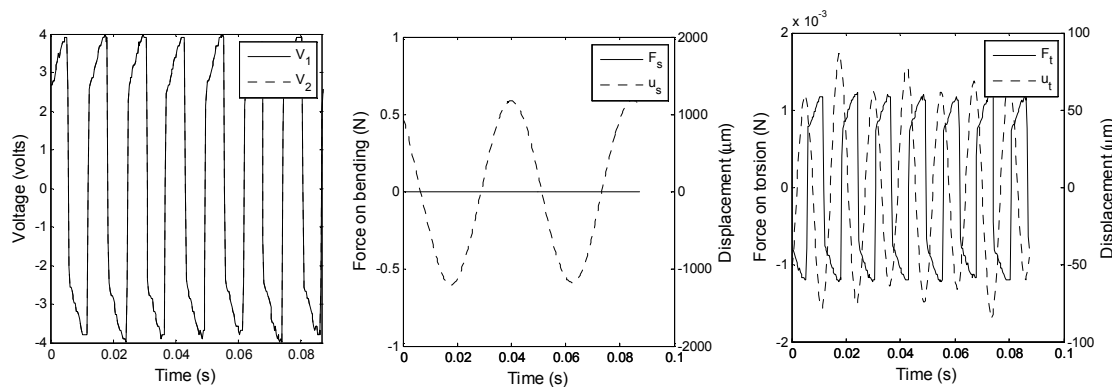


Figure 5.17: Experimental waveforms (CASE-B).

- CASE-D results: Two patches sharing an inductor with two switches. The electrical circuit is shown in Fig.5.18 and the experimental results are shown in Fig.5.18 which is agree with the simulation results. It can be seen that the voltages V_1 and V_2 are identical after each switching. Compared with the experiment of CASE-B, it is clear that the force F_s is enhanced about 100% leading to a better damping on the torsion. The bending mode motion is also reduced a little due to the extracted energy.
- Bidirectional SSDDET results: Two patches sharing an inductor with two switches. In bidirectional SSDDET control, the circuit is same with that in CASE-D. However, the switches switch follow the developed control law in Tab.5.3. The waveforms are plotted in Fig.5.18. It shows that both V_1 and V_2 increase

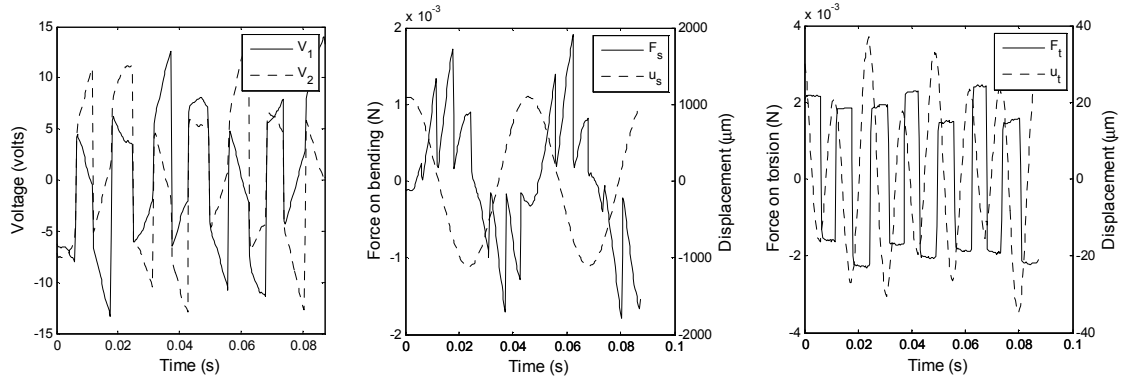


Figure 5.18: Experimental waveforms (CASE-D).

after each switching. That is one major difference with that in CASE-D (if V_1 increases, V_2 decreases and *vice versa*). That is to say both bending and torsional energy can not be extracted but not return back to the mechanical system. Therefore, a larger force F_s appears on the bending mode and it almost shows an opposite phase with the \dot{u}_s . Due to the greater transferred energy, the torsion mode can be damped more that that in CASE-D.

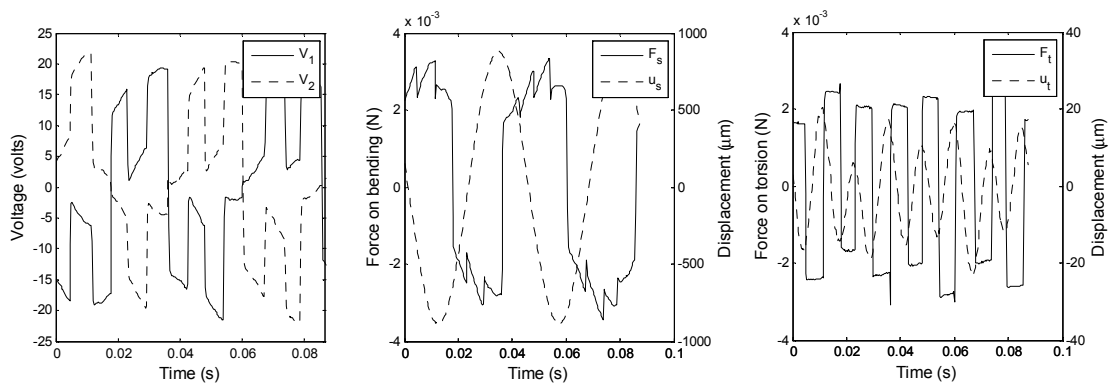


Figure 5.19: Experimental waveforms (CASE-E).

The damping on bending and torsion modes under different control strategies are plotted in Table.5.4. It shows that both damping and torsion modes motion can be reduced by the three methods. However, the damping on bending by CASE-B is attribute to the structure transfer function shift. In CASE-D and bidirectional SSDET, the force exerted on bending motion F_s almost have a opposite direction with the velocity. Nevertheless, its amplitude in bidirectional SSDET is higher than that in CASE-D. That can explain why the bidirectional SSDET performs better control on bending mode. The better damping on bending mode can also benefit the control on torsion mode in the two cases. Since the better damping

on torsion means the more energy is extracted from bending and transferred to damp the torsion mode. So, we can see that the bidirectional SSDET also shows the best control effect on torsion among these control methods.

	No control	Case-B	Case-D	Bi-SSDET
Bending mode (dB)	0	0.5	1.1	3.0
Torsion mode (dB)	0	3.4	12.4	16.8

Table 5.4: Damping comparison between different control strategies.

5.5 Conclusion

In this chapter, a new SSDET technique namely bidirectional SSDET is proposed. In this technique, we still have the energy source and target mechanical forms. In traditional SSDET technique, the energy transfer path is always from one patch group to another. But in bidirectional SSDET, this path can be changed depending on the situations of host structure motion. The chapter can be concludes in three parts as follows:

- First, a bending-torsion coupling vibration structure is introduced to illustrate our proposed method. We propose four connection possibilities between the two patches (namely Case-A, B, C and D) and simulate their behaviors in Simulink. Simulation waveforms indicate that all these four methods can show damping on torsion mode but most of them do not have a obvious damping effect on bending motion. It is found that the energy transfer in CASE-D is quite similar with that in traditional SSDET. Thanks to the transferred energy, CASE-D could perform better control on torsion mode than that in the rest three connections.
- Second, we propose the principles of bidirectional SSDET. Compared with traditional SSDET, the patches in bidirectional SSDET can extract all modes energy. Its electrical circuit is same with that of CASE-D, but their control laws are quite different. The control law of bidirectional SSDET is introduced in details. It can be concluded that the fact of bidirectional SSDET is to concentrate the energy on one patch at each transferring. The criterion of the patch selection is up to the signs relationship between u_t and \dot{u}_s . It can be also noticed that the voltage on the patch which receives the transferred energy do not be always inverted as in traditional SSDET. Simulation shows

that both voltages on two patches can be enhanced most of the time. That is to say can always extract energy from mechanical system but seldom return them back. It indicates a stronger damping effect than the other cases as we introduced before.

- Finally, An experiment is carried out on clamped plate which is excited under its first bending and torsional frequencies simultaneously as we introduced in the prototype. We verify the methods CASE-B, D and bidirectional SSDET in the experiment. The experiment waveforms show a good agreement with those in simulations. The damping comparisons shows that the proposed bidirectional SSDET can get a best damping both on bending and torsion mode among three methods.

Conclusion and perspectives

The main achievements of this thesis was the development and implementation of synchronized switch damping with energy transfer technique to reduce structural vibration. The distinguishing feature of this technique was that we used the energy which was pumped from vibrating structure or vibrating modes to damp another specific vibrating form.

In the first chapter, a comprehensive review of four representative piezoelectric shunt damping techniques was given. Among these methods (Resistive shunt damping, L-R resonant shunt damping, capacitive shunt damping and switched shunt damping), switched shunt damping techniques grew rapidly due to its low-power consumption, miniaturization and broadband control ability. The SSDET technique developed in this work is mainly based on one switched shunt damping technique *e.g.* Synchronized switch damping technique.

In chapter 2, a detailed review of synchronized switch damping technique was presented. By employing the classical mathematical model of piezo-coupled structure, we introduced three representative SSD techniques: SSDS, SSDI and SSDV which had been well studied in the past decade. We concluded the characteristics of these basic SSD treatments. (1) The switching occurs at the displacement extrema; (2) Piezoelectric elements converted mechanical energy into electrical energy all the time and finally dissipated it as heat. (3) The piezo-induced force always resisted the structure motion. The energy analysis revealed that the damping performance of SSD technique particularly depended on the piezoelectric voltage. SSDV could get a best damping between these methods due to the external energy, but that also brought the potential instability. SSDI can show a decent damping effect while keep unconditional stable. The multi-mode control abilities of SSD techniques were also summarized. We sorted these attempts into three catalogs. (1) Original SSD bandwidth control. The control law for single mode was directly applied to control the multi-mode control. (2) Mode distinguishing based bandwidth control. This control used numerical filter or modal observer to

distinguish the structure vibration mode for determining the switching instant. (3) Time window based bandwidth control. A time window was adopted to estimate the next switching instant. The power consumption was a critical issue in SSD technique. Some self-powered SSD techniques were introduced. Due to the smart circuit designs, these systems can feed themselves by using the extracted mechanical energy from the host structure. As a full review chapter, the BSD techniques were also concluded at the end although they are not exactly synchronized with displacement.

Chapter 3 brought the conception of synchronized switch damping with energy transfer. The goal of this technique was to damping target(could be one vibrating structure or one vibrating mode) by using energy which came from energy source (another vibrating structure or modes). At the beginning, we gave SSDET circuit and proposed its control law in detail. We divided the operation in two steps. One is to extract energy from source. The other is to transfer it for enhancing the voltage on source. The voltage waveforms during the energy transfer were exhibited in order to show how we transferred energy between source and target and why the damping on target can be improved. The mathematical models for SSDET were built by state-space representation in time domain and by Fourier transfer in frequency domain. Time domain simulation validated the effectiveness of the proposed control method and showed SSDET can get better damping then SSDI technique. The frequency domain simulations revealed the extracted power of the source was crucial to the damping on the target. At last, an enhanced control law was developed based on the threshold setting on source voltage. Numerical simulation results showed that applying an appropriate threshold can elevate the extracted power of source.

Chapter 4 experimentally verified SSDET by three test patterns. The experimental test bench was introduced at first. A SSDET experiment between two structures was implemented. Results showed that we successfully increased the damping of a four edge clamped plate by transferring the energy from a cantilever beam. The stability problems were discussed as well based on the results. Next, SSDET was carried out in one structure. The objective is to reduce torsion mode vibration by using the bending mode energy. The control for both harmonic and transient response were taken into account. The results demonstrates the effectiveness of SSDET in this case. The threshold setting was also be verified in this test. However, the piezoelectric elements should be distributed at the carefully selected position in this test. Finally, a SSDET experiment between multi patches was presented. In this scheme, we proposed a maximum energy based control law

in which only the source with maximum electrical energy could be connected into the SSDET circuit for energy transfer. Experimental results showed that more displacement suppression can be achieved by employing this scheme.

Chapter 5 developed a bidirectional SSDET technique. At first, we introduced a bending-torsion coupled vibrating structure with two piezoelectric patches bonded. We connected these two patches in four different patterns and simulated their electrical and dynamic behaviors in matlab/simulink. Based on the simulation results, the damping effects were estimated. The issue whether there is energy transfer between two modes in each method was also discussed. Then, bidirectional SSDET was presented. In this technique, there were still energy source motion and target motion. However, The piezoelectric elements in bidirectional SSDET can extract all modes energy from host structure but not extract only one mode energy as they did in traditional SSDET. The main idea of bidirectional SSDET is to concentrate the electrical energy on one patch at each switching. The bidirectional SSDET control law showed that the energy transfer path was bidirectional between two patches depending on the velocities of two modes. Experiments showed that bidirectional SSDET had multimode control ability that can achieve best damping among the proposed connections both on source and target mode.

Future work would focus on three aspects. (1) Since the control performance of SSDET technique depended on the extracted power of source. However, the system could lose its stability if the extracted power is too large. It is necessary to develop a more stable control law to avoid instability. (2) In current SSDET, we used energy from lower frequency motion (source) to damping the motion with higher frequency (target). In future SSDET, the target and source could exchange their roles. That means we can also use the energy from higher frequency motion to damp the lower frequency motion. (3) A significant issue for semi-passive control is the energy consumption. The ultimate goal for such a semi-passive control should be self-powered system. In this research, we still use dSPACE device to achieve the control. The future work can aim at developing a self-powered SSDET technique. One main difficulty is to on/off different switches with proper duration (The switching time of step 1 is changeable due to the voltage signs relationship). A practical method is to use the extreme low-power micro-controller to implement such operations. The power consumption of newly developed micro controller can be less than 500 nanowatt. Thus, it is possible to use partial extracted energy from source to power up this system. For instant, the extracted power in the experiment of chapter 4 have been reached to 0.2 milliwatt that is 400 times larger than the power need for extreme low power micro controller.

Bibliography

- [1] Lesieutre, G. A., “Vibration damping and control using shunted piezoelectric materials,” *Shock Vib. Dig* **30**, 187–195 (1998).
- [2] Wu, S. Y., “Multiple pzt transducers implemented with multiple mode piezoelectric shunting for passive vibration damping,” *Proc. SPIE: Smart Structures and Materials Conference: Passive Damping and Isolation, Huntington Beach, CA* **3672**, 112–122 (1999).
- [3] Kim, J., Ryu, Y.-H., and Choi, S.-B., “New shunting parameter tuning method for piezoelectric damping based on measured electrical impedance,” *Smart Mater. Struct.* **9**, 868–877 (2000).
- [4] Davis, C. L., “An actively tuned solid-state vibration absorber using capacitive shunting of piezoelectric stiffness,” *J. Sound Vib.* **232**, 601–617 (2000).
- [5] Kenji, M. and Kyohei, K., “Semi-active vibration suppression of large space structures with a variable axial stiffness member,” *AIAA/ASME/ASCE/AHS/ASC Structures, Structural Dynamics, and Materials Conference, 34th and AIAA/ASME Adaptive Structures Forum (La Jolla, CA)* **A93-33876 13-39**, 3305–3311 (1993).
- [6] Makihara, K., Onoda, J., and Minesugi, K., “Low-energy-consumption hybrid vibration suppression based on an energy-recycling approach,” *AIAA J.* **43(8)**, 1706–1715 (2005).
- [7] Badel, A., Sebald, G., Guyomar, D., Lallart, M., Lefeuvre, E., Richard, C., and Qiu, J., “Piezoelectric vibration control by synchronized switching on adaptive voltage sources: Towards wideband semi-active damping,” *J. Acoust. Soc. Am.* **119(5)**, 2815–2825 (2006).
- [8] Guyomar, D., Jayet, Y., Petit, L., Lefeuvre, E., Monnier, T., Richard, C., and Lallart, M., “Synchronized switch harvesting applied to selfpowered smart systems: Piezoactive microgenerators for autonomous wireless transmitters,” *Sensors and Actuators A: Physical* **138(1)**, 151 – 160 (2007).
- [9] Guyomar, D., Richard, T., and Richard, C., “Sound wave transmission reduction through a plate using piezoelectric synchronized switch damping technique,” *J. Intell. Mater. Syst. Struct.* **19**, 791–803 (2008).
- [10] Guyomar, D. and Badel, A., “Nonlinear semi passive multimodal vibration damping An efficient probabilistic approach,” *J. Sound Vib.* **294**, 249–268 (2006).

- [11] Corr, L. R. and Clark, W. W., “A novel semi-active multi-modal vibration control law for a piezoceramic actuator,” *J. Vib. Acoust.* **125**, 214–222 (2003).
- [12] Neubauer, M., Han, X., and Schwarzendahl, S. M., “Enhanced switching law for synchronized switch damping on inductor with bimodal excitation,” *J. Sound Vib.* **In Press, Corrected Proof**, – (2011).
- [13] Guyomar, D., Richard, C., and Mohammadi, S., “Semi-passive random vibration control based on statistics,” *J. Sound Vib.* **307**(3-5), 818 – 833 (2007).
- [14] Niederberger, D. and Morari, M., “An autonomous shunt circuit for vibration damping,” *Smart Mater. Struct.* **15**, 359–364 (2006).
- [15] Richard, C., Guyomar, D., and Lefevre, E., “Self-powered electronic breaker with automatic switching by detecting maxima or minima of potential difference between its power electrodes,” *Patent PCT/FR2005/003000*, Publication number: WO/2007/063194, (2007).
- [16] Shen, H., Qiu, J., Ji, H., Zhu, K., and Balsi, M., “Enhanced synchronized switch harvesting: a new energy harvesting scheme for efficient energy extraction,” *Smart Materials and Structures* **19**(11), 115017 (2010).
- [17] Lallart, M., Harari, S., Petit, L., Guyomar, D., Richard, T., Richard, C., and Gaudiller, L., “Blind switch damping(BSD): A self-adaptive semi-active damping technique,” *J. Sound Vib.* **328**, 29–41 (2009).
- [18] Lallart, M., *Amélioration de la conversion électroactive de matériaux piézoélectriques et pyroélectriques pour le contrôle vibratoire et la récupération d’énergie - Application au contrôle de santé structurale auto-alimenté*, PhD thesis, INSA de Lyon (2008).
- [19] Agrawal, A. K., “Response of light equipment on torsional building with passive tuned mass damper,” *Computers & Structures* **78**(4), 591 – 602 (2000).
- [20] Kagawa, Y., Tsuchiya, T., and NaotoWakatsuki, “Equivalent circuit representation of a vibrating structure with piezoelectric transducers and the stability consideration in the active damping control,” *Smart Mater. Struct.* **10**, 389–394 (2001).
- [21] Bruant, I., Coffignal, G., Léné, F., and Vergé, M., “Active control of beam structures with piezoelectric actuators and sensors: modeling and simulation,” *Smart Mater. Struct.* **10**, 404–408 (2001).
- [22] Ramaratnam, A. and Jalili, N., “A switched stiffness approach for structural vibration control: theory and real-time implementation,” *J. Sound Vib.* **291**(1-2), 258 – 274 (2006).
- [23] Onoda, J., Oh, H. U., and Minesugi, K., “Semi-active vibration suppression of truss structures by electro-rheological fluid,” *Acta Astronautica* **40**(11), 771 – 779 (1997).

- [24] Song, X., Ahmadian, M., Southward, S., and Miller, L., "Parametric study of nonlinear adaptive control algorithm with magneto-rheological suspension systems," *Communications in Nonlinear Science and Numerical Simulation* **12**(4), 584 – 607 (2007).
- [25] Giurgiutiu, V., "Review of smart-materials actuation solutions for aeroelastic and vibration control," *J. Intell. Mater. Syst. Struct.* **11**, 524–544 (2000).
- [26] Forward, R. L., "Electronic damping of vibrations in optical structures," *Appl. Opt.* **18**(5), 690–697 (1979).
- [27] Uchino, K. and Ishii, T., "Mechanical damper using piezoelectric ceramics," *Journal of Ceramic Society of Japan* **96**, 863–867 (1988).
- [28] Hagood, N. W. and Flotow, A. V., "Damping of structural vibrations with piezoelectric materials and passive electrical networks," *J. Sound Vib.* **146**(2), 243–268 (1991).
- [29] Lesieutre, G. and L.Davis, C., "Frequency-shaped passive damping using resistively-shunted piezoceramics," *Conference on Active Materials and Structures (Alexandria)* , 355–358 (1991).
- [30] Lesieutre, G. A., Yarlagadda, S., Yoshikawa, S., Kurtz, S. K., and Xu, Q. C., "Passively damped structural composite materials using resistively shunted piezoceramic fibers," *Journal of Materials Engineering and Performance* **2**, 887–892 (1992).
- [31] Tanimoto, T., K, H., and K, U., "Passive damping performance of an adaptive carbon-fiber reinforced plastics/lead zirconate titanate beam," *Japanese Journal of Applied Physics* **36**, 6110 6113 (1997).
- [32] Wu, S. Y., "Piezoelectric shunts with a parallel R-L circuit for structural damping and vibration control," *Proc. SPIE: Smart Structures and Materials, Passive damping and isolation* **2720**, 259–269 (1996).
- [33] Wu, S. and Bicos, A. S., "Structural vibration damping experiments using improved piezoelectric shunts," *Proc. SPIE: Smart Structures and Materials Conference: Passive Damping and Isolation, San Diego, CA* , 40–50 (1997).
- [34] Wu, S. Y., "Method for multiple mode shunting damping of structure vibration using a single pzt transducer," *Proc. SPIE: Smart Structures and Materials, Smart Structures and Intelligent Systems (Huntington Beach, CA)* **3672**, 159–168 (1998).
- [35] Wu, S.-Y., L., T. T., and A., R. S., "Piezoelectric shunt vibration damping of f-15 panel under high acoustic excitation," *Proc. SPIE. 7th International Symposium on Smart Structures and Materials, Newport Beach, CA* **3986**, 276–287 (2000).
- [36] Wu, S.-Y., "Broadband piezoelectric shunts for passive structural vibration control," *Proc. SPIE: Smart Structures and Materials Conference: Passive Damping and Isolation, San Diego, CA* **4331**, 251–261 (2001).

- [37] Behrens, S. and Mohammadi, S. O. R., “Current flowing multiple-mode piezoelectric shunt dampener,” *Proc. SPIE: Smart Structures and Materials Conference: Passive Damping and Isolation, San Diego, CA* **4697**, 217–226 (2002).
- [38] Ryu, Y.-H., Kim, J., and Cheong, C., “Piezoelectric shunting parameter estimation using electrical impedance models,” *Proc. SPIE: Smart Structures and Materials Conference: Passive Damping and Isolation, Newport Beach, CA* **3989**, 39–48 (2000).
- [39] Sun, H., Yang, Z., Li, K., Li, B., Xie, J., Wu, D., and Zhang, L., “Vibration suppression of a hard disk driver actuator arm using piezoelectric shunt damping with a topology-optimized PZT transducer,” *Smart Mater. Struct.* **18**, 065010 (2009).
- [40] Parka, J., Lima, S., Choia, S., Kima, J., and Parkb, Y., “Vibration reduction of a cd-rom drive base using a piezoelectric shunt circuit,” *J. Sound Vib.* **269**, 1111–1118 (2004).
- [41] Behrens, S. and Moheimani, S. O. R., “Optimal resistive elements for multiple mode shunt damping of a piezoelectric laminate beam,” *Proc. IEEE Conf. on Decision and Control (Sydney, Australia)* , 4018–4023 (2000).
- [42] Park, C., “Dynamics modelling of beams with shunted piezoelectric elements,” *J. Sound Vib.* **268**, 115–129 (2003).
- [43] Li, K., Yang, Z., Sun, H., and Zhang, L., “Profile and placement optimization for piezoelectric shunt damping system,” *World Forum on Smart Materials and Smart Structures Technology, Nanjing, China* , 493 (2007).
- [44] Fleming, A. J., Behrens, S., and Moheimani, S. O. R., “Reducing the inductance requirements of piezoelectric shunt damping systems,” *Smart Mater. Struct.* **12**, 57–64 (2003).
- [45] Fleming, A. J., Behrens, S., and Moheimani, S. O. R., “Synthetic impedance for implementation of piezoelectric shunt-damping circuits,” *Electronics letter* **36**, 1525–1526 (2000).
- [46] Behrens, S., Fleming, A. J., , and Moheimani, S. O. R., “New method for multiple-mode shunt damping of structural vibration using a single piezoelectric transducer,” *Proc. SPIE: Smart Structures and Materials, Damping and Isolation (Bellingham, WA)* **4331** (2001).
- [47] Behrens, S., Fleming, A. J., and Moheimani, S. O. R., “A broadband controller for shunt piezoelectric damping of structural vibration,” *Smart Mater. Struct.* **12**, 18–28 (2003).
- [48] Beck, B. S., Cunefare, K. A., and Ruzzene, M., “Active vibration control of a stiffened panel through application of negative capacitance shunts,” *Proc. SPIE: Smart Structures and Materials Conference: Active and Passive Smart Structures and Integrated Systems* , *San Diego, CA* **7977** (2011).
- [49] Davis, C. L., Lesieutre, G. A., and Dosch, J. J., “Tunable electrically shunted piezoceramic vibration absorber,” *Proc. SPIE: Smart Structures and Materials, Passive Damping and Isolation, Newport Beach, CA* **3045** (1997).

- [50] Davis, C. L. and Lesieutre, G. A., "Actively tuned solid state piezoelectric vibration absorber," *Proc. SPIE: Smart Structures and Materials Conference: Passive Damping and Isolation, San Diego, CA* **3327**, 169–182 (1998).
- [51] Kurdila, A., Lesieutre, G., Zhanga, X., Prazenicca, C., and Niezreckia, C., "Averaging analysis of state-switched piezoelectric structural systems," *Proc. SPIE: Smart Structures and Materials: Damping and Isolation, Bellingham, WA* **5760**, 413–422 (2005).
- [52] Tylikowski, A., "Control of circular plate vibrations via piezoelectric actuators shunted with a capacitive circuit," *Thin-Walled Structures* **39**, 84–94 (2001).
- [53] Lin, Q. and Ermanni, P., "Semi-active damping of a clamped plate using pzt," *International Journal of Solids and Structures* **41**, 1741–1752 (2004).
- [54] Larson, G. D. and Rogers, P. H., "State switched acoustic source," *The 128th Meeting of the Acoustical Society of America, Austin, Acoustic Society of America* **3317** (1994).
- [55] Cunefare, K. A., Sadegh, N., and Rogers, P. H., "State-switched absorber for semi-active structural control," *Journal of intelligent material systems and structures* **11**, 300–310 (2001).
- [56] Clark, W. W., "Semi-active vibration control with piezoelectric materials as variable stiffness actuators," *Proc. SPIE: Smart Structures and Materials, Passive damping and isolation (Newport Beach, CA)* **3672**, 123–130 (1999).
- [57] Clark, W. W., "Vibration Control with State-Switched Piezoelectric Materials," *J. Intell. Mater. Syst. Struct.* **11**, 263–271 (2000).
- [58] Clark, W. W. and Schoenly, J., "Evaluation of performance indices for tuning the switch timing of pulse-switched piezoelectric shunts for vibration control," *Proc. SPIE: Smart Structures and Materials, Damping and Isolation (Bellingham, WA)* **5760**, 402–412 (2005).
- [59] Corr, L. R., "Investigation of real-time switching of piezoceramic shunts for structural vibration control," *Ph.D These* (2001).
- [60] Corr, L. R. and Clark, W. W., "Comparison of low-frequency piezoelectric switching shunt techniques for structural damping," *Smart Mater. Struct.* **11**, 370–376 (2002).
- [61] Lallart, M., Guyomar, D., Jayet, Y., Petit, L., Lefeuvre, E., Monnier, T., Guy, P., and Richard, C., "Synchronized switch harvesting applied to self-powered smart systems: Piezoactive microgenerators for autonomous wireless receivers," *Sens. Actuators A: Phys.* **147**, 263–272 (2008).
- [62] Yuse, K., Monnier, T., Petit, L., Lefeuvre, E., Richard, C., and Guyomar, D., "Self-powered wireless health monitoring supplied by synchronized switch harvesting (SSH) method," *J. Intell. Mater. Syst. Struct.* **19**, 387–394 (2008).

- [63] Shen, H., Ji, H., Qiu, J., and Zhu, K., “A semi-passive vibration damping system powered by harvested energy,” *International Journal of Applied Electromagnetics and Mechanics* **13**(4), 219–233 (2009).
- [64] Lallart, M. and Guyomar, D., “An optimized self-powered switching circuit for non-linear energy harvesting with low voltage output,” *Smart Materials and Structures* **17**(3), 035030 (2008).
- [65] Balas, M. J., “Direct velocity feedback control of large space structures,” *Journal of Guidance, Control, and Dynamics* **2**(3), 252–253 (1979).
- [66] Yang, B., “Vibration control of gyroscopic systems via direct velocity feedback,” *J. Sound Vib.* **175**(4), 525–534 (1994).
- [67] Onoda, J., Endot, T., Tamaoki, H., and Watanabe, N., “Vibration suppression by variable-stiffness members,” *AIAA J.* **29**, 977–983 (1991).
- [68] Richard, C., Guyomar, D., Audigier, D., and Ching, G., “Semi-passive damping using continuous switching of a piezoelectric device,” *Proc. SPIE: Smart Structures and Materials, Passive damping and isolation (Newport Beach, CA)* **3672**, 104–111 (1999).
- [69] Corr, L. R. and Clark, W. W., “Energy dissipation analysis of piezoceramic semi-active vibration control,” *J. Intell. Mater. Syst. Struct.* **12**(11), 729–736 (2001).
- [70] Makihara, K., Onoda, J., and Minesugi, K., “A self-sensing method for switching vibration suppression with a piezoelectric actuator,” *Smart Mater. Struct.* **16**, 455–461 (2007).
- [71] Richard, C., Guyomar, D., Audigier, D., and Bassaler, H., “Enhanced semi-passive damping using continuous switching of a piezoelectric device on an inductor,” *Proc. SPIE: Smart Structures and Materials, Damping and Isolation (Newport Beach, CA)* **3989**, 288–299 (2000).
- [72] Lallart, M., Lefeuvre, E., Richard, C., and Guyomar, D., “Self-powered circuit for broadband, multimodal piezoelectric vibration control,” *Sens. Actuators A: Phys.* **143**, 377–382 (2008).
- [73] Ciminello, M., Calabro, A., Ameduri, S., and Concilio, A., “Synchronized switched shunt control technique applied on a cantilevered beam: numerical and experimental investigations,” *J. Intell. Mater. Syst. Struct.* **19**, 1089–1100 (2008).
- [74] Qiu, J., Ji, H., and Zhu, K., “Semi-active vibration control using piezoelectric actuators in smart structures,” *Frontiers of Mechanical Engineering in China* **4**, 242–251 (2009).
- [75] Onoda, J. and Makihara, K., “Performance of simple and sophisticated control in energy-recycling semi-active vibration suppression,” *J. Vib. Control* **14**(3), 417–436 (2008).
- [76] Makihara, K., Onoda, J., and Minesugi, K., “New approach to semi-active vibration isolation to improve the pointing performance of observation satellites,” *Smart Mater. Struct.* **15**, 342–350 (2006).

- [77] Makihara, K. and ONODA, J., "Using tuned electrical resonance to enhance bang-bang vibration control," *AIAA J.* **45(2)**, 497–504 (2007).
- [78] Makihara, K., Onoda, J., and Minesugi, K., "Behavior of piezoelectric transducer on energy-recycling semiactive vibration suppression," *AIAA J.* **44(2)**, 411–413 (2006).
- [79] Makihara, K., Onoda, J., and Tsuchihashi, M., "Investigation of performance in suppressing various vibrations with energy-recycling semi-active method," *Acta Astronautica* **58(10)**, 506 – 514 (2006).
- [80] Petit, L., Lefeuvre, E., Richard, C., and Guyomar, D., "A broadband semi passive piezoelectric technique for structural damping," *Proc. SPIE: Smart Structures and Materials, Damping and Isolation (Bellingham, WA)* **5386**, 414–425 (2004).
- [81] Lefeuvre, E., Badel, A., Petit, L., Richard, C., and Guyomar, D., "Semi-passive piezoelectric structural damping by synchronized switching on voltage sources," *J. Intell. Mater. Syst. Struct.* **17**, 653–660 (2006).
- [82] Ji, H., Qiu, J., Badel, A., Chen, Y., and Zhu, K., "Semi-active vibration control of a composite beam by adaptive synchronized switching on voltage sources based on LMS algorithm," *J. Intell. Mater. Syst. Struct.* **20**, 939–947 (2009).
- [83] Ciminello, M., Ameduri, S., and Concilio, A., "FE Modeling of an Innovative Vibration Control Shunt Technique," *J. Intell. Mater. Syst. Struct.* **19**, 875–887 (2008).
- [84] Badel, A., Lagache, M., Guyomar, D., Lefeuvre, E., and Richard, C., "Finite element and simple lumped modeling for flexural nonlinear semi-passive damping," *J. Intell. Mater. Syst. Struct.* **18**, 727–742 (2007).
- [85] Ciminello, M., Lecce, L., Ameduri, S., Calabr  s, A., and Concilio, A., "Multi-tone switching shunt control by a PZT network embedded into a fiberglass panel: design, manufacture, and test," *J. Intell. Mater. Syst. Struct.* **21**, 437–451 (2010).
- [86] Faiz, A., Guyomar, D., Petit, L., and Buttay, C., "Wave transmission reduction by a piezoelectric semi-passive technique," *Sensors and Actuators A: Physical* **128(2)**, 230 – 237 (2006).
- [87] Harari, S., *Contr  le modal semi-actif et actif   faible consommation  nerg tique par composants pi zo lectriques*, PhD thesis, INSA de LYON (2009).
- [88] Harari, S., Richard, C., and Gaudiller, L., "Semi-active control of a targeted mode of smart structures submitted to multimodal excitation," *Motion and Vibration Control* , 113–122 (2009).
- [89] Gaudiller, L., Harari, S., and Richard, C., "New semi-active multi-modal vibration control using piezoceramic components," *J. Intell. Mater. Syst. Struct.* **20(13)**, 1603–1613 (2009).

- [90] Ji, H., Qiu, J., and Xia, P., “Analysis of energy conversion in two-mode vibration control using synchronized switch damping approach,” *J. Sound Vib.* **In Press, Corrected Proof**, – (2011).
- [91] Ji, H., Qiu, J., Zhu, K., Chen, Y., and Badel, A., “Multi-modal vibration control using a synchronized switch based on a displacement switching threshold,” *Smart Mater. Struct.* **18**, 035016 (2009).
- [92] Ji, H., Qiu, J., Zhu, K., and Badel, A., “Two-mode vibration control of a beam using nonlinear synchronized switching damping based on the maximization of converted energy,” *J. Sound Vib.* **329**, 2751–2761 (2010).
- [93] Sodano, H. A., Lloyd, J., and Inman, D. J., “An experimental comparison between several active composite actuators for power generation,” *Smart Materials and Structures* **15**(5), 1211 (2006).
- [94] Adhikari, S., Friswell, M. I., and Inman, D. J., “Piezoelectric energy harvesting from broadband random vibrations,” *Smart Materials and Structures* **18**(11), 115005 (2009).
- [95] Anton, S. R. and Sodano, H. A., “A review of power harvesting using piezoelectric materials (2003-2006),” *Smart Materials and Structures* **16**(3), R1 (2007).
- [96] Anton, S. R., Erturk, A., and Inman, D. J., “Multifunctional self-charging structures using piezoceramics and thin-film batteries,” *Smart Materials and Structures* **19**(11), 115021 (2010).
- [97] Liao, Y. and Sodano, H. A., “Model of a single mode energy harvester and properties for optimal power generation,” *Smart Materials and Structures* **17**(6), 065026 (2008).
- [98] Badel, A., Guyomar, D., Lefeuvre, E., and Richard, C., “Efficiency enhancement of a piezoelectric energy harvesting device in pulsed operation by synchronous charge inversion,” *J. Intell. Mater. Syst. Struct.* **16**, 889–901 (2005).
- [99] Badel, A., *Récupération d’énergie et contrôle vibratoire par éléments piézoélectriques suivant une approche non linéaire*, PhD thesis, Université de Savoie/INSA de Lyon (2005).
- [100] Guyomar, D., Faiz, A., Petit, L., and Richard, C., “Wave reflection and transmission reduction using a piezoelectric semipassive nonlinear technique,” *J. Acoust. Soc. Am.* **19**(1), 285–298 (2006).
- [101] Thomson, W. T. and Dahleh, M. D., [*Theory of Vibration with Applications (5th Edition)*], Prentice Hall/Pearson (2005).

Publications

Journal papers

Li, K., Gauthier, J.-Y., and Guyomar, D., “Structural vibration control by synchronized switch damping energy transfer,” *J. Sound Vib.* **330**, 49–60 (2010).

Guyomar, D., Lallart, M., Li, K., Gauthier, J.-Y., and Monnier, T., “A self-synchronizing and low-cost structural health monitoring scheme based on zero crossing detection,” *Smart Mater. Struct.* **19**(4), 045017 (2010).

Li, K., Gauthier, J.-Y. and Guyomar, D., “Multimodal synchronized switch control with bidirectional energy transfer between piezoelectric patches for vibration damping,” **preparing to submit**.

Conference paper

Li, K., Gauthier, J.-Y., and Guyomar, D., “Nonlinear semi-passive vibration control based on synchronized switch damping with energy transfer between two modes,” *Proc. SPIE: Smart Structures and Materials Conference: Active and Passive Smart Structures and Integrated Systems V*, San Diego, CA **7977**(1), 797729 (2011).

French part

Chapitre 1 : Introduction générale

Les vibrations mécaniques indésirables ont tendance à détériorer le fonctionnement de la plupart des équipements. Cela peut se traduire par une fatigue prématurée des matériaux, une diminution des performances du système ou encore une augmentation du niveau de bruit acoustique. La structure peut, plus particulièrement, être endommagée en raison de grandes amplitudes de vibration lorsque les excitations se situent à des fréquences proches des fréquences propres du système. De grandes catastrophes tels que des écroulements de pont ou des crashes aériens sont arrivées à cause de problèmes de vibration. Le contrôle de ces vibrations est donc actuellement une préoccupation majeure des ingénieurs en mécanique.

Parmi les méthodes de contrôle de vibration, nous pouvons distinguer les méthodes passives, actives, semi-passives et semi-actives. De manière générale, les contrôles passifs sont toujours stables car il n'y a pas de contre-réaction externe directement exercée sur la structure à amortir. Ces méthodes sont souvent encombrantes et dépendantes des variations environnementales. A l'opposé, les contrôles actifs peuvent atteindre des performances robustes dans des grandes plages de fréquence mais consomment beaucoup d'énergie. De plus, des problèmes d'instabilité peuvent apparaître. Les méthodes semi-passives et semi-actives essaient de tirer profit des avantages des deux méthodes précédentes et sont actuellement des sujets de recherche très intenses dans le domaine du contrôle de vibration.

De nos jours, les matériaux intelligents sont de plus en plus utilisés en tant que capteur ou actionneur dans les systèmes de contrôle de vibration et plus particulièrement les matériaux piézoélectriques. Une technique classique consiste à connecter un circuit électrique ayant une impédance optimisée aux bornes des éléments piézoélectriques qui sont collés ou incorporés dans la structure à amortir. Un effet amortissant certain peut ainsi être observé lorsque la structure vibre autour de sa fréquence de résonance. Fondées sur ces bases, des techniques semi-passives

appelées en anglais Synchronized Switch Damping (S.S.D.) ont ainsi vu le jour et se sont développées. Les travaux sur ce thème couvrent beaucoup d'aspects tels que les principes, les lois de contrôle, les bandes passantes ainsi que quelques applications. Cependant, la plupart de ces recherches utilise un seul groupe d'éléments piézoélectriques dans le système de contrôle. Dans cette thèse, plusieurs groupes d'éléments sont collés sur la structure sans être définitivement connectés entre eux électriquement. Avec ce type de configuration, nous proposons un nouveau contrôle appelé Synchronized Switch Damping with Energy Transfer (S.S.D.E.T.). Un transfert d'énergie entre les groupes d'éléments piézoélectriques est ainsi effectué dans le but d'augmenter l'amortissement d'une structure ou d'un mode particulier en utilisant les autres structures ou modes.

Le manuscrit de thèse est organisé comme suit. Le chapitre 2 est une revue détaillée des techniques S.S.D. publiées. Le chapitre 3 présente les principes aussi bien que les lois de commande des techniques S.S.D.E.T. Des modèles mathématiques temporel et fréquentiel sont alors établis et des simulations numériques sous l'environnement Matlab/Simulink démontrent la faisabilité. Une loi de commande basée sur un seuil de tension est aussi abordée dans ce chapitre. Le chapitre 4 concerne la validation expérimentale. Trois types d'expérience ont été réalisés afin de montrer que le S.S.D.E.T. peut être appliqué entre différentes structures ou entre différents modes au sein d'une même structure. Les résultats expérimentaux montrent également que cette technique est aussi efficace pour les réponses purement harmoniques que pour des phases transitoires lors d'une perturbation en impulsion. Le chapitre 5 introduit les recherches préliminaires concernant le S.S.D.E.T. bidirectionnel. Un exemple impliquant deux éléments piézoélectriques couplés à deux modes est pris en compte. Différentes connections entre les éléments sont illustrées et le comportement dynamique de l'ensemble est étudié à l'aide de simulations. Ainsi, nous avons prouvé que le S.S.D.E.T. bidirectionnel permet d'améliorer l'amortissement. Des résultats expérimentaux comparent les différentes lois de contrôle et vont dans ce sens. Pour finir, le dernier chapitre apporte les conclusions et les perspectives de ces travaux de thèse.

Chapitre 2 : Etat de l'art des techniques d'amortissement par commutation synchronisée (S.S.D.)

Parmi les méthodes de contrôle de vibration semi-passives et semi-actives, les techniques d'amortissement par commutation synchronisée (S.S.D.) ont montré qu'elles étaient très efficaces. Comparées aux méthodes passives, le système de commande est robuste vis-à-vis des changements de propriétés dynamiques de la structure hôte soumise à des perturbations environnementales. Elles sont également compactes et légères, ce qui est approprié à des structures restreintes en poids ou en taille. Si l'on compare ces méthodes aux techniques purement actives, le S.S.D. est plus simple à implémenter et consomme moins d'énergie. Il peut même être auto-alimenté. Dans ces techniques, un interrupteur en série avec l'élément piézoélectrique, alternativement ouvert et fermé, permet d'obtenir une tension qui exerce toujours une force opposée à la vitesse de la structure. Cela se traduit donc par une dissipation d'énergie et un amortissement. En raison de ces avantages, ces techniques ont connu un essor important ces dernières années. Dans ce chapitre, nous établissons un état de l'art des techniques d'amortissement par commutation synchronisée.

D'abord, nous redonnons le modèle classique pour les structures couplées à des éléments piézoélectriques. Historiquement, les techniques S.S.D. sont issues des méthodes de contrôle de vibrations à raideur variable. Trois techniques représentatives (S.S.D.S., S.S.D.I. et S.S.D.V.) sont décrites sur le principe et avec leurs formes d'ondes correspondantes. Leurs points communs sont les suivants : (a) les commutations ont toujours lieu sur des extrema de déplacement ; (b) la tension aux bornes de l'élément piézoélectrique augmente (en valeur absolue) la plupart

du temps et reviens à zéro (S.S.D.S.) ou est inversée (S.S.D.I. ou S.S.D.V.) seulement durant la fermeture de l'interrupteur. Cela indique que l'énergie mécanique est convertie en énergie électrique et finalement dissipée en chaleur dans le circuit. L'énergie électrique ne peut donc pas être re-convertie en énergie mécanique. (c) Le signe de la tension aux bornes de l'élément piézoélectrique V est toujours le même que celui de la vitesse et donc la force exercée par l'élément piézoélectrique $-\alpha V$ admet un signe opposé à la vitesse. Les techniques S.S.D.S. et S.S.D.V. sont de bonnes candidates en ce qui concerne le recyclage d'énergie car l'énergie utilisée pour le contrôle est extraite de la structure hôte. Cependant la technique S.S.D.V. peut devenir instable car une partie de l'énergie provient d'une source externe de tension. Afin de contourner ce problème, une technique S.S.D.V. sur une source variable de tension a été proposée. Ainsi, la force est automatiquement ajustée en fonction de l'amplitude du déplacement de la structure à amortir.

Ensuite, nous introduisons une analyse énergétique pour les techniques S.S.D. précédentes. Cela montre que le pouvoir amortissant de chaque technique est particulièrement lié à l'amplitude de tension sur les éléments piézoélectriques. Généralement, une grande amplitude de tension donne un meilleur amortissement sur la structure hôte. En tant que pouvoir amortissant, les techniques sont ainsi classées comme suit : S.S.D.S. < S.S.D.I. < S.S.D.V. Mais le classement d'un point de vue consommation énergétique est le suivant S.S.D.S. = S.S.D.I. < S.S.D.V. Les fonctions de transfert sont aussi détaillées dans ce chapitre.

A la suite de cette partie, nous étudions les contrôles large bande et multimodaux utilisant des techniques S.S.D. qui ont été développées ces cinq dernières années. Les modèles mathématiques des méthodes multimodales sont généralement construits à partir de coordonnées modales. Les chercheurs établissent aussi des modèles par des méthodes à éléments finis. La différence principale entre les contrôles de mode unique et les contrôles multimodaux réside dans le choix de l'instant de commutation. Nous avons choisi de les regrouper en trois grandes parties. (a) Les méthodes avec un contrôle classique. Dans ces méthodes, les lois de commande sont identiques à celles des méthodes monomodales et, en effet, ce type de contrôle fonctionne pour excitation large-bande expérimentalement mais n'est pas du tout optimal. (b) Les méthodes basées sur une distinction des modes. Dans ces méthodes, les modes intéressants sont détectés à partir de signaux de mesure afin de déterminer les instant de commutation. (c) Les méthodes basées sur des fenêtres temporelles. Les instants de commutation sont déterminés à l'aide de prédictions statistiques qui sont obtenues à partir de mesures contenues dans une fenêtre de temps fixée.

Enfin, deux méthodes particulières sont décrites : les techniques auto-alimentées et les techniques non-synchronisées (B.S.D.). Dans les travaux exposés précédemment, les commutations sont couramment contrôlées par des systèmes à base de D.S.P. et donc l'énergie utilisée pour la commande des interrupteurs est grande. Des circuits spécialisés à partir d'éléments électroniques simples ont permis de montrer que les commutations pouvaient être pilotées sans aucune alimentation extérieure, l'énergie requise étant prise directement sur la structure mécanique à amortir. Des évolutions ont été également réalisées afin d'obtenir un pouvoir amortissant multimodal. Les techniques B.S.D., quant à elles, n'ont pas besoin de détecter les extrema de déplacement et la commande est ainsi plus aisée à implémenter. Ces techniques qui ne sont en effet pas des techniques synchronisées sur le déplacement, utilisent tout de même le même circuit électrique que les méthodes S.S.D. Nous verrons dans le chapitre suivant que ces techniques ont un point commun avec les travaux de cette thèse concernant l'amortissement par commutation synchronisée avec transfert d'énergie.

Chapitre 3 : Principes généraux de l'amortissement par commutation synchronisée avec transfert d'énergie.

Dans ce chapitre, nous proposons une nouvelle déclinaison des techniques S.S.D appelée amortissement par commutation synchronisée avec transfert d'énergie (S.S.D.E.T.). Dans cette méthode de commande, l'énergie de vibration est transférée entre les éléments piézoélectriques dans le but d'obtenir un effet amortissant. Trois points importants sont ainsi détaillés.

Premièrement, nous introduisons le but du S.S.D.E.T. Celui-ci est d'amortir le mouvement d'une vibration (cible) en utilisant l'énergie mécanique d'une autre vibration (source). Une caractéristique nouvelle est donc que la source d'énergie n'est plus une source artificielle mais une autre structure vibrante ou une autre mode de vibration. Un schéma électrique est donc proposé afin de réaliser cet échange. Dans ce circuit, une inductance est utilisée pour stocker de l'énergie de manière intermédiaire entre la source et la cible. La loi de commande correspondante comporte deux phases : stockage de l'énergie mécanique provenant de la source dans l'inductance et transfert de celle-ci vers l'élément piézoélectrique qui contrôle la vibration cible. Les formes d'onde durant le transfert sont détaillées, quatre possibilités peuvent apparaître en fonction des signes des tensions de la source et de la cible.

Deuxièmement, des modèles mathématiques sont construits dans les domaines temporels et fréquentiels. Dans cette partie, nous introduisons comment identifier les paramètres du modèle dans le cas d'une structure couplée à des éléments piézoélectriques. Dans le cadre de la modélisation temporelle, une représentation d'état est adoptée afin de décrire le comportement du système lors de ces

différentes phases de fonctionnement. Des simulations numériques ont été implémentées à l'aide de Matlab/Simulink pour les techniques S.S.D.E.T. et S.S.D.I. Comparé au S.S.D.I., le S.S.D.E.T. peut augmenter l'amortissement de la structure cible à travers une meilleure inversion de la tension. De plus, la structure source est aussi amortie car une énergie mécanique est extraite. Une étude dans le domaine fréquentiel a permis d'obtenir des équations décrivant l'amortissement lorsque la structure est excitée à la fréquence de résonance. Une équation est dérivée à partir de calculs statistiques et permet d'obtenir la relation entre la puissance extraite de la source et l'effet amortissant sur la cible. Cela permet également d'examiner quantitativement l'effet des différents paramètres sur l'efficacité de l'amortissement.

Troisièmement, une amélioration des lois de commande est proposée en se basant sur le modèle développé. Une augmentation de la puissance extraite, et donc de l'amortissement de la cible, peut être réalisée simplement à partir d'un seuil de tension sur la source. Cette augmentation de puissance extraite est ainsi opérée en diminuant le nombre de transfert. En comparant avec la loi de commande originale, des simulations numériques ont montré que ce nouveau contrôle améliore sensiblement l'efficacité lorsque le rapport des fréquences entre la source et la cible est grand.

Chapitre 4 : Essais expérimentaux et discussions autour de l'amortissement par commutation synchronisée avec transfert d'énergie.

Dans ce chapitre, des essais expérimentaux sont présentés afin de prouver l'efficacité des techniques S.S.D.E.T. Trois différentes expériences ont ainsi été mises en place pour tester ces techniques.

Le premier banc expérimental est constitué de deux structures mécaniques : une poutre encastrée à son extrémité et une plaque encastrée sur les quatre côtés. Ce type de système est intéressant car il n'y a aucun couplage mécanique direct entre les deux structures. La vibration source est le premier mode de flexion de la poutre et la vibration cible est la plaque qui vibre à son premier mode (mode 1-1). Les résultats montrent que le S.S.D.E.T. peut augmenter considérablement l'amortissement de la plaque par rapport au S.S.D.I. De plus, les résultats expérimentaux sont en bon accord avec les simulations temporelles. Ainsi, plus la vibration de la poutre est importante (ce qui indique une grande puissance transférée), plus l'amortissement de la plaque est bon.

La deuxième expérience porte sur les premiers modes de flexion et de torsion d'une plaque encastrée sur un seul côté. En raison des couplages entre les deux modes, les éléments piézoélectriques sont divisés en deux groupes et placés de manière à obtenir un couplage maximum pour chaque mode. La source d'énergie correspond au mode de flexion et la cible est le mode de torsion. Les résultats montrent que le S.S.D.E.T. est efficace également dans ces circonstances et de plus l'effet du seuil sur la tension de la source est vérifié. Les résultats expérimentaux

sont comparés avec ceux du modèle mathématique dans le domaine fréquentiel. La puissance extraite est également comparée avec les résultats de simulation pour l'effet du seuil. Les prédictions théoriques sont cohérentes à la vue de ces résultats. Des essais ont de plus été réalisés pour tester les techniques S.S.D.E.T. lors des transitoires suite à un choc sur la plaque.

Le troisième test a été mené pour montrer que le S.S.D.E.T. pouvait être utilisé pour des systèmes contenant plus de deux groupes d'éléments piézoélectriques. Ainsi, trois modes de vibration sont considérés à partir de deux structures mécaniques. La cible est le mode de torsion de la plaque encastrée sur un côté, et la source peut être une poutre en acier ou le mode torsion de cette même plaque. Le choix entre les deux sources est fait sur la base d'une comparaison entre les énergies électriques des deux sources au moment du transfert d'énergie. Avec ce type de stratégie, nous avons montré qu'une plus grande puissance pouvait être transférée et donc qu'un meilleur amortissement de la cible était obtenu.

De plus, la stabilité des techniques S.S.D.E.T. est discutée lors de ces expériences. Il a été montré que la fréquence de vibration de la source se retrouvait dans le déplacement de la cible. Cette composante est d'autant plus grande que l'amplitude de la source est importante. Nous avons aussi mis en évidence que le système pouvait perdre sa stabilité lorsque la puissance transférée était trop importante. Cela peut être expliqué par deux raisons : (a) le déplacement n'est plus sinusoïdal lorsque l'amortissement est très grand, le détecteur d'extrema ne peut donc plus détecter correctement les instants de commutation. (b) En raison de la forme non sinusoïdale de la tension, la force correspondante peut exciter des modes résiduels dans la structure.

Chapitre 5 : S.S.D.E.T. bidirectionnel : une recherche préliminaire

Les techniques S.S.D.E.T. que nous avons détaillé dans les chapitres précédents ont deux caractéristiques. (1) La tension aux bornes d'un groupe d'éléments piézoélectriques est toujours sinusoïdale en circuit ouvert même si la structure hôte est en excitation bimodale. Cela indique qu'un élément ne peut extraire de l'énergie mécanique qu'à partir d'un mode de vibration. (2) La source est toujours un groupe d'élément et la cible en est un autre.

Dans ce chapitre, nous proposons une technique S.S.D.E.T. bidirectionnelle qui possède des caractéristiques différentes sur ces deux points. Un groupe d'éléments piézoélectriques peut extraire de l'énergie de plusieurs modes et n'est plus défini de manière permanente comme étant une source ou une cible. Afin de la comparer avec les méthodes traditionnelles, nous étudierons quatre circuits classiques SSD qui sont les suivants: (1) Cas A : Les groupes d'éléments sont connectés de manière isolée à un circuit S.S.D.I. (2) Cas B : Les groupes d'éléments sont connectés en parallèle puis à un circuit S.S.D.I. (3) Cas C : Les groupes d'éléments sont connectés en série puis à un circuit S.S.D.I. (4) Cas D : Les groupes d'éléments ont chacun leur interrupteur mais sont connectés à la même inductance.

Le chapitre est ainsi organisé de la manière suivante. Premièrement, une structure mécanique vibrante mettant en IJuvre deux modes (flexion et torsion) est introduite afin d'illustrer nos propos. Nous proposons les quatre possibilités de connexion entre deux groupes d'éléments (cas A, B, C et D) et simulons leurs comportements sous Matlab/Simulink. Les résultats indiquent que toutes les méthodes permettent d'obtenir un amortissement sur le mode de torsion mais la plupart d'entre elles n'ont pas d'effet substantiel sur le mode de flexion. De plus, des similitudes peuvent être établies entre les méthodes S.S.D.E.T. et le Cas D. En

raison d'un transfert d'énergie entre les deux groupes d'éléments (via l'inductance partagée) un plus grand amortissement est atteint par rapport aux trois autres cas.

Deuxièmement, nous introduisons les principes de base du S.S.D.E.T. bidirectionnel. Les groupes d'éléments piézoélectriques sont connectés électriquement comme le cas D mais le contrôle des interrupteurs est très différent. Les lois de contrôle du S.S.D.E.T. bidirectionnel sont détaillées dans le manuscrit. Le but est de concentrer toute l'énergie électrique sur un seul groupe d'éléments après chaque commutation. Le critère de sélection du groupe se fait à partir des signes du déplacement du mode cible et de la vitesse du mode source. Nous pouvons également remarquer que la tension sur le groupe d'éléments qui reçoit l'énergie transférée n'est pas forcément inversée comme dans le cas du S.S.D.E.T. classique. Des simulations montrent que les tensions sur les deux groupes d'éléments augmentent en valeur absolue la plupart du temps, c'est-à-dire que l'énergie est extraite du système mécanique et plus rarement envoyée vers celui-ci. Cela a pour effet un meilleur pouvoir amortissant que les autres cas introduits précédemment.

Finalement, un test expérimental a été mené sur une poutre encadrée excitée simultanément sur deux modes de flexion et de torsion. Les cas B, D et le S.S.D.E.T. bidirectionnel ont été testés et les formes d'ondes sont cohérentes avec les simulations. Les comparaisons montrent que le S.S.D.E.T. bidirectionnel peut engendrer un meilleur amortissement sur la cible ainsi que sur la source parmi les trois méthodes testées.

FOLIO ADMINISTRATIF

THÈSE SOUTENUE DEVANT L'INSTITUT NATIONAL DES SCIENCES APPLIQUÉES DE LYON

NOM : **LI**
(avec précision du nom de jeune fille, le cas échéant)

DATE de SOUTENANCE : **xx Septembre 2011**

Prénom : **Kaixiang**

TITRE : **Amortissement vibratoire avec échange d'énergie synchronisé entre des éléments piézoélectriques**

NATURE : **Doctorat**

Numéro d'ordre : **2011-ISAL-xxxx**

École Doctorale : **Électronique, Électrotechnique et Automatique de Lyon**

Spécialité: **Énergie et Systèmes**

Cote B.I.U. - Lyon : T 50/210/19 / et bis CLASSE :

RÉSUMÉ :

Les matériaux évolués tels que les matériaux composites ou les fibres de carbone sont de plus en plus utilisés dans l'industrie. Ils rendent les structures plus légères et plus résistantes mais en contrepartie, ils apportent de nouveaux problèmes de vibration. De nombreuses recherches sont ainsi en cours pour apporter des solutions afin d'éliminer les vibrations indésirables tout en restant compactes, légères, intelligentes et modulaires. Récemment, des techniques de contrôle non-linéaires, dénommées en anglais S.S.D. (Synchronized Switch Damping) ont été proposées et validées. Ces méthodes font commuter un élément piézoélectrique collé à la structure mécanique à amortir sur un circuit électrique de manière synchronisée avec la déformation de celle-ci. Un effet amortissant peut ainsi être obtenu en utilisant l'énergie de vibration de la structure mécanique elle-même. Basée sur ces concepts, une nouvelle technique appelée S.S.D.E.T. (Synchronized Switch Damping with Energy Transfer) est proposée dans ce manuscrit. Cette méthode permet d'amortir une vibration en utilisant de l'énergie extraite à partir d'autres vibrations. Les résultats de ce travail de thèse sont présentés de la manière suivante. Premièrement, le principe et les lois de commande de la technique S.S.D.E.T. sont introduits. Ainsi, un modèle mathématique est établi et permet de vérifier les concepts proposés par simulation. Ensuite, des validations expérimentales menées sur différentes configurations sont décrites et démontrent l'augmentation de l'amortissement sur un système composé de deux structures mécaniquement indépendantes, sur un système composé d'une seule structure qui vibre selon plusieurs modes et sur une combinaison des deux précédents. Enfin, une extension de la technique S.S.D.E.T. est introduite dans un cadre d'échange d'énergie bidirectionnel. Celle-ci permet d'obtenir un amortissement privilégié sur un mode tout en conservant un contrôle correct des autres modes.

MOTS-CLÉS : matériaux piézoélectriques, technique d'amortissement par commutation synchronisée, contrôle de vibration non-linéaire, semi-passif, semi-actif, transfert d'énergie

Laboratoire(s) de recherche : **Laboratoire de Génie Électrique et Ferroélectricité(LGEF) - INSA Lyon**

Directeur de thèse : **Pr. Daniel GUYOMAR**

Co-directeur de thèse : **Dr. Jean-Yves GAUTHIER**

Président du Jury : **Pr.**

Composition du Jury :

Pr. Emmanuel FOLTETE, Dr. Jean-Yves GAUTHIER

Pr. Daniel GUYOMAR, Pr. Mohamed ICHCHOU

Dr. Dejan VASIC, Pr. Zhichun YANG